The Effects of Benzalkonium Chloride Disinfectants on Lipid Homeostasis and Neurodevelopment

Josi M. Herron

A dissertation
submitted in partial fulfillment of the
requirements for the degree of

Doctor of Philosophy

University of Washington
2019

Reading Committee:
Libin Xu, Chair
Edward Kelly
Zhengui Xia

Program Authorized to Offer Degree:
Environmental and Occupational Health Sciences – Public Health

University of Washington

Abstract

The Effects of Benzalkonium Chloride Disinfectants on Lipid Homeostasis and Neurodevelopment

Josi M. Herron

Chair of Supervisory Committee:
Assistant Professor Libin Xu
Departments of Medicinal Chemistry and Environmental and Occupational Health Sciences

Developmental neurotoxicity (DNT) is one of the least tested health effects of the more than 80,000 chemicals registered for use today. In order to more efficiently test chemicals for DNT, more knowledge is needed on mechanisms that trigger adverse neurodevelopmental outcomes. Lipids are critical for neurodevelopment; therefore, disruption of lipid homeostasis by chemicals is expected to have detrimental effects on this process. However, few have investigated this as a possible mechanism of DNT.

In preliminary studies, we demonstrated that benzalkonium chloride compounds (BACs) alter cholesterol biosynthesis and lipid homeostasis in neuronal cells. BACs are the most commonly used quaternary ammonium compound (QAC) disinfectants. They are applied in food processing lines, health care facilities, residential settings, and are common ingredients in over-the-counter cosmetics, hand sanitizers, and pharmaceutical products. Therefore, exposure to BACs is prevalent given the diversity of applications and may occur through dermal/eye contact, inhalation, and ingestion. Recent studies demonstrate that BAC

exposure leads to an increased incidence of neural tube defects *in utero* and increased apoptosis of neural progenitor cells (NPCs). However, the effects of BACs on neurodevelopment as a result of altered lipid homeostasis has not been investigated.

In my dissertation work, I characterized the effects of BACs on lipid homeostasis and neurodevelopmental processes. First, I showed that BACs potently inhibit cholesterol biosynthesis in mouse and human neuronal cells. Building on this work, I showed that BACs can cross the blood-placental barrier and enter the developing mouse brain following *in utero* exposure via maternal diet. Further transciptomic analyses of the developing brain elucidated key signaling pathways affected by BACs, including cholesterol biosynthesis, liver X receptor-retinoid X receptor (LXR/RXR) signaling, and glutamate receptor signaling. Mass spectrometry analysis revealed decreases in total sterol levels and downregulation of triglycerides and diglycerides, which were consistent with the upregulation of genes involved in sterol biosynthesis and uptake, as well as inhibition of LXR signaling. Finally, I investigated the effects of BACs on neurospheres, free floating structures of NPCs, which are used as a three-dimensional (3-D) *in vitro* model of neurodevelopment. I found that BACs depleted the pool of NPCs and increased apoptosis, which contributed to a reduction in neurosphere growth. Transcriptome analysis revealed that BACs activated the integrated stress response, a mechanism used by cells to adapt to a variety of stressors including oxidative stress, mitochondrial dysfunction, nutrient deficiency, or hypoxia.

Altogether, the findings of this dissertation demonstrate that a class of commonly used disinfectants alter lipid homeostasis and impact neurodevelopmental processes. These data add to a growing body of literature reporting the adverse effects of BACs on neurodevelopment. Importantly, this work supports a novel mechanism by which environmental chemicals may target neurodevelopment.

Table of Contents

List of Figures

List of Tables

List of Abbreviations

3-D	Three-dimensional
7-DHC	7-dehydrocholesterol
7-DHD	7-dehydrodesmosterol
8-DHC	8-dehydrocholesterol
BAC	Benzalkonium chloride compound
BTEC	Benzyltriethylammonium chloride
Cer	Ceramide
DEG	Differentially expressed gene
DG	Diacylglycerol
DHA	Docosahaexanoic acid
DHCEO	3β,5α-dihydroxycholest-7-en-6-one
DHCR7	3β-hydroxysterol-Δ^7-reductase
DNT	Developmental neurotoxicity
DSSTox	Distributed Structure-Searchable Toxicity
EBP	3β-hydroxysterol-Δ^8,Δ^7-isomerase
ER	Endoplasmic reticulum
GC-MS	Gas chromatography-mass spectrometry
GO	Gene ontology
HexCer	Hexosylceramide
Hh	Hedgehog
HILIC	Hydrophilic-interaction liquid chromatography
HPLC	High-performance liquid chromatography
IM	Ion mobility
IPA	Ingenuity Pathway Analysis
LC	Liquid chromatography
LXR/RXR	Liver X receptor-retinoid X receptor
MS	Mass spectrometry
MS/MS	Tandem mass spectrometry
NPC	Neural progenitor cell
NTD	Neural tube defect
PCA	Principal component analysis
PCP	Phencyclidine

PND	Postnatal day
PUFA	Polyunsaturated fatty acid
QAC	Quaternary ammonium compound
RT-qPCR	Real time-quantitative polymerase chain reaction
SAR	Structure activity relationship
SLOS	Smith-Lemli-Opitz syndrome
TG	Triacylglycerol
UHPLC	Ultra-high performance liquid chromatography

Acknowledgements

First and foremost, I would like to thank my doctoral advisor, Dr. Libin Xu, for his incredible mentorship and support over the past four years. Libin has been a source of invaluable guidance and has always been supportive of my research endeavors. He has reviewed countless abstracts, proposals, posters, presentations, and manuscripts – fostering my development into a scientist and professional. Every time I entered Libin's office full of despair when experiments did not pan out, I left with a fresh perspective and a path forward. I cannot thank Libin enough for allowing me the opportunity to be his first graduate student.

I also thank Drs. Terrance Kavanagh, Edward Kelly, Zhengui Xia, and Qingcheng Mao for serving on my Doctoral Advisory committee and providing thoughtful feedback on this work. I would like to extend further gratitude to Terry for allowing me to work in his lab as an undergraduate, his continued support throughout my time in graduate school, and his collaboration on my research. Thanks also to Zhengui and Ed Kelly for serving on my Dissertation Reading Committee.

A special thank you also goes to current and former members of the Xu lab. This journey would not have been possible, and definitely not as fun, without the encouragement, guidance, and friendship of Dr. Kelly Hines. I also thank Dr. Hideaki Tomita for his welcome advice and countless bags of ketchup chips. Finally, thanks to Cecilia Tran and Amy Li for working by my side on various experiments.

Most importantly, I would not be who or where I am today without the love and support from those most special to me. Mom and Dad, I can only hope that one day my work ethic, integrity, and perseverance will match yours. Thanks for all you have done for me. Kacy, Molly, and Marca, thank you for being the three best sisters and friends that anyone could have. Andrew, you have been a loving partner throughout this challenging time. Thank you for always seeing the best in me and staying positive when I needed it most.

Lastly, I would like to acknowledge the financial support for this work: the University of Washington Environmental Pathology/Toxicology Training Program (NIH T32 ES007032-39), the Eunice Kennedy Shriver National institute for Child Health and Human Development (R01 HD092659), the University of Washington Interdisciplinary Center for Exposures, Diseases, Genomics and Environment (P30ES007033), National Institute of Health grants (R00 HD0732700 and P30 ES000267), and the University of Washington Department of Medicinal Chemistry.

Chapter 1: Introduction

1.1 Environmental Chemicals and Neurodevelopmental Disorders

Neurodevelopment requires the careful coordination of a variety of complex processes including cell proliferation, differentiation, migration, apoptosis, and synaptic pruning (Rice and Barone Jr., 2000). This period of developmental plasticity is considered a window of susceptibility, as exposure to environmental insults could interfere with developmental processes, leading to permanent changes in brain structure and function, known as developmental neurotoxicity (DNT). The Organisation for Economic Co-operation and Development and United States Environmental Protection Agency have defined DNT as the adverse effects of chemicals on the nervous system associated with exposure during development (OECD, 2006; US EPA, 1998). The association of neurodevelopmental disorders, including delays, deficits, and neuropsychiatric diagnoses, with exposure to environmental chemicals is well established and exemplified by well-known developmental neurotoxicants. These include ethanol, polychlorinated biphenyls, lead, methylmercury, organophosphate pesticides, polybrominated diethyl ether flame retardants, and air pollution (Bennett et al., 2016; Grandjean, Kishi, and Kogevinas, 2017).

An alarming increase in children's neurodevelopmental disorders has raised society's concern about the contribution of chemical exposures (Bennett et al., 2016; Fritsche et al., 2017; Grandjean, Kishi, and Kogevinas, 2017; Bal-Price et al., 2018). In 2006-2008, it wass estimated that 1 in 6 children in the United States had a developmental disability, 17% more than the decade prior (Boyle et al., 2011). A majority of these children had cognitive disabilities, including attention deficit hyperactivity disorder, intellectual disability, autism, and seizures (Boyle et al., 2011). Importantly, these disorders are costly and cause lifelong disability (Grandjean and Landrigan, 2006).

Prevention of neurodevelopmental disorders caused by exposure to environmental chemicals is impeded by gaps in testing chemicals for DNT and the amount of evidence required for regulation (Grandjean and Landrigan, 2006). Of the more than 80,000 chemicals registered for use in the United States, only 200 have undergone DNT testing (Smirnova et al., 2014). To more efficiently characterize the DNT hazard posed by environment chemicals, an emphasis has been placed on understanding mechanisms by which exposure to environmental chemicals results in neurodevelopmental disorders (Bal-Price and Meek, 2017; Rock and Patisaul, 2018).

1.2 Altered Lipid Homeostasis as a Mechanism of Developmental Neurotoxicity

Lipids and Neurodevelopment

The brain is one of the most lipid rich organs, second to adipose tissue, with lipids accounting for approximately half of the brain's dry weight (Hussain et al., 2019). The brain rapidly builds up its lipid content during development, which is maintained throughout adulthood (Betsholtz, 2015). The mammalian brain contains eight categories of lipids (Adibhatla and Hatcher, 2008). Of these, sphingolipids, glycerophospholipids and cholesterol are present in high amounts and in almost equal ratios (Korade and Kenworthy, 2008).

Sphingolipids are made from the initial synthesis of ceramide and subsequent attachment of different head groups to ceramides to produce complex sphingolipids (Olsen and Færgeman, 2017). Docosahexaenoic acid (DHA), a long-chain polyunsaturated fatty acid (PUFA), is supplied to the developing brain through placental transfer during gestation and becomes incorporated into membrane glycerophospholipids (Lauritzen et al., 2016). Peak brain deposition of DHA coincides with rapid brain growth (Meldrum and Simmer, 2016). Cholesterol can also be obtained from maternal circulation, however a significant amount is synthesized by the fetus (Woollett, 2011). Moreover, after formation of the blood brain barrier, cholesterol in the brain must be synthesized locally (Zhang and Liu, 2015). Cholesterol

biosynthesis is a complex process involving many intermediates but can be broadly divided into two segments: pre-squalene and post-squalene syntheses. In pre-squalene synthesis, isoprenoids formed from the mevalonate pathway undergo a series of condensation reactions that leads first to squalene and then to squalene epoxide upon epoxidation. In post-squalene synthesis, cyclization of squalene epoxide leads to the first sterol in the pathway, lanosterol, which is diverted into one of two pathways that both progress through a series of dehydrogenations, reductions, and demethylations (**Figure 1.1**) (Kelley and Herman, 2001).

Rather than being used for energy storage, brain lipids are used in a variety of processes, which ultimately contributes to the brain's structure and function (Betsholtz, 2015). One of the processes where lipids play a critical role is neurodevelopment. Changes in the composition of sphingolipids has been correlated with several neurodevelopmental milestones in the human brain, including neural tube formation, neuronal differentiation, axonogenesis, and synaptogenesis (Olsen and Færgeman, 2017). Long chain PUFAs, including DHA, act as precursors of signaling molecules and activators of gene transcription factors (Lauritzen et al., 2016). DHA is essential for neurogenesis, the process by which neural cell types are generated from neural stem cells (Coti Bertrand, O'Kusky, and Innis, 2006; Katakura et al., 2009). Cholesterol also plays important roles in neurodevelopment – serving an essential role in Hedgehog (Hh) signaling (Byrne et al., 2016; Cooper et al., 2003; Porter, Young, and Beachy, 1996; Zhang et al., 2018), which is an important mediator of neurogenesis (Komada et al., 2008); synapse formation and function (Koudinov and Koudinova, 2001; Mauch et al., 2001); and myelination (Saher et al., 2005).

Given the importance of lipids in neurodevelopment, it is expected that alterations in lipid homeostasis, perhaps by exposure to environmental chemicals, would impact neurodevelopment. Effects on brain cholesterol may be especially detrimental as it must be synthesized locally following the formation of the blood-brain barrier.

Consequences of Altered Cholesterol Biosynthesis

Alterations in cholesterol homeostasis, especially the deficiency of cholesterol and accumulation of its precursors, contribute to a variety of malformations and disorders (**Figure 1.1**) (Porter and Herman, 2011). Smith-Lemli-Opitz syndrome (SLOS) is the most common cholesterol biosynthesis disorder, with an estimated incidence of approximately 1 in 50,000 births among those of European ancestry (Tierney et al., 2006). SLOS is caused by mutations in the gene encoding the last step of cholesterol biosynthesis, 3β-hydroxysterol-Δ^7-reductase (DHCR7), resulting in reduced enzymatic activity. This defect leads to greatly elevated levels of 7-DHC and decreased levels of cholesterol in all tissues and fluids (Korade et al., 2010). The small molecule and known teratogen, AY9944, induces a pharmacological model of SLOS in rats by potently inhibiting DHCR7, reproducing the above-mentioned biochemical defects (Kolf-Clauw et al., 1996; Roux, Horvath, and Dupuis, 1979; Roux et al., 1980). Clinical features of SLOS include effects on brain development such as microcephaly, holoprosencephaly, and agenesis of the corpus callosum; mental retardation and hyperactivity; growth retardation and postnatal failure to thrive; and facial and limb malformations (Porter and Herman, 2011).

Ethanol and retinoic acid, two well-known developmental neurotoxicants, have also been shown to alter cholesterol homeostasis in the developing brain through the upregulation of cholesterol transporters and increased cholesterol efflux, which leads to reduced levels of cholesterol (Chen, Costa, and Guizzetti, 2011a; Zhou et al., 2014). Interestingly, fetal alcohol syndrome, a hallmark of gestational ethanol exposure, shares many clinical features with SLOS (Guizzetti and Costa, 2007). Based on these findings, Guizzetti et al (2011) concluded

that chemicals capable of affecting cholesterol homeostasis should be regarded as potential developmental neurotoxicants.

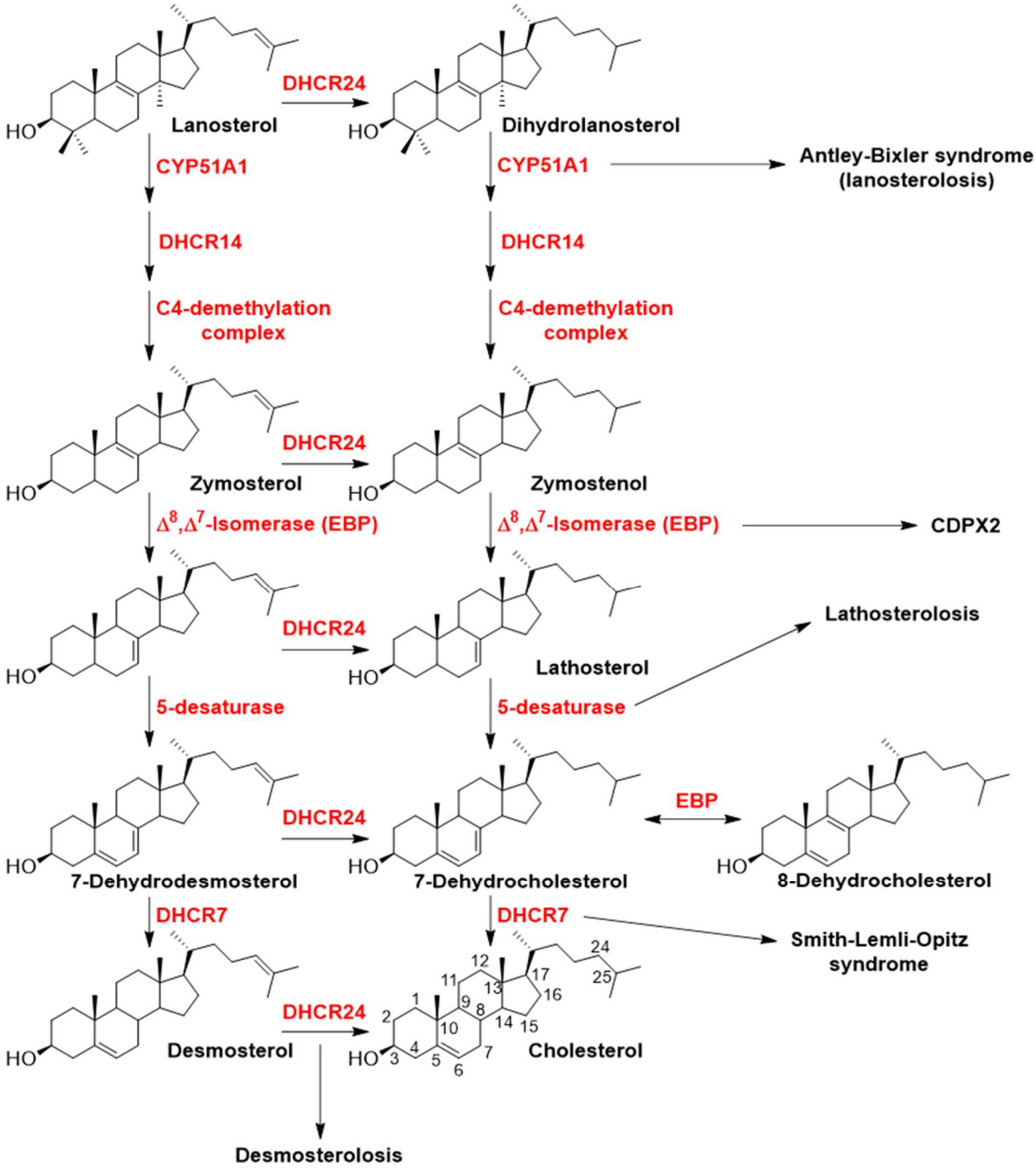

Figure 1.1. Post-squalene cholesterol biosynthetic pathway and examples of disorders associated with defects at specific steps.

1.3 Benzalkonium Chloride Compounds, an Emerging Class of Developmental Neurotoxicants

In the early part of my graduate studies, we found that benzalkonium chloride compounds (BACs) display high structural similarity to AY9944 and demonstrated that BACs inhibit cholesterol biosynthesis in neuronal cells (Chapter 2; Herron et al., 2016) in a chain length-dependent manner. Furthermore, in a collaborative work with a postdoctoral fellow in the Xu Lab, Dr. Kelly Hines, we found that BACs also alter the lipidome of neuronal cells in a chain length-dependent manner (Hines, Herron, and Xu, 2017). These findings suggest that BACs may have adverse impacts on neurodevelopment through altered cholesterol and lipid homeostasis, which laid the foundation for my dissertation work.

BACs belong to a larger class of disinfectants called quaternary ammonium compound (QACs). QACs are cationic surfactants used as disinfectants in various domestic, industrial, and medical applications (Tandukar et al., 2013). BACs are also found in over-the-counter cosmetics, hand sanitizers, and pharmaceutical products (Kim et al., 2018). Given the diversity of applications, exposure to BACs is prevalent and expected to occur through dermal/eye contact, inhalation, and ingestion. However, literature on exposure levels in humans is scarce. Contact dermatitis, asthma symptoms, eye and mucous irritation, and injuries of the gastrointestinal tract have been reported from direct exposure to QACs (BNOEMC, 2015).

More recent studies have reported effects on neurodevelopment associated with exposure to BACs. Hrubec et al (2017) suggested that QACs should be considered *bona fide* teratogens, based on an increased incidence of neural tube defects observed in rodents exposed *in utero* to an environmentally relevant mixture of QACs that contains BACs. NTDs are closely associated with defects in the proliferation of neural progenitor cells (NPCs), a population of cells which have important roles in the developing brain (Hirata et al., 2001;

Ishibashi et al., 1995; Zhong et al., 2000). Additionally*, in vitro* BAC exposure decreased proliferation and increased apoptosis and oxidative stress in cultured NPCs (Ryu et al., 2018). However, the effects of BACs on neurodevelopment as a result of altered lipid homeostasis has not yet been investigated.

1.4. Summary and Objectives of Dissertation Research

Exposure to environmental chemicals has been associated with increased risk for neurodevelopmental disorders. However, there is limited knowledge on mechanisms that trigger these adverse outcomes. To fill this gap, I proposed a novel mechanism that environmental toxicants can affect neurodevelopment – through disruption of lipid homeostasis, as lipids, including cholesterol, sphingolipids, and glycerophospholipids, are essential for neurodevelopment. As mentioned above, my early structure activity studies demonstrated that BAC disinfectants inhibit cholesterol biosynthesis and alter the lipidome of neuronal cells. Therefore, the focus of my dissertation was to characterize the effects of BACs on neurodevelopment as a result of altered lipid homeostasis.

The overarching hypothesis was that **BACs modulate lipid homeostasis and impair neurodevelopment.** The specific aims for this dissertation were to: **(1) Characterize consequences of *in utero* BAC exposure on lipid homeostasis and neurodevelopment *in vivo,* and (2) elucidate the effects of BACs on neurodevelopment and investigate underlying mechanisms.**

In this dissertation, Chapter 2 describes the establishment of BACs as potent inhibitors of cholesterol biosynthesis in neuronal cell lines. Chapter 3 builds from the findings of Chapter 2 and the collaborative study with Dr. Kelly Hines (Hines et al., 2017), describing the effect of *in utero* BAC exposure on lipid homeostasis and the transcriptome of the developing brain. Chapter 4 describes the developmental neurotoxicity posed by BACs in a three-dimensional

in vitro model of neurodevelopment. Finally, Chapter 5 summarizes conclusions of these works and provides perspectives on future directions.

1.5. References

Adibhatla, R. M., & Hatcher, J. F. (2007). Role of Lipids in Brain Injury and Diseases. *Future Lipidology, 2*(4), 403–422. doi:10.2217/17460875.2.4.403

Bal-Price, A., and Meek, M. E. B. (2017). Adverse outcome pathways: Application to enhance mechanistic understanding of neurotoxicity. *Pharmacology and Therapeutics*, *179*, 84–95. https://doi.org/10.1016/j.pharmthera.2017.05.006

Bal-Price, A., Pistollato, F., Sachana, M., Bopp, S. K., Munn, S., and Worth, A. (2018). Strategies to improve the regulatory assessment of developmental neurotoxicity (DNT) using in vitro methods. *Toxicology and Applied Pharmacology*, *354*, 7–18. https://doi.org/10.1016/j.taap.2018.02.008

Bennett, D., Bellinger, D. C., Birnbaum, L. S., Bradman, A., Chen, A., Cory-Slechta, D. A., … Witherspoon, N. O. (2016). Project TENDR: Targeting environmental neuro-developmental risks. the TENDR consensus statement. *Environmental Health Perspectives*, *124*(7), A118–A122. https://doi.org/10.1289/EHP358

Betsholtz, C. (2015, June 26). Lipid transport and human brain development. *Nature Genetics*, Vol. 47, pp. 699–701. https://doi.org/10.1038/ng.3348

Boyle, C. A., Boulet, S., Schieve, L. A., Cohen, R. A., Blumberg, S. J., Yeargin-Allsopp, M., … Kogan, M. D. (2011). Trends in the prevalence of developmental disabilities in US children, 1997-2008. *Pediatrics*, *127*(6), 1034–1042. https://doi.org/10.1542/peds.2010-2989

BNOEMC (2015) Quaternary ammonium compounds in cleaning products: Health and safety information for health professionals. Bellevue/NYU Occupational & Environmental Medicine Clinic, Retrieved from: https://med.nyu.edu/pophealth/sites/default/files/pophealth/QACs%20Info%20for%20Physicians_18.pdf

Byrne, E. F. X., Sircar, R., Miller, P. S., Hedger, G., Luchetti, G., Nachtergaele, S., … Siebold, C. (2016). Structural basis of Smoothened regulation by its extracellular domains. *Nature*, *535*(7613), 517–522. https://doi.org/10.1038/nature18934

Chen, J., Costa, L. G., and Guizzetti, M. (2011a). Retinoic acid isomers up-regulate ATP binding cassette A1 and G1 and cholesterol efflux in rat astrocytes: Implications for their therapeutic and teratogenic effects. *Journal of Pharmacology and Experimental Therapeutics*, *338*(3), 870–878. https://doi.org/10.1124/jpet.111.182196

Chen, J., Costa, L. G., and Guizzetti, M. (2011b). Retinoic acid isomers up-regulate ATP binding cassette A1 and G1 and cholesterol efflux in rat astrocytes: Implications for their therapeutic and teratogenic effects. *Journal of Pharmacology and Experimental Therapeutics*, *338*(3), 870–878. https://doi.org/10.1124/jpet.111.182196

Cooper, M. K., Wassif, C. A., Krakowiak, P. A., Taipale, J., Gong, R., Kelley, R. I., … Beachy, P. A. (2003). A defective response to Hedgehog signaling in disorders of cholesterol biosynthesis. *Nature Genetics*, *33*(4), 508–513. https://doi.org/10.1038/ng1134

Coti Bertrand, P., O'Kusky, J. R., and Innis, S. M. (2006). Maternal Dietary (n-3) Fatty Acid Deficiency Alters Neurogenesis in the Embryonic Rat Brain. *The Journal of Nutrition*, *136*(6), 1570–1575. https://doi.org/10.1093/jn/136.6.1570

Fritsche, E., Crofton, K. M., Hernandez, A. F., Hougaard Bennekou, S., Leist, M., Bal-Price, A., … Gourmelon, A. (2017). OECD/EFSA workshop on developmental neurotoxicity (DNT): The use of non-animal test methods for regulatory purposes. *ALTEX*, *34*(2), 311–315. https://doi.org/10.14573/altex.1701171

Grandjean, P., and Landrigan, P. (2006, December 16). Developmental neurotoxicity of industrial chemicals. *Lancet*, Vol. 368, pp. 2167–2178. https://doi.org/10.1016/S0140-6736(06)69665-7

Grandjean, Philippe, Kishi, R., and Kogevinas, M. (2017, March 1). Prevention of Developmental Neurotoxicity. *Epidemiology*, Vol. 28, pp. 157–158. https://doi.org/10.1097/EDE.0000000000000601

Guizzetti, M., and Costa, L. G. (2007). Cholesterol homeostasis in the developing brain: a possible new target for ethanol. *Human and Experimental Toxicology*, *26*(4), 355–360. https://doi.org/10.1177/0960327107078412

Herron, J., Reese, R. C., Tallman, K. A., Narayanaswamy, R., Porter, N. A., and Xu, L. (2016). Identification of environmental quaternary ammonium compounds as direct inhibitors of cholesterol biosynthesis. *Toxicological Sciences*, *151*(2), 261–270. https://doi.org/10.1093/toxsci/kfw041

Hines, K. M., Herron, J., and Xu, L. (2017). Assessment of altered lipid homeostasis by HILIC-ion mobility-mass spectrometry-based lipidomics. *Journal of Lipid Research*, *58*(4), 809–819. https://doi.org/10.1194/jlr.D074724

Hirata, H., Tomita, K., Bessho, Y., and Kageyama, R. (2001). Hes1 and Hes3 regulate maintenance of the isthmic organizer and development of the mid/hindbrain. *EMBO Journal*, *20*(16), 4454–4466. https://doi.org/10.1093/emboj/20.16.4454

Hrubec, T. C., Melin, V. E., Shea, C. S., Ferguson, E. E., Garofola, C., Repine, C. M., … Hunt, P. A. (2017). Ambient and Dosed Exposure to Quaternary Ammonium Disinfectants Causes Neural Tube Defects in Rodents. *Birth Defects Research*, *109*(14), 1166–1178. https://doi.org/10.1002/bdr2.1064

Hussain, G., Wang, J., Rasul, A., Anwar, H., Imran, A., Qasim, M., … Sun, T. (2019, January 25). Role of cholesterol and sphingolipids in brain development and neurological diseases. *Lipids in Health and Disease*, Vol. 18. https://doi.org/10.1186/s12944-019-0965-z

Ishibashi, M., Ang, S. L., Shiota, K., Nakanishi, S., Kageyama, R., and Guillemot, F. (1995). Targeted disruption of mammalian hairy and Enhancer of split homolog-1 (HES-1) leads to up-regulation of neural helix-loop-helix factors, premature neurogenesis, and severe neural tube defects. *Genes and Development*, *9*(24), 3136–3148. https://doi.org/10.1101/gad.9.24.3136

Katakura, M., Hashimoto, M., Shahdat, H. M., Gamoh, S., Okui, T., Matsuzaki, K., and Shido, O. (2009). Docosahexaenoic acid promotes neuronal differentiation by regulating basic helix-loop-helix transcription factors and cell cycle in neural stem cells. *Neuroscience*, *160*(3), 651–660. https://doi.org/10.1016/j.neuroscience.2009.02.057

Kelley, R. I., and Herman, G. E. (2001). Inborn errors of sterol biosynthesis. *Annu Rev Genomics Hum Genet*, *2*, 299–341. Retrieved from

http://genom.annualreviews.org/cgi/content/full/2/1/299

Kim, M., Weigand, M. R., Oh, S., Hatt, J. K., Krishnan, R., Tezel, U., … Konstantinidis, K. T. (2018). Widely used benzalkonium chloride disinfectants can promote antibiotic resistance. *Applied and Environmental Microbiology*, *84*(17). https://doi.org/10.1128/AEM.01201-18

Kolf-Clauw, M., Chevy, F., Wolf, C., Siliart, B., Citadelle, D., and Roux, C. (1996). Inhibition of 7-dehydrocholesterol reductase by the teratogen AY9944: A rat model for Smith-Lemli-Opitz syndrome. *Teratology*, *54*(3), 115–125. https://doi.org/10.1002/(SICI)1096-9926(199609)54:3<115::AID-TERA1>3.0.CO;2-2

Komada, M., Saitsu, H., Kinboshi, M., Miura, T., Shiota, K., and Ishibashi, M. (2008). Hedgehog signaling is involved in development of the neocortex. *Development*, *135*(16), 2717–2727. https://doi.org/10.1242/dev.015891

Korade, Z., and Kenworthy, A. K. (2008). Lipid rafts, cholesterol, and the brain. *Neuropharmacology*, Vol. 55, pp. 1265–1273. https://doi.org/10.1016/j.neuropharm.2008.02.019

Korade, Z., Xu, L., Shelton, R., and Porter, N. A. (2010). Biological activities of 7-dehydrocholesterol-derived oxysterols: Implications for Smith-Lemli-Opitz syndrome. *Journal of Lipid Research*, *51*(11), 3259–3269. https://doi.org/10.1194/jlr.M009365

Koudinov, A. R., and Koudinova, N. V. (2001). Essential role for cholesterol in synaptic plasticity and neuronal degeneration. *The FASEB Journal : Official Publication of the Federation of American Societies for Experimental Biology*, *15*(10), 1858–1860.

Lauritzen, L., Brambilla, P., Mazzocchi, A., Harsløf, L. B. S., Ciappolino, V., and Agostoni, C. (2016, January 4). DHA effects in brain development and function. *Nutrients*, Vol. 8. https://doi.org/10.3390/nu8010006

Mauch, D. H., Nägier, K., Schumacher, S., Göritz, C., Müller, E. C., Otto, A., and Pfrieger, F. W. (2001). CNS synaptogenesis promoted by glia-derived cholesterol. *Science*, *294*(5545), 1354–1357. https://doi.org/10.1126/science.294.5545.1354

Meldrum, S., and Simmer, K. (2016). Docosahexaenoic acid and neurodevelopmental outcomes of term infants. *Annals of Nutrition and Metabolism*, *69*(1), 23–28. https://doi.org/10.1159/000448271

OECD. (2006). Test No. 426: Developmental Neurotoxicity Study. *OECD Guidelines for the Testing of Chemicals*, *1*(4), 1–26. https://doi.org/10.1787/9789264067394-en

Olsen, A. S. B., and Færgeman, N. J. (2017). Sphingolipids: Membrane microdomains in brain development, function and neurological diseases. *Open Biology*, Vol. 7. https://doi.org/10.1098/rsob.170069

Porter, F. D., and Herman, G. E. (2011, January). Malformation syndromes caused by disorders of cholesterol synthesis. *Journal of Lipid Research*, Vol. 52, pp. 6–34. https://doi.org/10.1194/jlr.R009548

Porter, J. A., Young, K. E., and Beachy, P. A. (1996). Cholesterol modification of hedgehog signaling proteins in animal development. *Science*, *274*(5285), 255–259. https://doi.org/10.1126/science.274.5285.255

Rice, D., and Barone Jr., S. (2000). Critical Periods of Vulnerability for the Developing Nervous System : Evidence from Humans and Animal Models Critical Periods of Vulnerabilityfor the Developing Nervous System : Evidence from Humans and Animal

Models Development of the Brain in Utero. *Environmental Health Perspectives*, *108*(January), 511–533. https://doi.org/10.1289/ehp.00108s3511

Rock, K. D., and Patisaul, H. B. (2018, March 1). Environmental Mechanisms of Neurodevelopmental Toxicity. *Current Environmental Health Reports*, Vol. 5, pp. 145–157. https://doi.org/10.1007/s40572-018-0185-0

Roux, C, Horvath, C., and Dupuis, R. (1979). Teratogenic action and embryo lethality of AY 9944R. Prevention by a hypercholesterolemia-provoking diet. *Teratology*, *19*(1), 35–38. https://doi.org/10.1002/tera.1420190106

Roux, Ch., Dupuis, R., Horvath, C., and Talbot, J.-N. (1980). Teratogenic Effect of an Inhibitor of Cholesterol Synthesis (AY 9944) in Rats: Correlation with Maternal Cholesterolemia. *The Journal of Nutrition*, *110*(11), 2310–2312. https://doi.org/10.1093/jn/110.11.2310

Ryu, O., Park, B. K., Bang, M., Cho, K. S., Lee, S. H., Gonzales, E. L. T., … Kwon, K. J. (2018). Effects of several cosmetic preservatives on ros-dependenapoptosis of rat neural progenitor cells. *Biomolecules and Therapeutics*, *26*(6), 608–615. https://doi.org/10.4062/biomolther.2017.221

Saher, G., Brügger, B., Lappe-Siefke, C., Möbius, W., Tozawa, R. I., Wehr, M. C., … Nave, K. A. (2005). High cholesterol level is essential for myelin membrane growth. *Nature Neuroscience*, *8*(4), 468–475. https://doi.org/10.1038/nn1426

Smirnova, L., Hogberg, H. T., Leist, M., and Hartung, T. (2014). Developmental neurotoxicity - challenges in the 21st century and in vitro opportunities. *ALTEX*, *31*(2), 129–156. https://doi.org/10.14573/altex.1403271

Tandukar, M., Oh, S., Tezel, U., Konstantinidis, K. T., and Pavlostathis, S. G. (2013). Long-term exposure to benzalkonium chloride disinfectants results in change of microbial community structure and increased antimicrobial resistance. *Environmental Science and Technology*, *47*(17), 9730–9738. https://doi.org/10.1021/es401507k

Tierney, E., Bukelis, I., Thompson, R. E., Ahmed, K., Aneja, A., Kratz, L., and Kelley, R. I. (2006). Abnormalities of cholesterol metabolism in autism spectrum disorders. *American Journal of Medical Genetics, Part B: Neuropsychiatric Genetics*, *141*(6), 666–668. https://doi.org/10.1002/ajmg.b.30368

US EPA. (1998). Health effects guidelines OPPTS 870.6300 Developmental Neurotoxicity Study, EPA/ 712/c-98/239.Office of Prevention Pesticides and Toxic Substances.

Woollett, L. A. (2011). Review: Transport of maternal cholesterol to the fetal circulation. *Placenta*, *32*(SUPPL. 2). https://doi.org/10.1016/j.placenta.2011.01.011

Zhang, J., and Liu, Q. (2015). Cholesterol metabolism and homeostasis in the brain. *Protein and Cell*, *6*(4), 254–264. https://doi.org/10.1007/s13238-014-0131-3

Zhang, Y., Bulkley, D. P., Xin, Y., Roberts, K. J., Asarnow, D. E., Sharma, A., … Beachy, P. A. (2018). Structural Basis for Cholesterol Transport-like Activity of the Hedgehog Receptor Patched. *Cell*, *175*(5), 1352-1364.e14. https://doi.org/10.1016/j.cell.2018.10.026

Zhong, W., Jiang, M. M., Schonemann, M. D., Meneses, J. J., Pedersen, R. A., Jan, L. Y., and Jan, Y. N. (2000). Mouse numb is an essential gene involved in cortical neurogenesis. *Proceedings of the National Academy of Sciences of the United States of America*, *97*(12), 6844–6849. https://doi.org/10.1073/pnas.97.12.6844

Zhou, C., Chen, J., Zhang, X., Costa, L. G., and Guizzetti, M. (2014). Prenatal ethanol exposure up-regulates the cholesterol transporters ATP-binding cassette A1 and G1 and reduces cholesterol levels in the developing rat brain. *Alcohol and Alcoholism*, *49*(6), 626–634. https://doi.org/10.1093/alcalc/agu049

Chapter 2: Identification of Environmental Quaternary Ammonium Compounds as Direct Inhibitors of Cholesterol Biosynthesis

2.1. Introduction

Cholesterol plays important roles in embryonic development (Porter et al., 1996), synapse formation and function (Koudinov and Koudinova, 2001; Mauch et al., 2001), and myelination (Saher et al., 2005). Almost all cholesterol in the brain is synthesized locally and independently (Bjorkhem and Meaney, 2004). The Xu Lab has been interested in the cholesterol biosynthesis disorder, Smith-Lemli-Opitz syndrome (SLOS), which is caused by defective 3β-hydroxysterol-Δ^7-reductase (DHCR7) (Fitzky et al., 1998; Wassif et al., 1998; Waterham et al., 1998). This defect leads to greatly elevated levels of cholesterol precursors, including 7-dehydrocholesterol (7-DHC) and 8-dehydrocholesterol (8-DHC), and decreased levels of cholesterol (Tint et al., 1994; Tint et al., 1995) (**Figure 2.1A**). The formation of 8-DHC is due to the activity of 3β-hydroxysterol-Δ^8,Δ^7-isomerase (EBP). The SLOS phenotype includes multiple congenital malformations, developmental delay, cognitive impairment, and behavior problems (Bukelis et al., 2007; Nowaczyk and Irons, 2012; Porter and Herman, 2011; Sikora et al., 2006). Previous work reported that 7-DHC and 8-DHC are exceptionally prone to peroxidation and their oxidation products, *i.e.*, oxysterols, contribute to the pathophysiology of SLOS (Korade et al., 2010, 2013, and 2014; Xu et al., 2012 and 2013).

Interestingly, some small molecules, such as AY9944 (a known teratogenic agent) and BM15.766, can potently inhibit DHCR7, leading to the same biochemical defect as seen in SLOS, *i.e.*, increased levels of 7-DHC and decreased levels of cholesterol. Because of this, AY9944 and BM15.766 have been used to create a pharmacological animal model of SLOS (Fliesler et al., 2004; Kolf-Clauw et al., 1996 and 1997; Xu et al., 1995). Many other small molecules have been reported to affect different steps of cholesterol biosynthesis. For example, antipsychotic drugs such as haloperidol, ziprasidone, risperidone, aripiprazole, and

trazodone were found to inhibit DHCR7 *in vitro* (Canfran-Duque, 2013) and in patients treated with these medications (Hall, 2013); a breast cancer drug, tamoxifen, and an infertility drug, clomifene, were found to inhibit EBP (Moebius, 1998).

Much work has been done by the US EPA to screen environmental molecules for their biological activities, such as their effect on key transcription regulators (Martin et al., 2010), various receptor signaling pathways (Sipes et al., 2013), and zebrafish development (Padilla et al., 2012). However, none of the previous reports addressed the effect of environmental agents on cholesterol biosynthesis, which is important to development as discussed above. Thus, we aim to identify environmental molecules and drugs that display similar structures to DHCR7 inhibitors and that can inhibit cholesterol biosynthesis, potentially leading to the same biochemical defect as observed in SLOS.

In this study, we rely on the Distributed Structure-Searchable Toxicity (DSSTox) Database Network (Kavlock and Dix, 2010; Richard and Williams, 2002) to carry out an initial *in silico* screening to identify structures similar to AY9944, one of the most potent inhibitors of DHCR7 known to date. The reason to choose AY9944 over BM15.766 as a model inhibitor here is because AY9944 displays almost 100 times higher potency than BM15.766 (Moebius et al., 1998). The DSSTox was built by EPA's National Center for Computational Toxicology in order to facilitate structure-activity studies and enable predictive toxicology. One feature of DSSTox is that it can calculate the similarity score (Tanimoto similarity coefficient) (Schneider, 2000) of the molecules in the database (over 10,000 so far) to a given chemical structure and rank these structures based on their similarity.

In this chapter, the following findings are reported: 1) identification of benzalkonium chlorides (BACs) as a class of compounds that are highly similar structurally to AY9944 and BAC can inhibit the Dhcr7 in both mouse and human neuroblastoma cell lines; 2) structure-activity studies suggest that the potency of BACs as Dhcr7 inhibitors decrease with the length

of the hydrocarbon chain: C10 > C12 >> C14 > C16; 3) cholesterol biosynthesis-related genes were upregulated and a cholesterol efflux gene was downregulated in the cells upon exposure to BACs; and 4) 7-DHC-derived oxysterols were observed in cells exposed to BACs.

2.2. Results

In silico screening of environmental and pharmaceutical small molecules for potential DHCR7 inhibitors using DSSTox and identification of BACs as DHCR7 inhibitors in cells

Using the DSSTox Database Network as described above, we found that there are six classes of molecules that show > 45% of structural similarity to AY9944 (**Figure 2.1B**), including the antiseptic benzalkonium chloride compounds (BACs), the recreational drug phencyclidine (PCP), the anesthetic drug ketamine, mucus expectorant bromhexine, and the industrial chemical benzyltriethylammonium chloride (BTEC). Among them, BAC displays the highest similarity to AY9944 at 72.9%.

Neuro2a cells, a mouse neuroblastoma cell line, were chosen to test the effect of each compound or compound mixture (BAC) on cholesterol biosynthesis because these cells express high levels of Dhcr7 and *Dhcr7*-knockdown Neuro2a cells have been demonstrated to be a useful model for studying SLOS (Korade et al., 2009; Korade et al., 2010; Xu et al., 2011a). Briefly, Neuro2a cells were exposed to each compound at 100 nM, lipids were extracted, and sterols were analyzed by GC-MS. We found that BAC is indeed a potent inhibitor of Dhcr7, leading to significant accumulation of 7-DHC and 7-dehydrodesmosterol (7-DHD) at 100 nM (**Figure 2.1C** and **Figure S.1A**). Importantly, BAC as a mixture is only slightly less potent than the positive control, AY9944. We note that in control Neuro2a cells, the baseline levels of desmosterol is high, possible due to intrinsic low expression or activity of 3β-hydroxysterol-Δ^{24}-reductase (Dhcr24). As a result of this, the level of 7-DHD also increased when Dhcr7 was inhibited (**Figure S.1A**). In a subsequent experiment, we found

that BAC mix can inhibit Dhcr7 even at 1 nM, as indicated by the formation of 7-dehydrodesmosterol (**Figure S.1B**).

We then carried out similar experiments using a human neuroblastoma cell line, SK-N-SH. We found that the BAC mixture can also inhibit DHCR7 effectively at 100 nM (**Figure 2.1D**). Interestingly, bromhexine displayed high potency in inhibiting DHCR7, a drastic increase from its potency in Neuro2a cells, which suggests that there may be some structural differences in the human DHCR7 enzyme from its mouse equivalent. We also note that BAC mixture did not affect the level 8-DHC as much as AY9944 did.

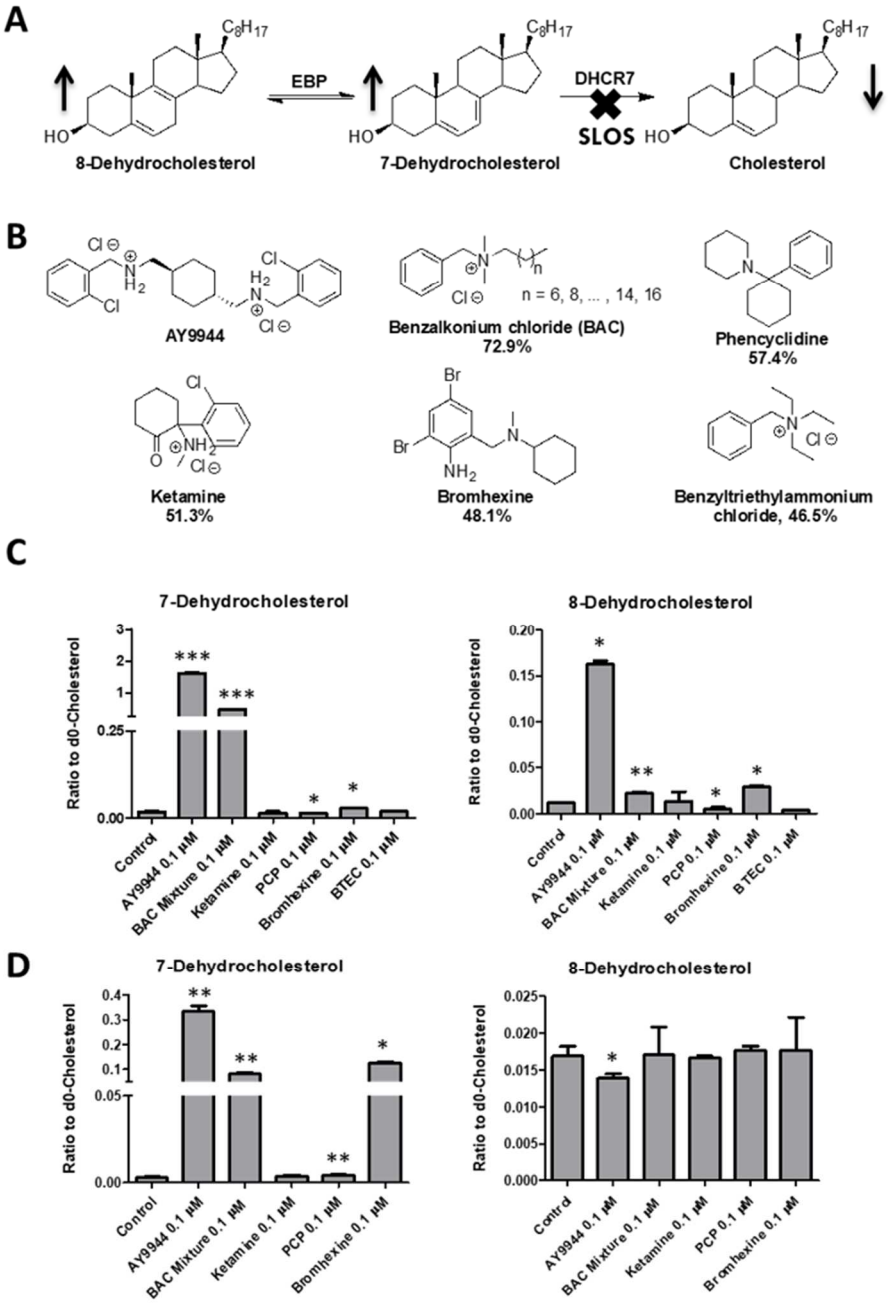

Figure 2.1. (A) The enzymatic step, DHCR7, affected in Smith-Lemli-Opitz syndrome; (B) Structures of the known cholesterol biosynthesis inhibitor and similar environmental agents (similarity score to AY9944 obtained from DSSTox are shown underneath each structure); (C) Effect of the compounds similar to AY9944 on cholesterol biosynthesis in Neuro2a cells and (D) in human SK-N-SH cells after incubation in lipid-free medium for 48 hrs, shown as the ratios of the cholesterol precursors to cholesterol. *, $p < 0.05$; **, $p < 0.005$; ***, $p < 0.0005$; $n = 3$; all statistical analyses are relative to Control using Student's *t*-test.

Structure-activity studies of individual BACs as inhibitors of Dhcr7

BACs are a class of quaternary ammonium compounds (QACs) that differ by the length of the alkyl side-chain. In this study, we chose the most common components of BACs, *i.e.*, those with an alkyl chain of C10, C12, C14 or C16. We first examined the cytotoxicity of individual BACs on the Neuro2a cells using MTS assay after 24 or 48 hrs of treatment. Cell viability results after 48 hrs are shown in **Figure 2.2A**, which suggests that BAC-C16 is the most toxic component, followed by C14, C12 and C10, with IC50 values of 0.5 μM, 2.5 μM, 5 μM, and >10 μM, respectively. A similar trend in cytotoxicity was observed after 24 hr of treatment as shown in **Figure S.2**. The SK-N-SH cells displayed similar vulnerability to BAC using the same cytotoxicity test (**Figure 2.2B**).

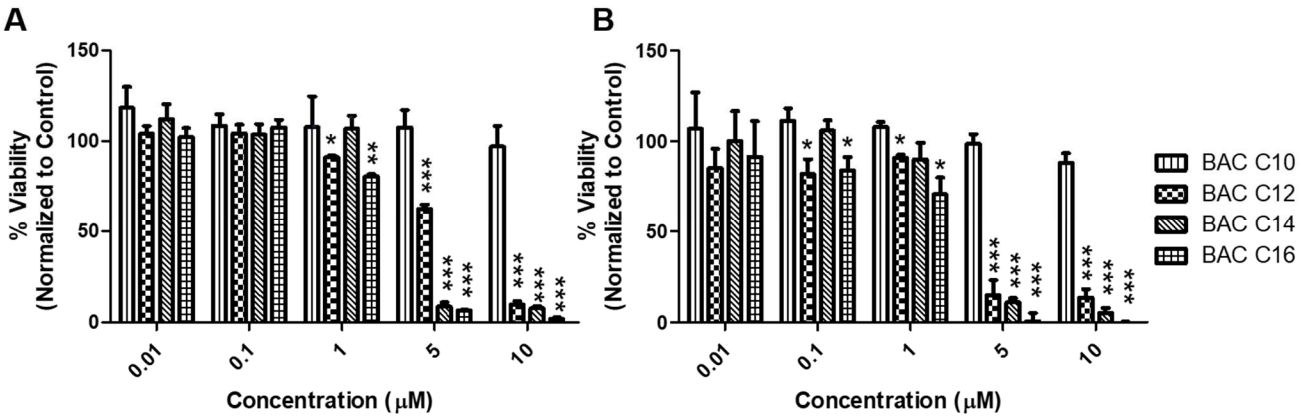

Figure 2.2. Cytotoxicity of individual BACs on (A) Neuro2a cells and (B)SK-N-SH cells after 48 hrs of treatment. *, $p < 0.05$; **, $p < 0.005$; ***, $p < 0.0005$; n = 3; all statistical analyses are relative to Control using Student's *t*-test.

As the main mechanism of action of BACs against microbes is through disruption of the lipid membrane (Gilbert and Moore, 2005; McDonnell and Russell, 1999), quantification of the incorporation of individual BACs to the cells would reflect such action. Thus, we developed a fast and sensitive analytical method using isotope-dilution UPLC-MS/MS. Deuterated (d_7)-standards of BAC-C10, C12, C14, and C16 were synthesized following known chemistry (see Materials and Methods). After testing two different UPLC columns (reverse

phase C8 and C18), we established an UPLC-MS/MS method that allows complete analysis of all four BACs within three minutes (**Figure S.3**). After incubating the Neuro2a cells in the presence of individual BAC, BAC was extracted by Folch solution in the presence of the deuterated standards and was analyzed by UPLC-MS/MS.

As shown in the **Figure 2.3A**, the incorporation levels increase with the chain length of the BAC (C10 << C12 < C14 < C16), which appears to reflect their cLogP values of 2.1, 3.2, 4.2 and 5.3, respectively. Accordingly, the levels of individual BACs in the corresponding media decrease with the chain length (**Figure 2.3B**). Thus, the cytotoxicity of each BAC is consistent with its level of incorporation into the cells. To examine whether membrane-breakage contributed to the cytotoxicity, we carried out cell permeability test using a membrane integrity assay based on the release of lactate dehydrogenaseand found that no BAC led to cell leakage at 1 μM or lower (**Figure 2.4**), which suggests that at 100 nM, the effect of BAC was not caused by the breakage of the cell membrane.

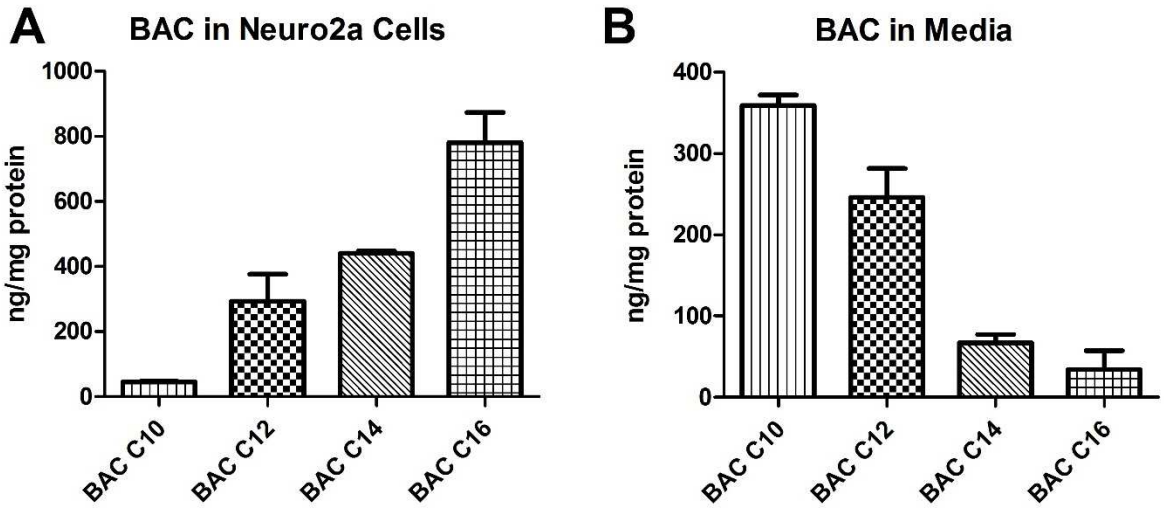

Figure 2.3. Levels of BACs (A) incorporated into Neuro2a cells and (B) in the media after being exposed to the respective compounds at 100 nM for 48 hrs. BACs were analyzed by UPLC-MS/MS as described in Materials and Methods. Experiment conducted by co-author Rohini Narayanaswamy.

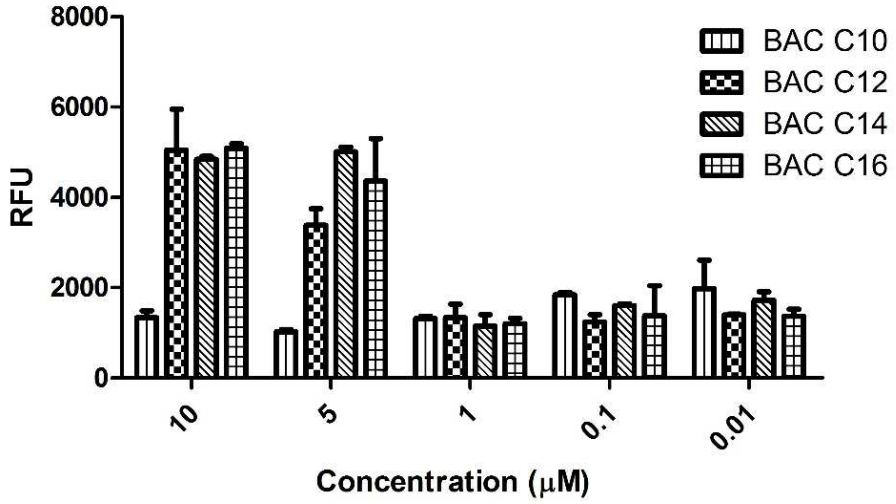

Figure 2.4. Cell membrane permeability test using CytoTox-ONE™ Homogeneous Membrane Integrity Assay (which measures the release of lactate dehydrogenase) indicates that no BAC leads to membrane leakage at 1 μM or lower, while BAC-C12, C14 and C16 led to membrane leakage at 5 and 10 μM. BAC-C10 did not lead to leakage at any concentration. Higher fluorescence intensity indicates more leakage.

To understand the structural features of BACs that are responsible for their potency as Dhcr7 inhibitor, Neuro2a cells were exposed to individual BACs at the non-cytotoxic concentration (100 nM), and the sterol profiles were analyzed by GC-MS (**Figure 2.5**). We found that both BAC-C10 and BAC-C12 inhibit Dhcr7 potently, leading to much elevated levels of 7-DHC and 7-DHD, while C14 and C16 are not very good inhibitors, suggesting that the proper length of the side chain plays a critical role for binding to the active site of Dhcr7. This result suggests that BAC-C10 is a much more potent inhibitor of Dhcr7 than it appears to be as it was incorporated at a much lower level than other BACs (**Figure 2.3**). We also observed that BAC-C10 and C12 are also inhibitors of EBP as indicated by the formation of zymosterol and zymostenol, although at much lower potency. Interestingly, although BAC-C14 and C16 did not inhibit any steps of the cholesterol biosynthesis examined here, they both led to significantly lower levels of desmosterol while they did not affect the total levels of cholesterol (**Figure 2.5I**).

To confirm the effect of BACs on the total cholesterol homeostasis, gene expression analysis was carried out on related genes by qPCR, including *Srebf2*, *Hmgcr*, *Ebp*, and *Dhcr7*. We found that all BACs led to significant upregulation of the genes that are related to cholesterol biosynthesis (**Figure 2.6A**) and downregulation of *Abca1*, the gene that is responsible for cholesterol efflux (**Figure 2.6B**). All these observed gene expression changes suggest feedback response to the inhibition of the cholesterol biosynthesis by BAC. It is worth noting that although BAC-C14 and C16 did not show high potency in inhibiting cholesterol biosynthesis, they behaved similarly to C10 and C12 on the regulation of the cholesterol homeostasis-related genes. This observation suggests that BAC-C14 and C16 could interact with other proteins that regulate cholesterol biosynthesis and remain to be identified. The decreased levels of desmosterol in response to BAC-C14 and C16 treatment (without any precursors being accumulated) also provided support to this notion.

7-DHC-derived oxysterols are formed in BAC-treated cells

Because of the high reactivity of 7-DHC toward free radical peroxidation (Xu et al., 2009; 2010), one would expect the formation of 7-DHC-derived oxysterols in BAC-treated cells. Thus, lipids were extracted from the cells that were treated with individual BAC for two days, and the 7-DHC oxysterol biomarker, 3β,5α-dihydroxycholest-7-en-6-one (DHCEO) (Xu et al., 2011a), was analyzed by normal phase HPLC-MS/MS (Xu et al., 2011a, 2011b, and 2013). We found that DHCEO was indeed formed in cells that were treated with AY9944, BAC-C10, or BAC-C12, but not with BAC-C14 and BAC-C16, which is consistent with the profile of the cholesterol precursors under these conditions (**Figure 2.7A**). The levels of DHCEO are proportional to the levels of 7-DHC as shown in **Figure 2.7B**.

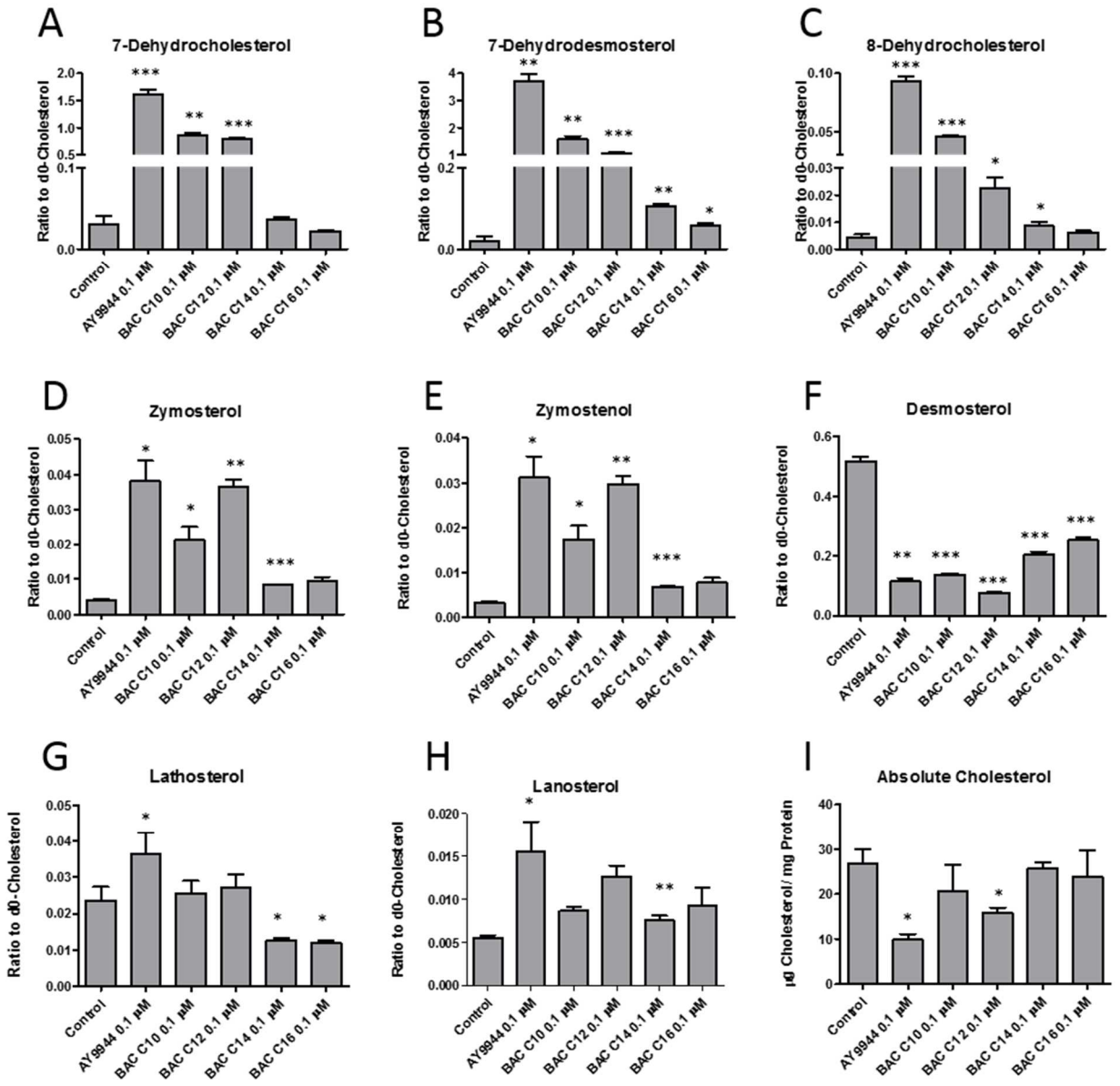

Figure 2.5. Structure-activity studies on the effect of individual BACs on the cholesterol biosynthesis. The Neuro2a cells were exposed to individual BACs at 100 nM in lipid-free medium for 48 hrs and the levels of cholesterol and its precursors were analyzed by GC-MS as described in the Materials and Methods. *, $p < 0.05$; **, $p < 0.005$; ***, $p < 0.0005$; $n = 3$; all statistical analyses are relative to Control using Student's *t*-test.

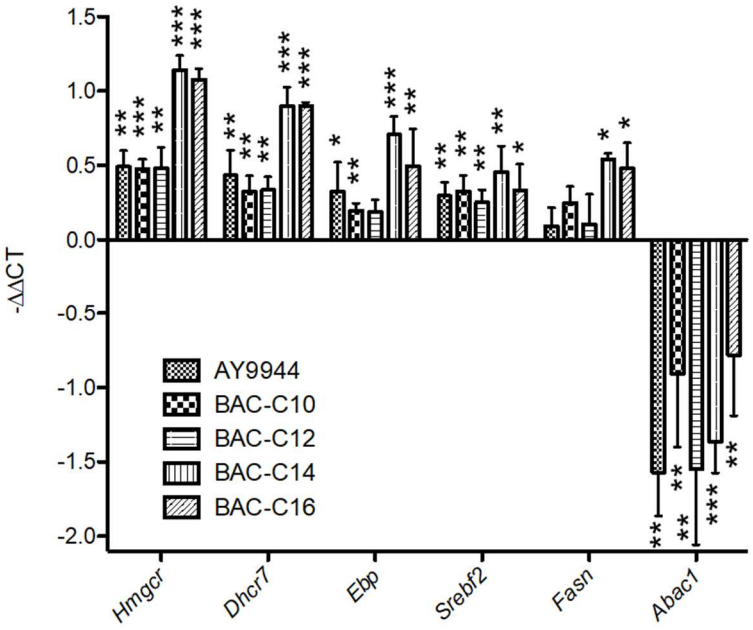

Figure 2.6. Effect of individual BACs on expression of the genes related to cholesterol biosynthesis and cholesterol efflux as analyzed by qPCR in Neuro2a cells after treatment of each compound at 100 nM for 20 hrs. The expression level of each gene was normalized to *Actin*. *, P < 0.05; **, p < 0.005; ***, p < 0.0005; four biological replicates for each group and four technical replicates for each sample were used; all statistical analyses are relative to Control using Student's *t*-test.

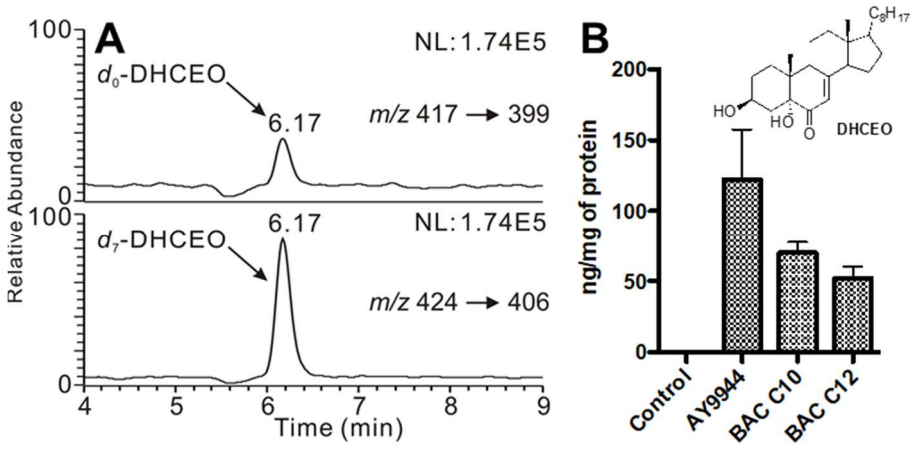

Figure 2.7. Normal phase HPLC-MS/MS analysis (A) and quantitation (B) of DHCEO using d_7-DHCEO as the internal standard in Neuro2a cells treated with different compounds at 100 nM for two days.

2.3. Discussion

Environmental factors have been implicated in neurodevelopmental and neurodegenerative diseases, such as autism, Parkinson's disease, and Alzheimer's disease (Hallmayer et al., 2011; Kanthasamy et al., 2012; Landrigan et al., 2005). Cholesterol biosynthesis disorders are characterized by defects in embryonic and neural development (Porter and Herman, 2011). Thus, it seems to be plausible that inhibition of cholesterol biosynthesis by non-genetic factors, such as small molecules in the environment or prescriptions, could also contribute to such developmental disorders.

In this study, the DSSTox Database Network allowed us to carry out initial structural screening of environmental molecules and drugs based on their similarity to AY9944, which led to the identification of BACs as a class of molecules that inhibit Dhcr7, the enzyme that was affected in the cholesterol biosynthesis disorder, SLOS. Structure-activity relationship (SAR) studies allowed us to identify BAC-C10 and C12 to be the active components that are responsible for the inhibition of Dhcr7 while also serving as a less potent inhibitor of Ebp. On the other hand, although BAC-C14 and C16 did not lead to accumulation of sterol precursors, they both lowered the levels of desmosterol, a major sterol in Neuro2a cells (approximately 50% of the levels of cholesterol in control Neuro2a cells), suggesting that they likely inhibit the cholesterol biosynthesis at an earlier step. More broad scale lipidomic analysis could reveal the particular steps that were affected by BAC-C14 and C16. The observed upregulation of cholesterol biosynthesis-related genes suggests that BACs act as direct inhibitors of the enzymes involved in the biosynthesis. This SAR study suggests that the benzyl group, dimethyl, and proper length of the side chain are critical for binding to the active site of Dhcr7. Interestingly, a recently reported potent inhibitor of Dhcr7 also displays the benzyl dialkyl amine moiety (Horling et al., 2012), which seems to be consistent with our findings. We note that this new inhibitor is only about 2 times more potent than AY9944 based on their

comparison with BM15.766 (no direct comparison with AY9944 was done in this study) (Horling et al., 2012; Moebius et al., 1998). Similarity between BAC/AY9944 and BM15.766 appears to be much smaller.

Significantly, even at non-cytotoxic concentrations, BACs can potently inhibit Dhcr7. This suggests that exposure of BACs could have severe consequences even when there is no apparent acute toxicity. It has been reported that orally administered BAC can cross the blood-brain barrier in rats (a 1.2 μg/g concentration in serum leads to 0.2 μg/g in brain) (Xue et al., 2002; 2004), which suggests that BAC could post threat to the central nervous system. On the other hand, vaginal treatment of pregnant rats with BAC led to fetal death, reduced litter size, and birth defects (Buttar, 1985). A recent study by Hrubec, Hunt, and coworkers demonstrated that chronic consumption of QAC-containing food (including BAC) led to significantly decreased fertility and fecundity in mice, as well increased mortality of the dam (Melin et al., 2014). The latter report suggests that BAC may penetrate the blood-placenta barrier. The inhibition of cholesterol biosynthesis by BACs could contribute to some of the deleterious effects on embryonic development.

The observation of a 7-DHC-derived oxysterol, DHCEO, in BAC-C10 and C12-treated cells further confirmed that these cells resemble the biochemical features of SLOS cells and tissues. DHCEO was established as a biomarker of the oxidation of 7-DHC and was observed at the highest level (3.5 μM) among all oxysterols in the brain of a *Dhcr7*-KO mouse (Xu et al., 2011a). Importantly, DHCEO exerts a variety of biological activities, such as affecting expression of the genes related to cholesterol biosynthesis (Korade et al., 2010) and cell growth and inducing differentiation and arborization of neuronal cells (Xu et al., 2012). Thus, 7-DHC-derived oxysterols could be a major contributor to the biological consequences of exposure to BACs.

Quaternary ammonium compounds (QAC), including BACs, have been used as antimicrobials for more than 50 years (Gilbert and Moore, 2005), exerting their effect on microbes mainly through the disruption of the negatively charged lipid membrane mediated by its positively charged head group (Gilbert and Moore, 2005; McDonnell and Russell, 1999). QACs are widely used in cleaning products (such as Lysol and Clorox solutions, wipes, and hand sanitizers), medical products (such as eye and nasal drops), and the food processing industries (Gilbert and Moore, 2005; Holah et al., 2002; McDonnell and Russell, 1999; Ratani et al., 2012). High levels of QAC have been found in grapefruit seed extracts (Takeoka et al., 2005), food additives (Kröckel et al., 2003), fruits (The Federal Institute for Risk Assessment (BfR) of Germany, 2012a; The Federal Institute for Risk Assessment (BfR) of Germany, 2012b), and processed food such as milk and other dairy products (The Federal Institute for Risk Assessment (BfR) of Germany, 2012a; The Federal Institute for Risk Assessment (BfR) of Germany, 2012b). Thus, the sources of exposure of BACs to human beings are diverse and the levels are potentially high. These reports, combined with the high potency of BACs as cholesterol inhibitor (nM in Neuro2a cells and SK-N-SH cells), suggest that BACs could be a legitimate threat to human health.

A number of deleterious effects of the usage of QAC have been reported. For example, long-term use of BAC-preserved eye and nasal drops can cause ocular and corneal surface diseases (Baudouin et al., 2010; De Saint Jean et al., 1999; Leung et al., 2008; Pisella et al., 2002), and aggravate rhinitis medicamentosa (Graf, 2001), respectively. Evidence also suggests that BAC exposure can lead to occupational asthma (Burge and Richardson, 1994; Purohit et al., 2000). More importantly, BAC was found to be toxic to peripheral neurons when applied at μM concentrations directly to the serosa of an exteriorized portion of intestine from anesthetized rats and in cultures of mouse ganglion cells (Herman and Bass, 1989; Sarkar et al., 2012). Significantly, BACs (Roccal in the study) stopped the development of over 50% of

the clam eggs and completely killed the larvae even at 0.2 ppm (equivalent to approximately 500 nM when calculating using the molecular weight of BAC-C16) (Davis and Hidu, 1969). The inhibition effect of BACs on cholesterol biosynthesis could provide an alternative or additional mechanism for these observed toxicities.

In summary, a combination of *in silico* screening and *in vitro* tests led to the discovery of a class of common antiseptic compounds, BACs, being potent inhibitors of the last step of cholesterol biosynthesis, Dhcr7. This finding suggests that exposure to these compounds at critical developmental stages could contribute to the pathogenesis of developmental disorders. An epidemiological study may be warranted in order to systematically assess the risk of exposure to BACs.

2.4. Materials and Methods

Materials

HPLC grade solvents (hexanes, 2-propanol, methanol and water) were purchased from Thermo Fisher Scientific Inc. [25,26,26,26,27,27,27-d_7]-7-DHC and d_7-DHCEO were prepared as reported previously (Xu et al., 2011a; 2011b). Non-deuterated BAC mixture, individual BACs (C10, C12, C14 and C16), ketamine, phencyclidine, bromhexine, benzyltriethylammonium chloride, dimethylalkyl amines with different lengths of alkyl chains and d_7-benzyl chloride were purchased from Sigma-Aldrich Co. d_7-BACs were synthesized as described below. All sterol standards were purchased from Avanti Polar Lipids unless otherwise noted.

Cell cultures and treatment with different compounds

Mouse Neuro2a and human SK-N-SH neuroblastoma cell lines were purchased from the American Type Culture Collection (Rockville, MD). Both cell lines were maintained in DMEM supplemented with L-glutamine, 10% fetal bovine serum (FBS; Thermo Scientific HyClone,

Logan, UT), and penicillin/streptomycin at 37 ºC and 5% CO_2. For treatment of Neuro2a cells with different chemicals, the cells were plated in 100mm plates at the density of 1.0 x 10^6 cells/plate and left to adhere overnight. The following day, the media was replaced with DMEM high glucose media without serum, but with the addition of N2-supplement, L-glutamine and penicillin/streptomycin, and with or without the chemicals at the concentrations specified in the main text (stock solutions of the chemicals were made in DMSO at 1000x concentrations). 0.1% DMSO was used as the vehicle control and AY9944, a known Dhcr7 inhibitor, was used as the positive control. The SK-N-SH cells were maintained and treated the same way as the Neuro2a cells.

Lipid extraction, analysis of sterols by GC-MS, and analysis of oxysterol by HPLC-MS/MS

Cell pellets were lysed using 150 µL of lysis buffer (120 mM NaCl, 50 mM Hepes, 1% IGEPAL, 1% saturated PMSF) and the protein weight measured with the BioRad-DC protein Assay Kit. Before lipid extraction, internal standards, d_7-cholesterol and $^{13}C_3$-lanosterol (1 µg of each) were added to each sample. To extract the lipids, 1 mL of NaCl aqueous solution (0.9%) and 4mL of Folch solution (chloroform:methanol = 2:1, containing 1mM BHT and 1 mM PPh_3) was added to the cell lysates. The mixture was briefly vortexed and centrifuged for 5 min. The lower organic phase was taken and dried under nitrogen. The samples were re-dissolved in 300 µL of methylene chloride and 150 µL of the sample was transferred to a GC vial and then blown dry by nitrogen or argon. 20 µL of acetonitrile and 40 µL of BSTFA were added to each sample before being analyzed by GC-MS.

GC-MS analysis was performed on a Shimadzu QP2010 instrument with a DB-5 column, electron ionization and a single-quadrupole mass analyzer. The injector temperature is 280 °C. The column temperature program starts at 220 °C, then increases to 275 °C at 15 °C/min, then to 280 °C at 1 °C/min and maintain for 2 min, then increases to 315 °C at 15 °C/min and maintain for 2.5 min. The interface temperature is 270 °C and the MS operates

at 70 eV. The *m/z* values for monitoring cholesterol, d_7-cholesterol, lanosterol, $^{13}C_3$-lanosterol, 7-dehydrocholesterol, 8-dehydrocholesterol, 7-dehydrodesmosterol, desmosterol, lathosterol, zymostenol and zymosterol are 329, 336, 393, 396, 325, 325, 349, 343, 458, 458, and 456, respectively. The levels of cholesterol and lanosterol were calculated based on their isotope-labeled internal standards. The levels of other sterols were calculated based on their relative response to the internal standard d_7-cholesterol. A typical chromatogram for the analysis of the sterol standards by this method is included in the supporting information (**Figure S.4** in supporting information documentation).

Oxysterols were analyzed by normal phase HPLC-MS/MS as described previously (Xu et al., 2011a and 2013). Endogenous DHCEO (*m/z* 399 → *m/z* 381) were quantified by comparing its relative response to the d_7-DHCEO (*m/z* 406 → *m/z* 388) internal standard. HPLC column and conditions: Phenomenex Luna 4.6 × 150 mm Si column; 3 μm particle size; 1.0 mL/min; elution solvent: 10% 2-propanol in hexanes.

Analysis of BACs by LC-MS/MS

Prior to extraction, a known amount of deuterated internal standards (d_7-BAC-C10, d_7-BAC-C12, d_7-BAC-C14 and d_7-BAC-C16) were added to each cell lysate sample. The extraction was performed the same as described above. The dried extracts were re-dissolved in Water (0.1% formic acid)/ [Acetonitrile/2-propanol (0.1% formic acid) (50/50)] (30/70). The samples were stored at -80^{0}C until analysis using HPLC- Electrospray Ionization (ESI)-MS/MS. LC separations were performed on a Waters Acquity UPLC system equipped with autosampler (Waters, Milford, MA). HPLC conditions: Phenomenex Kinetex C18, 100A (100 x 2.1 mm) column; 1.7 μm particle size; mobile phase solvent: Water (0.1% formic acid)/[Acetonitrile/2-propanol (0.1% formic acid) (50/50)] (30/70); isocratic solvent at 0.200 ml/min flow rate; 10 μL injection volume. MS detections were done using a ThermoFinnigan TSQ tandem mass spectrometer (ThermoFisher, Waltham, MA) and data was acquired using

Finnigan Xcalibur software package. MS condition: spray voltage, 3200 V; sheath gas pressure, 8 psi; sweep gas pressure, 0 psi; aux gas pressure, 3 psi; capillary temperature, 205.68 °C; tube lens, 103.61 V; skimmer offset, 14 V; collision pressure, 1.5 mTorr; collision energy, 14 V.

Cell viability and membrane integrity assay

To determine the toxicity of each component of BAC, cell viability studies were performed on Neuro2A cells at 2 different time points (24 hours and 48 hours). Neuro2a cells were plated in 96 well plates at the density of 5,000 cells/well and left in the incubator to adhere overnight. The following day, the media was replaced with 200 µL of DMEM high glucose media without serum with the addition of N2-supplement, L-glutamine and penicillin/streptomycin and BAC at various concentrations in DMSO. DMSO levels were kept below 0.1% and the final concentration levels of BAC were: 10 µM, 5µ M, 1 µM, 100 nM, 10 nM. 0.1% DMSO was used as a vehicle control. The Neuro2a cells were kept in culture for 24 hours and 48 hours in the presence of BAC. The CellTiter-Glo Luminescent Cell Viability Assay (Promega, cat #G7570) was performed to determine the cell viability as described previously (Xu et al., 2010). In parallel, CytoTox-ONE™ Homogeneous Membrane Integrity Assay (Promega, cat # G7890) based on the releasing of lactate dehydrogenase was performed to examine the cell membrane integrity. Statistical significance was determined via Student's t-test (Excel).

Gene expression studies

Neuro2a cells were plated in 6 well plates at the density of 0.1 x 10^6 cells/well and left in the incubator to adhere to the plate overnight. The following day, the media was replaced with DMEM high glucose media without serum and the addition of N2-supplement, L-glutamine and penicillin/streptomycin with or without chemicals. Total RNA was isolated from the cells using the RNeasy Mini Kit (Qiagen, catalog #74104). The concentration of total RNA

was measured on a Nanodrop instrument. RNA (200 ng) from each sample was reverse transcribed to cDNA using a reverse transcriptase PCR kit (Life Technologies, catalog #4368814). Quantitative PCR (qPCR) was performed with an Applied Biosystems 7300 Machine. A 2X mastermix was prepared (Rox dye, 2x SYBR green, 100μM dNTPs, 25mM MgCl2, and 10x buffer) and each reaction contained the 2X mastermix, gene-specific primers, Taq polymerase and cDNA (from 2ng of RNA). The primers were designed using the primer software on <http://frodo.wi.mit.edu/>. The primers were designed to yield 90-110 bp PCR amplicons and were 20-22 bp long. Primers for *Srebf2* and *Fasn* were as reported (Yang et al., 2001). The primers used are shown in **Table 2.1**. All samples were run in quadruplicate. Significance was determined by Student's t-test (Microsoft Excel).

Table 2.1. Primers for qPCR studies in Neuro2a cells.

Gene name	Protein name		Sequence
mHmgcr	3-Hydroxy-3-Methylglutaryl-CoA Reductase	Forward	AACTATTGCACCGACAAGAAGC
		Reverse	CACCTCTCTCACCACCTTGG
mDhcr7	7-dehydrocholesterol reductase	Forward	CCAAGAAGGTGCCATTACTCC
		Reverse	TTCACAAACCAGAGGATGTGG
mSrebp-2	Sterol Regulatory Element Binding Protein-2	Forward	GCGTTCTGGAGACCATGGA
		Reverse	ACAAAGTTGCTCTGAAAACAAATCA
mFasn	fatty acid synthase	Forward	GCTGCGGAAACTTCAGGAAAT
		Reverse	AGAGACGTGTCACTCCTGGACTT
mEbp	3β-hydroxysterol-Δ^8,Δ^7-isomerase	Forward	TCACGTGGCTGTTGTCTAGC
		Reverse	CCCTCGATCACAAGGTGAAT
mAbca1	ATP-binding cassette, sub-family A-1	Forward	AGGTGATGTTTCTGACCAACG
		Reverse	GTTGAGGGACTTGATCTTCAGG

Synthesis

Reactions were monitored by TLC and the plates were visualized by UV and stained with phosphomolybdic acid or Ninhydrin. A general procedure for the synthesis of d_7-BACs using dimethylalkylamine and d_7-benzyl chloride is described below:

Basic Dowex was washed with CH_2Cl_2, acetone, and ethanol. The Dowex (0.90 g, 1g/mmol of amine) was added to a solution of *N*,*N*-dimethylhexadecylamine (0.20 mL, 0.84 mmol) and d_7-benzyl chloride (0.10 mL, 0.87 mmol) in ethanol (4 mL), then the reaction mixture was heated to reflux. After 2 h, the reaction mixture was cooled and filtered. The filtrate was concentrated, then redissolved in CH_2Cl_2 and dried over $MgSO_4$. The solution was filtered, concentrated, and the product dried under high vacuum. The product (0.30 g, 100%) was isolated as a colorless oil. All BACs were synthesized following the same procedure and their NMR data follows.

d_7-C10-BAC: colorless oil; ^{1}H NMR (300 MHz, $CDCl_3$) δ 3.35-3.29 (m, 2H), 3.03 (s, 6H), 1.56 (br s, 2H), 1.07 and 0.99 (br s, 14H), 0.63 (t, 3H, *J* = 6.4 Hz); ^{13}C NMR (75 MHz, $CDCl_3$) δ 132.9 (m), 128.3 (m), 127.1, 63.5, 49.2, 31.6, 29.1, 29.0, 28.9, 26.1, 22.7, 22.4, 13.9; HRMS (ESI) calculated 283.3125 (M - Cl), observed 283.3133.

d_7-C12-BAC: colorless oil; ^{1}H NMR (300 MHz, $CDCl_3$) δ 3.40-3.35 (m, 2H), 3.10 (s, 6H), 1.61 (br s, 2H), 1.12 and 1.05 (br s, 18H), 0.69 (t, 3H, *J* = 6.9 Hz); ^{13}C NMR (75 MHz, $CDCl_3$) δ 132.6 (m), 128.3 (m), 127.2, 63.5, 49.3, 31.7, 29.4, 29.3, 29.2, 29.12, 29.08, 26.2, 22.7, 22.5, 13.9; HRMS (ESI) calculated 311.3438 (M - Cl), observed 311.3444.

d_7-C14-BAC: colorless oil; ^{1}H NMR (300 MHz, $CDCl_3$) δ 3.38-3.36 (m, 2H), 3.10 (s, 6H), 1.61 (br s, 2H), 1.11 and 1.06 (br s, 22H), 0.68 (t, 3H, *J* = 7.0 Hz); ^{13}C NMR (75 MHz, $CDCl_3$) δ 132.6 (m), 128.3 (m), 127.2, 63.5, 49.3, 31.7, 29.5, 29.44, 29.39, 29.3, 29.21,

29.15, 29.1, 26.2, 22.8, 22.5, 13.9; HRMS (ESI) calculated 339.3751 (M - Cl), observed 339.3744.

d_7-C16-BAC: white powder; ^{1}H NMR (300 MHz, $CDCl_3$) δ 3.45-3.39 (m, 2H), 3.18 (s, 6H), 1.67 (br s, 2H), 1.18 and 1.13 (br s, 26H), 0.75 (t, 3H, *J* = 7.0 Hz); ^{13}C NMR (75 MHz, $CDCl_3$) δ 132.6 (m), 128.3 (m), 127.2, 63.5, 49.4, 31.8, 29.6, 29.52, 29.45, 29.32, 29.26, 29.2, 29.1, 26.2, 22.8, 22.6, 14.0; HRMS (ESI) calculated 367.4064 (M - Cl), observed 367.4063.

2.5. Acknowledgements

This chapter contains the research article: Josi Herron, Rosalyn Reese, Keri A. Tallman, Rohini Narayanaswamy, Ned A. Porter, and Libin Xu, Identification of Environmental Quaternary Ammonium Compounds as Direct Inhibitors of Cholesterol Biosynthesis. *Toxicological Sciences* 2016, 151(2): 261-270.

Financial support for this research was provided in part by the National Institutes of Health grants R00 HD073270, a pilot grant of NIH P30 ES000267 to Libin Xu, and startup funds to Libin Xu from the Department of Medicinal Chemistry, School of Pharmacy of the University of Washington. We also thank Dr. Karoly Mirnics for the use of the tissue culture facility and qPCR instrument at Vanderbilt University and for helpful discussion on the project. We also would like to thank Dr. Zeljka Korade for sharing the design of the *mEbp* primers.

2.6. References

Baudouin, C., A. Labbe, H. Liang, A. Pauly, and F. Brignole-Baudouin. 2010. Preservatives in eyedrops: the good, the bad and the ugly. *Prog. Retin. Eye Res.* 29:312-334.

Bjorkhem, I., and S. Meaney. 2004. Brain cholesterol: long secret life behind a barrier. *Arterioscler. Thromb. Vasc. Biol.* 24:806-815.

Bukelis, I., F.D. Porter, A.W. Zimmerman, and E. Tierney. 2007. Smith-Lemli-Opitz syndrome and autism spectrum disorder. *Am. J. Psychiatry*. 164:1655-1661.

Burge, P.S., and M.N. Richardson. 1994. Occupational asthma due to indirect exposure to lauryl dimethyl benzyl ammonium chloride used in a floor cleaner. *Thorax*. 49:842-843.

Buttar, H.S. 1985. Embryotoxicity of benzalkonium chloride in vaginally treated rats. *J. Appl. Toxicol.* 5:398-401.

Canfran-Duque, A., et al. 2013. Atypical antipsychotics alter cholesterol and fatty acid metabolism in vitro. *J. Lipid Res.* 54:310-324.

Davis, H.C., and H. Hidu. 1969. Effects of pesticides on embryonic development of clams and oysters and on survival and growth of the larvae. *Fish. Bull*. 67:393-404.

De Saint Jean, M., F. Brignole, A.F. Bringuier, A. Bauchet, G. Feldmann, and C. Baudouin. 1999. Effects of benzalkonium chloride on growth and survival of Chang conjunctival cells. *Invest. Ophthalmol. Vis. Sci.* 40:619-630.

Fitzky, B.U., M. Witsch-Baumgartner, M. Erdel, J.N. Lee, Y.K. Paik, H. Glossmann, G. Utermann, and F.F. Moebius. 1998. Mutations in the Delta 7-sterol reductase gene in patients with the Smith-Lemli-Opitz syndrome. *Proc. Natl. Acad. Sci. U. S. A.* 95:8181-8186.

Fliesler, S.J., N.S. Peachey, M.J. Richards, B.A. Nagel, and D.K. Vaughan. 2004. Retinal degeneration in a rodent model of Smith-Lemli-Opitz syndrome: electrophysiologic, biochemical, and morphologic features. *Arch. Ophthalmol.* 122:1190-1200.

Gilbert, P., and L.E. Moore. 2005. Cationic antiseptics: diversity of action under a common epithet. *J. Appl. Microbiol.* 99:703-715.

Graf, P. 2001. Benzalkonium chloride as a preservative in nasal solutions: re-examining the data. *Respir. Med.* 95:728-733.

Hall, P., et al. 2013. Aripiprazole and trazodone cause elevations of 7-dehydrocholesterol in the absence of Smith-Lemli-Opitz Syndrome. *Mol. Genet. Metab.* 110:176–178.

Hallmayer, J., S. Cleveland, A. Torres, J. Phillips, B. Cohen, T. Torigoe, J. Miller, A. Fedele, J. Collins, K. Smith, L. Lotspeich, L.A. Croen, S. Ozonoff, C. Lajonchere, J.K. Grether, and N. Risch. 2011. Genetic heritability and shared environmental factors among twin pairs with autism. *Arch. Gen. Psychiatry*. 68:1095-1102.

Herman, J.R., and P. Bass. 1989. Enteric neuronal ablation: structure-activity relationship in a series of alkyldimethylbenzylammonium chlorides. *Fundam. Appl. Toxicol.* 13:576-584.

Holah, J.T., J.H. Taylor, D.J. Dawson, and K.E. Hall. 2002. Biocide use in the food industry and the disinfectant resistance of persistent strains of Listeria monocytogenes and Escherichia coli. *Symp. Ser. Soc. Appl. Microbiol.*:111S-120S.

Horling, A., C. Muller, R. Barthel, F. Bracher, and P. Imming. 2012. A new class of selective and potent 7-dehydrocholesterol reductase inhibitors. *J. Med. Chem.* 55:7614-7622.

Kanthasamy, A., H. Jin, V. Anantharam, G. Sondarva, V. Rangasamy, and A. Rana. 2012. Emerging neurotoxic mechanisms in environmental factors-induced neurodegeneration. *Neurotoxicology*. 33:833-837.

Kavlock, R., and D. Dix. 2010. Computational toxicology as implemented by the U.S. EPA: providing high throughput decision support tools for screening and assessing chemical exposure, hazard and risk. *J. Toxicol. Environ. Health B Crit. Rev.* 13:197-217.

Kolf-Clauw, M., F. Chevy, B. Siliart, C. Wolf, N. Mulliez, and C. Roux. 1997. Cholesterol biosynthesis inhibited by BM15.766 induces holoprosencephaly in the rat. *Teratology*. 56:188-200.

Kolf-Clauw, M., F. Chevy, C. Wolf, B. Siliart, D. Citadelle, and C. Roux. 1996. Inhibition of 7-dehydrocholesterol reductase by the teratogen AY9944: a rat model for Smith-Lemli-Opitz syndrome. *Teratology*. 54:115-125.

Korade, Z., A.K. Kenworthy, and K. Mirnics. 2009. Molecular consequences of altered neuronal cholesterol biosynthesis. *J. Neurosci. Res.* 87:866-875.

Korade, Z., L. Xu, F.E. Harrison, R. Ahsen, S.E. Hart, O.M. Folkes, K. Mirnics, and N.A. Porter. 2014. Antioxidant Supplementation Ameliorates Molecular Deficits in Smith-Lemli-Opitz Syndrome. *Biol. Psychiatry*. 75:215-222.

Korade, Z., L. Xu, K. Mirnics, and N.A. Porter. 2013. Lipid biomarkers of oxidative stress in a genetic mouse model of Smith-Lemli-Opitz syndrome. *J. Inherit. Metab. Dis.* 36:113-122.

Korade, Z., L. Xu, R. Shelton, and N.A. Porter. 2010. Biological activities of 7-dehydrocholesterol-derived oxysterols: implications for Smith-Lemli-Opitz syndrome. *J. Lipid Res.* 51:3259-3269.

Koudinov, A.R., and N.V. Koudinova. 2001. Essential role for cholesterol in synaptic plasticity and neuronal degeneration. *FASEB J.* 15:1858-1860.

Kröckel, L., W. Jira, and D. Wild. 2003. Identification of benzalkonium chloride in food additives and its inefficacy against bacteria in minced meat and raw sausage batters. *Eur. Food Res. Technol.* 216:402-406.

Landrigan, P.J., B. Sonawane, R.N. Butler, L. Trasande, R. Callan, and D. Droller. 2005. Early environmental origins of neurodegenerative disease in later life. *Environ. Health Perspect.* 113:1230-1233.

Leung, E.W., F.A. Medeiros, and R.N. Weinreb. 2008. Prevalence of ocular surface disease in glaucoma patients. *J. Glaucoma*. 17:350-355.

Martin, M.T., D.J. Dix, R.S. Judson, R.J. Kavlock, D.M. Reif, A.M. Richard, D.M. Rotroff, S. Romanov, A. Medvedev, N. Poltoratskaya, M. Gambarian, M. Moeser, S.S. Makarov, and K.A. Houck. 2010. Impact of environmental chemicals on key transcription regulators and correlation to toxicity end points within EPA's ToxCast program. *Chem. Res. Toxicol.* 23:578-590.

Mauch, D.H., K. Nagler, S. Schumacher, C. Goritz, E.C. Muller, A. Otto, and F.W. Pfrieger. 2001. CNS synaptogenesis promoted by glia-derived cholesterol. *Science*. 294:1354-1357.

McDonnell, G., and A.D. Russell. 1999. Antiseptics and disinfectants: activity, action, and resistance. *Clin. Microbiol. Rev.* 12:147-179.

Melin, V.E., H. Potineni, P. Hunt, J. Griswold, B. Siems, S.R. Werre, and T.C. Hrubec. 2014. Exposure to common quaternary ammonium disinfectants decreases fertility in mice. *Reprod. Toxicol.* 50:163-170.

Moebius, F.F., et al. 1998. Pharmacological analysis of sterol delta8-delta7 isomerase proteins with [3H]ifenprodil. *Mol Pharmacol*. 54:591-598.

Moebius, F.F., B.U. Fitzky, J.N. Lee, Y.K. Paik, and H. Glossmann. 1998. Molecular cloning and expression of the human delta7-sterol reductase. *Proc. Natl. Acad. Sci. U. S. A.* 95:1899-1902.

Nowaczyk, M.J., and M.B. Irons. 2012. Smith-Lemli-Opitz syndrome: phenotype, natural history, and epidemiology. *Am. J. Med. Genet. C Semin. Med. Genet.* 160C:250-262.

Padilla, S., D. Corum, B. Padnos, D.L. Hunter, A. Beam, K.A. Houck, N. Sipes, N. Kleinstreuer, T. Knudsen, D.J. Dix, and D.M. Reif. 2012. Zebrafish developmental screening of the ToxCast Phase I chemical library. *Reprod. Toxicol.* 33:174-187.

Pisella, P.J., P. Pouliquen, and C. Baudouin. 2002. Prevalence of ocular symptoms and signs with preserved and preservative free glaucoma medication. *Br. J. Ophthalmol.* 86:418-423.

Porter, F.D., and G.E. Herman. 2011. Malformation syndromes caused by disorders of cholesterol synthesis. *J. Lipid Res.* 52:6-34.

Porter, J.A., K.E. Young, and P.A. Beachy. 1996. Cholesterol modification of hedgehog signaling proteins in animal development. *Science*. 274:255-259.

Purohit, A., M.C. Kopferschmitt-Kubler, C. Moreau, E. Popin, M. Blaumeiser, and G. Pauli. 2000. Quaternary ammonium compounds and occupational asthma. *Int. Arch. Occup. Environ. Health*. 73:423-427.

Ratani, S.S., R.M. Siletzky, V. Dutta, S. Yildirim, J.A. Osborne, W. Lin, A.D. Hitchins, T.J. Ward, and S. Kathariou. 2012. Heavy metal and disinfectant resistance of Listeria monocytogenes from foods and food processing plants. *Appl. Environ. Microbiol.* 78:6938-6945.

Richard, A.M., and C.R. Williams. 2002. Distributed structure-searchable toxicity (DSSTox) public database network: a proposal. *Mutation research*. 499:27-52.

Saher, G., B. Brugger, C. Lappe-Siefke, W. Mobius, R. Tozawa, M.C. Wehr, F. Wieland, S. Ishibashi, and K.A. Nave. 2005. High cholesterol level is essential for myelin membrane growth. *Nat. Neurosci.* 8:468-475.

Sarkar, J., S. Chaudhary, A. Namavari, O. Ozturk, J.H. Chang, L. Yco, S. Sonawane, V. Khanolkar, J. Hallak, and S. Jain. 2012. Corneal neurotoxicity due to topical benzalkonium chloride. *Invest. Ophthalmol. Vis. Sci.* 53:1792-1802.

Schneider, G. 2000-. Analysis of Chemical Space. *In* Madame Curie Bioscience Database [Internet]. Landes Bioscience, Austin (TX).

Sikora, D., K. Pettit-Kekel, J. Penfield, L. Merkens, and R. Steiner. 2006. The near universal presence of autism spectrum disorders in children with Smith-Lemli-Opitz syndrome. *Am. J. Med. Genet.* 140A:1511-1518.

Sipes, N.S., M.T. Martin, P. Kothiya, D.M. Reif, R.S. Judson, A.M. Richard, K.A. Houck, D.J. Dix, R.J. Kavlock, and T.B. Knudsen. 2013. Profiling 976 ToxCast chemicals across 331 enzymatic and receptor signaling assays. *Chem. Res. Toxicol.* 26:878-895.

Takeoka, G.R., L.T. Dao, R.Y. Wong, and L.A. Harden. 2005. Identification of benzalkonium chloride in commercial grapefruit seed extracts. *J. Agric. Food Chem.* 53:7630-7636.

The Federal Institute for Risk Assessment (BfR) of Germany. 2012a. Health assessment of benzalkonium chloride residues in food. *BfR opinion No*

032/2012:http://www.bfr.bund.de/cm/349/health-assessment-of-benzalkonium-chloride-residues-in-food.pdf.

The Federal Institute for Risk Assessment (BfR) of Germany. 2012b. Health assessment of didecyldimethylammonium chloride (DDAC) residues in food. *BfR opinion No 027/2012*:http://www.bfr.bund.de/cm/349/health-assessment-of-didecyldimethylammonium-chloride-ddac-residues-in-food.pdf.

Tint, G.S., M. Irons, E.R. Elias, A.K. Batta, R. Frieden, T.S. Chen, and G. Salen. 1994. Defective cholesterol biosynthesis associated with the Smith-Lemli-Opitz syndrome. *N. Engl. J. Med.* 330:107-113.

Tint, G.S., M. Seller, R. Hughes-Benzie, A.K. Batta, S. Shefer, D. Genest, M. Irons, E. Elias, and G. Salen. 1995. Markedly increased tissue concentrations of 7-dehydrocholesterol combined with low levels of cholesterol are characteristic of the Smith-Lemli-Opitz syndrome. *J. Lipid Res.* 36:89-95.

Wassif, C.A., C. Maslen, S. Kachilele-Linjewile, D. Lin, L.M. Linck, W.E. Connor, R.D. Steiner, and F.D. Porter. 1998. Mutations in the human sterol Delta(7)-reductase gene at 11q12-13 cause Smith-Lemli-Opitz syndrome. *American Journal of Human Genetics*. 63:55-62.

Waterham, H.R., F.A. Wijburg, R.C. Hennekam, P. Vreken, B.T. Poll-The, L. Dorland, M. Duran, P.E. Jira, J.A. Smeitink, R.A. Wevers, and R.J. Wanders. 1998. Smith-Lemli-Opitz syndrome is caused by mutations in the 7-dehydrocholesterol reductase gene. *Am J Hum Genet*. 63:329-338.

Xu, G., G. Salen, S. Shefer, G.C. Ness, T.S. Chen, Z. Zhao, L. Salen, and G.S. Tint. 1995. Treatment of the cholesterol biosynthetic defect in Smith-Lemli-Opitz syndrome reproduced in rats by BM 15.766. *Gastroenterology*. 109:1301-1307.

Xu, L., T.A. Davis, and N.A. Porter. 2009. Rate Constants for Peroxidation of Polyunsaturated Fatty Acids and Sterols in Solution and in Liposomes. *J. Am. Chem. Soc.* 131:13037-13044.

Xu, L., Z. Korade, and N.A. Porter. 2010. Oxysterols from free radical chain oxidation of 7-dehydrocholesterol: product and mechanistic studies. *J. Am. Chem. Soc.* 132:2222-2232.

Xu, L., Z. Korade, D.A. Rosado, Jr., K. Mirnics, and N.A. Porter. 2013. Metabolism of oxysterols derived from nonenzymatic oxidation of 7-dehydrocholesterol in cells. *J. Lipid Res.* 54:1135-1143.

Xu, L., Z. Korade, D.A. Rosado, W. Liu, C.R. Lamberson, and N.A. Porter. 2011a. An oxysterol biomarker for 7-dehydrocholesterol oxidation in cell/mouse models for Smith-Lemli-Opitz syndrome. *J. Lipid Res.* 52:1222-1233.

Xu, L., W. Liu, L.G. Sheflin, S.J. Fliesler, and N.A. Porter. 2011b. Novel oxysterols observed in tissues and fluids of AY9944-treated rats - a model for Smith-Lemli-Opitz Syndrome. *J. Lipid Res.* 52:1810-1820.

Xu, L., K. Mirnics, A.B. Bowman, W. Liu, J. Da, N.A. Porter, and Z. Korade. 2012. DHCEO accumulation is a critical mediator of pathophysiology in a Smith-Lemli-Opitz syndrome model. *Neurobiol. Dis.* 45:923-929.

Xue, Y., Y. Hieda, K. Kimura, T. Nishiyama, and T. Adachi. 2002. Sensitive determination of benzalkonium chloride in blood and tissues using high-performance liquid chromatography with solid-phase extraction. *Leg. Med. (Tokyo)*. 4:232-238.

Xue, Y., Y. Hieda, Y. Saito, T. Nomura, J. Fujihara, K. Takayama, K. Kimura, and H. Takeshita. 2004. Distribution and disposition of benzalkonium chloride following various routes of administration in rats. *Toxicol. Lett.* 148:113-123.

Yang, J., J.L. Goldstein, R.E. Hammer, Y.A. Moon, M.S. Brown, and J.D. Horton. 2001. Decreased lipid synthesis in livers of mice with disrupted Site-1 protease gene. *Proc. Natl. Acad. Sci. U. S. A.* 98:13607-13612.

Chapter 3: Multi-omics Investigation Reveals Benzalkonium Chloride Disinfectants Alter Sterol and Lipid Homeostasis in the Mouse Neonatal Brain

3.1. Introduction

As reviewed in Chapter 1, the brain is the one of the most lipid-rich organs, second to adipose tissue. Lipids, including glycerophospholipids, sphingolipids, and cholesterol, play important roles in neurodevelopment. Alterations in cholesterol homeostasis contribute to a variety of other malformations and disorders (Porter and Herman, 2010). Additionally, some known developmental neurotoxicants, such as retinoic acid and ethanol, have been shown to modulate cholesterol homeostasis (Chen, Costa, and Guizzetti, 2011; Zhou et al., 2014). Therefore, it is plausible that environmental chemicals capable of disrupting cholesterol and lipid homeostasis could be potential developmental neurotoxicants.

In Chapter 2, we screened for environmental molecules and drugs that could inhibit cholesterol biosynthesis in a manner similar to AY9944, a teratogenic small molecule used to induce a pharmacological model of SLOS in rats. We found that benzalkonium chloride (BAC), a widely used quaternary ammonium compound (QAC) disinfectant, displays high structural similarity to AY9944 (Herron et al., 2016). We further found that short-chain BACs (C10 and C12) potently inhibit DHCR7 while long-chain BACs (C14 and C16) suppress the formation of other cholesterol precursors, such as zymosterol, lathosterol, and desmosterol (Herron et al., 2016). In a subsequent collaborative work with a postdoctoral fellow, Dr. Kelly Hines, where I carried out BAC exposure experiments, we found that exposure to BACs also altered the lipidome of neuronal cells, in a manner dependent on the BAC alkyl chain length (Hines, Herron, and Xu, 2017). Given the important role of lipids in neurodevelopment, these findings indicate that environmental exposure to BACs during developmental stages could adversely affect neurodevelopment.

Recently, QACs have been suggested to be *bona fide* teratogens, based on an increased incidence of neural tube defects (NTDs) observed in both mice and rats exposed *in utero* to an environmentally relevant mixture of QACs that contains BACs (Hrubec et al., 2017). NTDs are closely associated with defects in neural progenitor cell (NPC) proliferation and neurogenesis (Hirata et al., 2001; Ishibashi et al., 1995; Zhong et al., 2000). Lipid metabolism has been shown to influence NPC proliferation and neurogenesis, as a variety of lipids are used as building blocks for membranes, energy sources, and signaling entities (Knobloch et al., 2013; Bieberich, 2012; Dietschy and Turley, 2004; Edmond, 1992; Salem et al., 2001; Spitzer, 1973; Warshaw and Terry, 1976). Thus, disruption of lipid metabolism by BACs might contribute to the previously reported NTDs and other neurodevelopmental outcomes. However, the ability of BACs to enter the fetal brain and alter sterol and lipid homeostasis has not yet been investigated. Therefore, the objective of this chapter was to test the hypothesis that *in utero* exposure to BACs alters sterol and lipid homeostasis in the developing brain.

3.2. Results

Distribution of BACs in PND0 tissues and maternal circulation

To examine whether BACs can enter the embryonic brain, dams were exposed one-week prior to mating and throughout gestation to control Nutra-Gel diet or Nutra-Gel diet with added d_7-BAC C12 or d_7-BAC C16 (120 mg/kg/day) (**Figure 3.1A-B**). This dosing regimen was adapted from Hrubec *et al*, who had previously demonstrated that 120 mg/kg/day of an environmentally relevant mixture of QACs, including BACs, increased the incidence of NTDs in both mice and rats (Hrubec et al., 2017). In the current study, BACs were found at low nM levels in various PND0 tissues, including the brain and liver (**Figure 3.1C-D**). d_7-BAC C12 levels were higher in the brain and liver of neonates than in the control neonates (**Figure 3.1C**), whereas d_7-BAC C16 levels were only significantly higher in the brain (**Figure 3.1D**).

Levels in the neonatal tissues corresponded to approximately 20 nM BAC in the maternal circulation (**Figure 3.1C-D**).

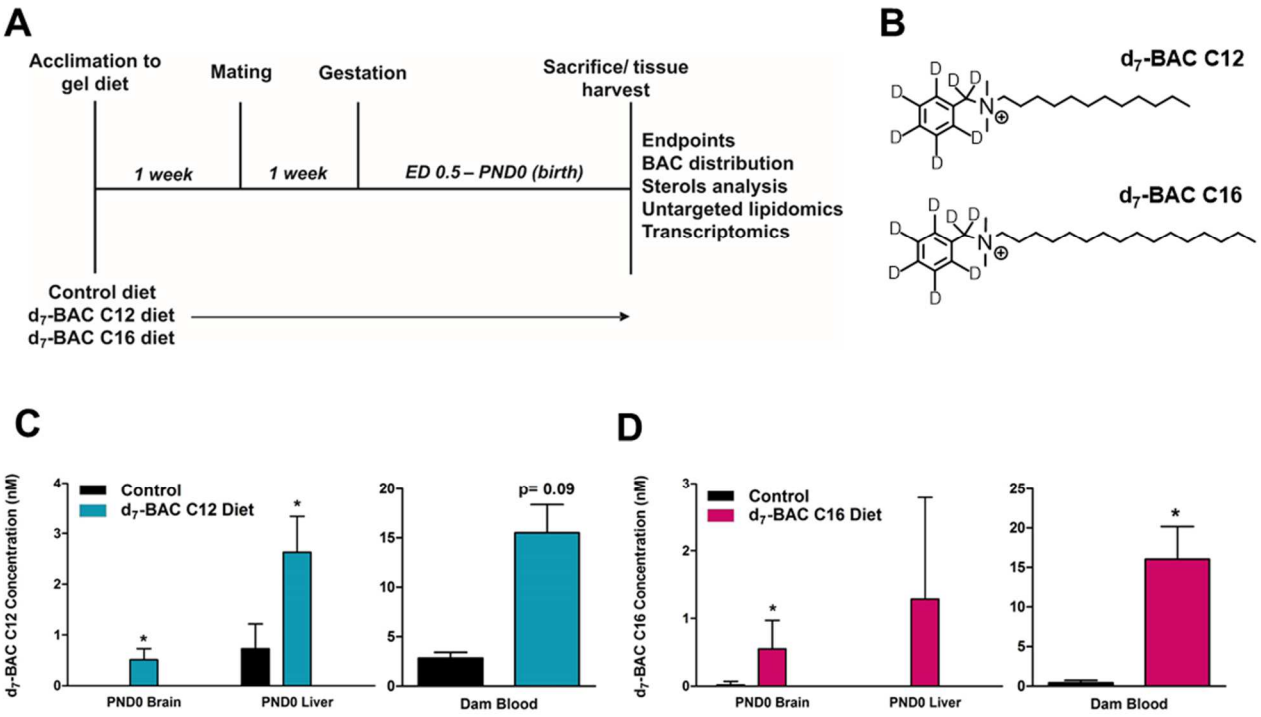

Figure 3.1. Experimental design, structure of deuterium (d_7)-labelled BACs, and BAC tissue distribution analysis. (A) Dams were exposed prior to mating and gestation. At birth, neonates and dams were sacrificed and tissues were harvested to be used for the described endpoints. (B) Structures of d_7-BAC C12 (top) and d_7-BAC C16 (bottom). (C) Concentration of d_7-BAC C12 in control and exposed neonatal brain and liver and dam blood determined by UHPLC-MS/MS. (D) Concentration of d_7-BAC C16 in control and exposed neonatal brain and liver and dam blood determined by UHPLC-MS/MS. n = 5-7 biological replicates per condition for PND0 tissues and n = 2-3 biological replicates per condition for dam blood; all statistical analyses are relative to control using Student's t-test assuming unequal variances; * $P < 0.05$; ** $P < 0.005$; *** $P < 0.0005$.

As additional evidence of systemic BAC exposure, BAC metabolites that entailed cytochrome P450-mediated oxidations of the alkyl chain were observed in the neonatal brain exposed to d_7-BAC C12 and in the circulation of dams exposed to either BAC but not in the control mice (**Figure 3.2**) (Seguin et al., 2019). Overall, these results indicate that BACs do indeed cross the blood-placenta barrier, enter the fetus, and reach the developing brain.

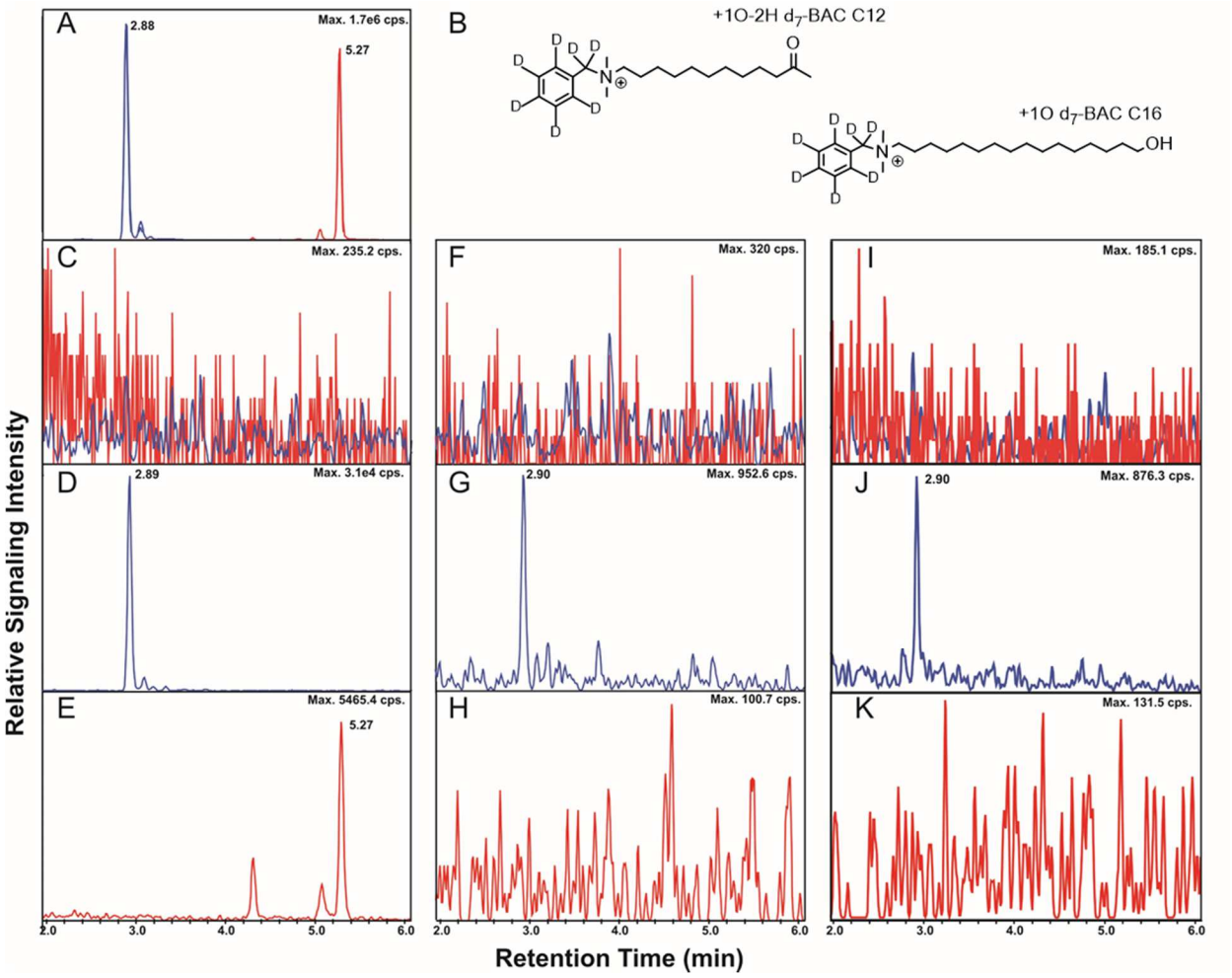

Figure 3.2. (A) Chromatogram of the major BAC metabolites +1O-2H d_7-BAC C12 (blue) and +1 O d_7-BAC C16 (red) and (B) corresponding structures. Metabolites in dam blood: (C) control dam blood, no metabolites detected; (D) d_7-BAC C12 -exposed dam blood; and (E) d_7-BAC C16 -exposed dam blood. Metabolites in neonatal brain: (F) control neonatal brain, no metabolites detected; (G) d_7-BAC C12 -exposed neonatal brain; and (H) d_7-BAC C16 -exposed neonatal brain, no metabolite detected. Metabolites in neonatal liver: (I) control neonatal liver, no metabolites detected; (J) d_7-BAC C12 -exposed neonatal liver, and (K) d_7-BAC C16 -exposed neonatal liver, no metabolite detected.

Assessment of sterol homeostasis in PND0 brains

BAC compounds of different alkyl chain lengths have been shown to alter cholesterol biosynthesis (**Figure 3.3A**) in neuronal cell lines (Herron et al., 2016). However, the ability of BACs to alter sterol homeostasis during neurodevelopment has not been characterized.

Therefore, levels of sterols in lipid extracts from control and exposed PND0 brains were assessed using a UHPLC-MS/MS we developed (**Appendix A**; Herron et al., 2018).

Using this UHPLC-MS/MS method, decreased sterol levels were observed in both BAC C12 and BAC C16 exposed brains (**Figure 3.3B-I**). Exposure to BAC C12 had a more pronounced effect on sterol levels, significantly decreasing levels of total sterols as well as the precursors, 7- and 8-DHC, 7-DHD, desmosterol, and lanosterol, with a trend of decreased cholesterol and other cholesterol precursors. BAC C16 also lead to significantly decreased levels of 7-DHD, lanosterol, and lathosterol with a trend of decreased total sterols, cholesterol, and other cholesterol precursors. The decrease in lanosterol, as well as sterol metabolites downstream of lanosterol, indicate that BACs inhibit biosynthesis upstream of the post-squalene cholesterol biosynthetic pathway in neonatal brains.

Untargeted analysis of the PND0 brain lipidome

We have previously demonstrated that BAC compounds altered lipid homeostasis in treated neuronal cells, leading to decreased levels of triacylglycerols (TGs), diacylglycerols (DGs), and ceramides (Cers) by both BAC-C12 and BAC-C16 and varied changes to phospholipids and sphingomyelins in a manner dependent on the alkyl chain length (Hines, Herron, and Xu, 2017). In the current study, significant alterations in the lipidome of BAC C12- and BAC C16- exposed neonatal brains were also observed, as determined by our HILIC-IM-MS lipidomics method (**Figure 3.4**). Principal component analysis (PCA) revealed group separation dependent on exposure, with BAC-exposed brains separating from control brains along PC-1 (accounting for 64.0% of the variance), although some overlap is observed

(**Figure 3.4A**). BAC-C12 exposed brains further separated from BAC-C16 samples along PC-2 (accounting for 13.3% of the variance).

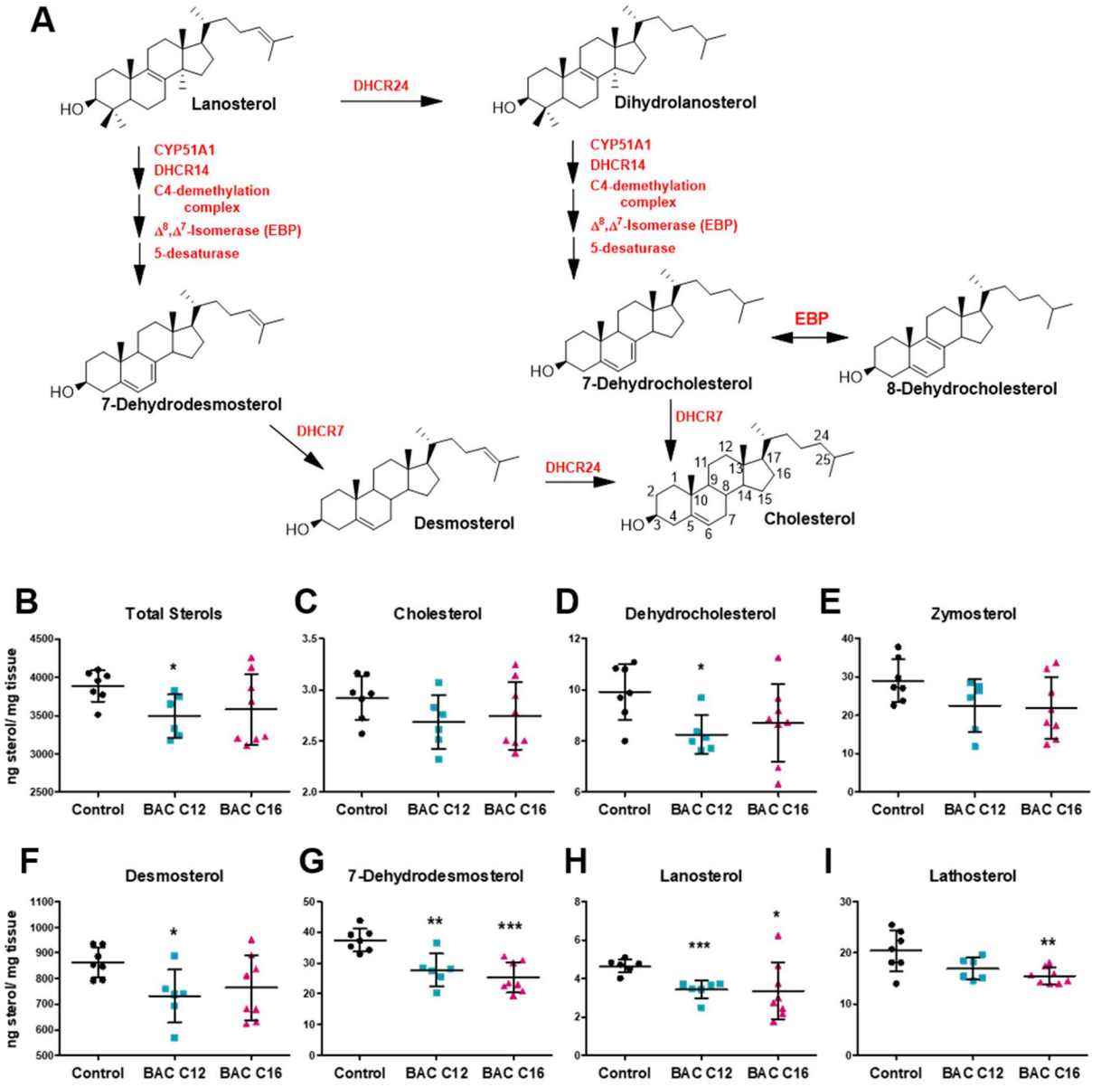

Figure 3.3. Lipid extracts from neonatal brains exposed in utero to BAC C12 or C16 were analyzed to assess changes to sterols involved in the post-squalene cholesterol biosynthetic pathway (see cholesterol biosynthesis scheme in panel A). (B) Total sterol levels, as well as (C) cholesterol, (D) dehydrocholesterol, (E) zymosterol, (F) desmosterol, (G) 7-dehydrodesmosterol, (H) lanosterol, and (I) lathosterol were quantified in each neonatal brain. N = 5-7 biological replicates per condition; all statistical analyses are relative to control using Student's t-test assuming unequal variances; * $P < 0.05$; ** $P < 0.005$; *** $P < 0.0005$.

Significantly altered lipid species were identified by retention time and *m/z* (**Table S.1**). Changes in lipid classes, including DGs, TGs, hexosylceramides (HexCers), and Cers, contributed to the group separations observed in the PCA. BACs altered these lipid species in a manner dependent on the alkyl chain length. BAC C12 exposure led to an overall decrease in DGs and TGs in the neonatal brains, whereas BAC C16 exposure also decreased the levels of these lipids albeit not reaching statistical significance due to large error (**Figure 3.4B**). Furthermore, BAC C16 significantly decreased the levels of Cers and HexCers (**Figure 3.4C**). The reduction in the levels of TGs, DGs, and Cers is consistent with what was previously observed in neuronal cells exposed to BACs (Hines et al., 2017).

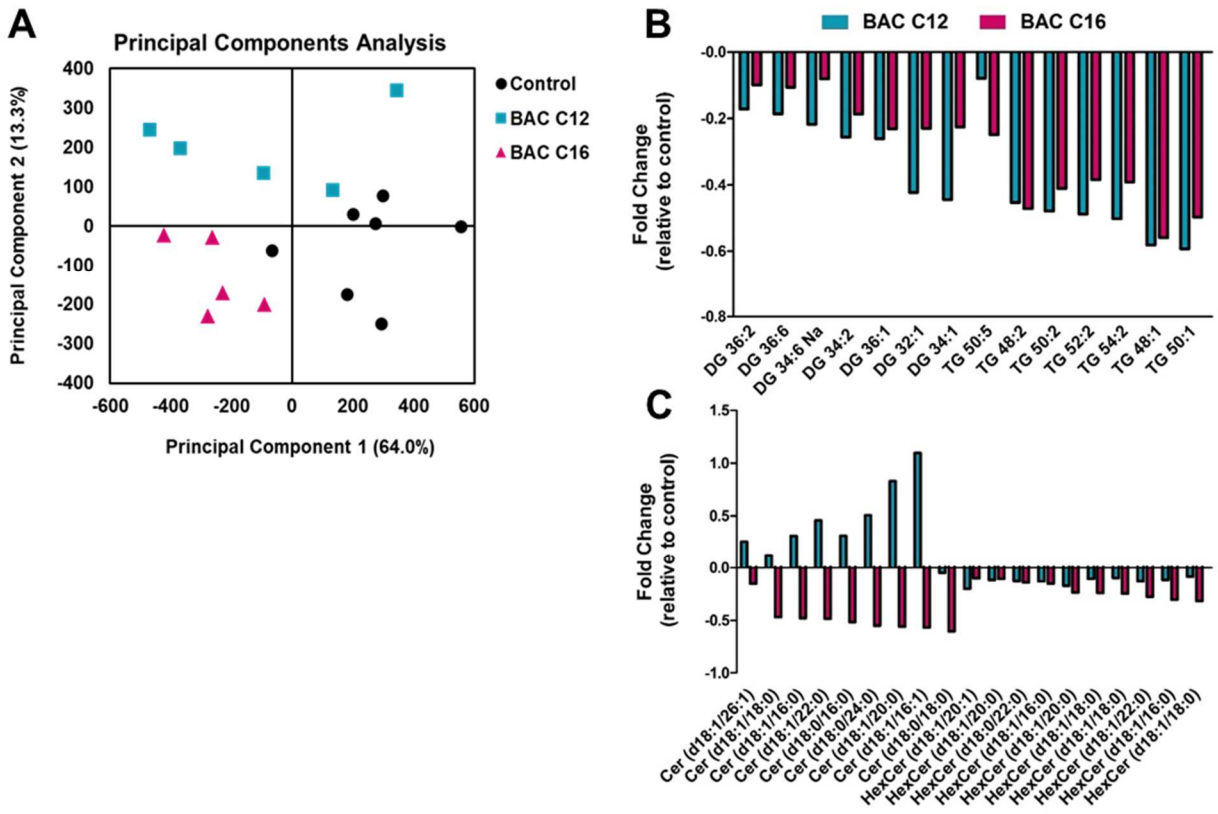

Figure 3.4. Results from lipidomic analysis of neonatal brains exposed to BAC C12 or BAC C16. (A) Various lipid species including DGs, TGs, Cers, HexCers are main contributors to the group separation in the PCA. (B) Both BACs decreased DGs and TGs, although this trend did not reach statistical significance for BAC C16. (C) BAC C16 significantly decreased Cers and HexCers, whereas BAC C12 had little effect on these lipids. n = 5-7 biological replicates per condition; data filtered by ANOVA P value < 0.05.

Global changes in gene expression profiles in BAC-exposed PND0 brains

To elucidate mechanisms underlying the observed decreases in sterols and lipids, transcriptomic changes in control and BAC-exposed neonatal brains were investigated using RNA sequencing. Overall, BAC C12 showed more significant gene expression changes than BAC C16. Compared to controls, *in utero* exposure to BAC C12 altered the expression of 507 genes in PND0 brains, whereas *in utero* exposure to BAC C16 altered the expression of 139 genes (adjusted P <0.05) (**Figure 3.5A-B**). BAC C12 up-regulated 308 genes and down-regulated 199 genes, whereas BAC C16 up-regulated 65 genes and down-regulated 74 genes. Among the differentially expressed genes (DEGs), 77 genes were co-regulated by both BACs, whereas 430 genes were uniquely regulated by BAC C12 and 62 genes were uniquely regulated by BAC C16. Among the commonly regulated genes, 46 of the genes were up-regulated and 31 were down-regulated.

Ingenuity pathway analysis of DEGs in BAC-exposed PND0 brains

Functional characterization of DEGs was conducted using Ingenuity Pathway Analysis (IPA). IPA revealed the most significantly altered canonical pathways of DEGs in the control versus BAC C12 comparison and the control versus BAC C16 comparison (**Figure 3.5C; Table S.2**). For the control versus BAC C12 comparison, the top 5 significantly altered canonical pathways included the "Superpathway of Cholesterol Biosynthesis" (8 genes), "liver X receptor-retinoid X receptor (LXR/RXR) activation" (14 genes), "thyroid hormone receptor-retinoid X receptor (TR/RXR) Activation" (11 genes), "Glutamate Receptor Signaling" (8 genes), and "Acute Phase Response Signaling" (13 genes) (**Figure 3.5C; Table S.2**). The "Superpathway of Cholesterol Biosynthesis" was predicted to be activated, whereas the "LXR/RXR activation" and "Acute Phase Response Signaling" pathways were predicted to be

inhibited. Predictions of activation or inhibition is inferred from the activation z-score which is calculated based on the match between the gene expression pattern expected from the IPA

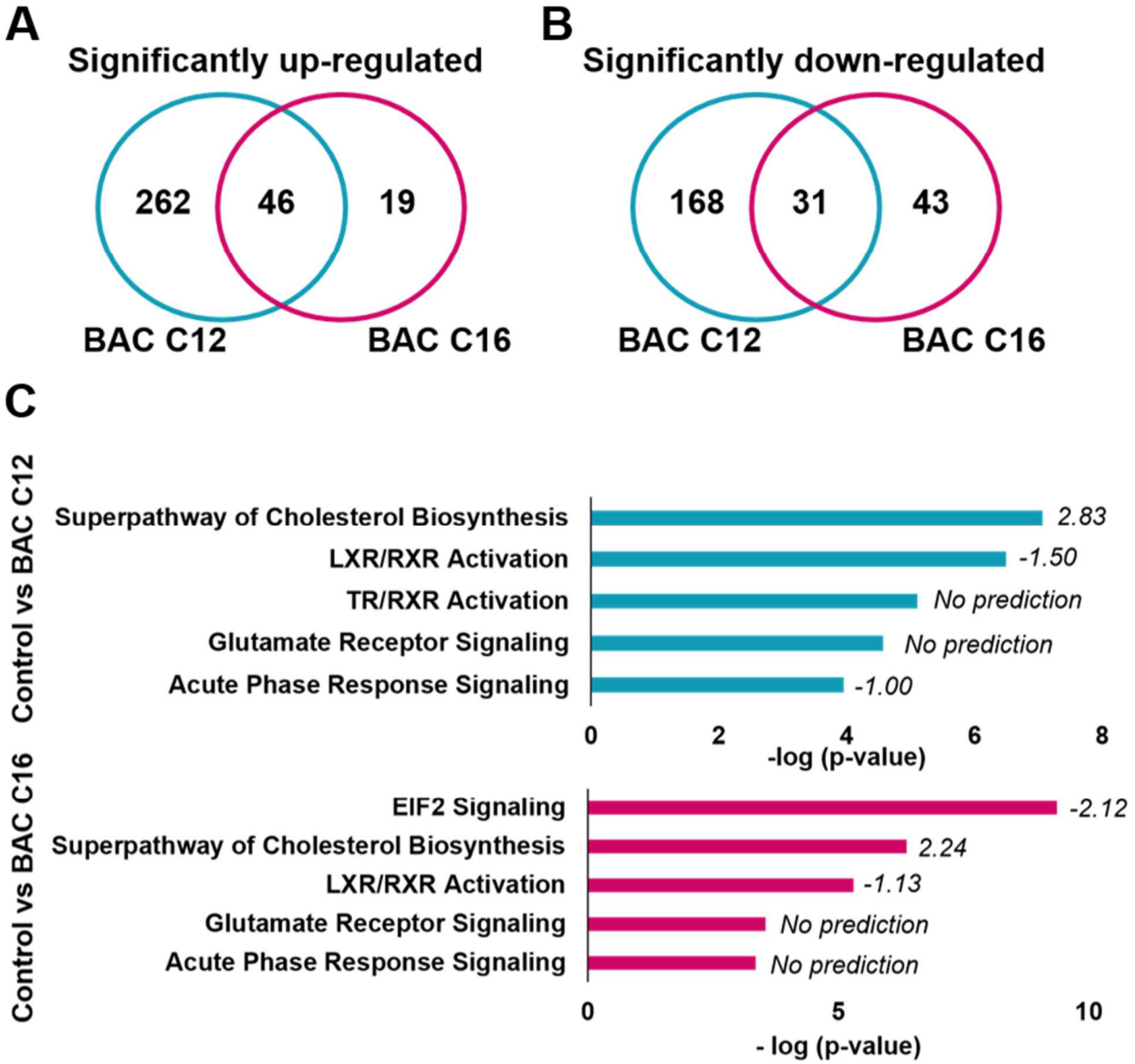

Figure 3.5. Venn diagrams of genes commonly or uniquely expressed in neonatal brains exposed *in utero* to BAC C12 or BAC C16: (A) upregulated genes or (B) downregulated genes. BAC C12 exposure led to an upregulation of 308 genes whereas BAC C16 upregulated 65 genes. Of the genes with increased expression, 46 were co-regulated by the BACs. BAC C12 exposure also led to a downregulation of 199 genes whereas BAC C16 upregulated 74 genes. Of the genes with decreased expression, 31 were co-regulated by the BACs. (C) Top 5 canonical signaling pathways significantly altered in neonatal brains exposed *in utero* to BAC C12 or BAC C16. The BACs altered many of the same pathways, however TR/RXR Activation was unique to BAC C12 and EIF2 Signaling was unique to BAC C16. Z-score activation values to right of bar for each pathway, positive number indicates activation whereas negative

number indicates inhibition of pathway. n = 4 biological replicates per condition; adjusted $P < 0.05$.

Knowledge Base and the expression ("increase" or "decreased") of DEGs within the dataset. Activation z-scores were not predicted for the "TR/RXR Activation" or "Glutamate Receptor Signaling" pathways, likely due to ambiguity in the direction of gene expression changes in these pathways. For the control versus BAC C16 comparison, the top 5 significantly altered canonical pathways included "EIF2 signaling", "Superpathway of Cholesterol Biosynthesis" (5 genes), "LXR/RXR Activation" (7 genes), "Glutamate Receptor Signaling" (4 genes), and "Acute Phase Response Signaling" (6 genes) (**Figure 3.5C; Table S.2**). The "Superpathway of Cholesterol Biosynthesis" was predicted to be activated, whereas the "EIF2 signaling" and "LXR/RXR activation" pathways were predicted to be inhibited. Activation z-scores were not predicted for the "Acute Phase Response Signaling" or "Glutamate Receptor Signaling" pathways.

The upstream analysis module of IPA also predicted transcriptional regulators of gene expression and whether they were activated or inhibited (**Tables S.3-4**). Of particular interest was the identification of the upstream regulator of sterol and lipid homeostasis, SREBP cleavage-activating protein (SCAP), as one of the most significantly activated transcriptional regulators in both the control versus BAC C12 and control versus BAC C16 comparisons (**Figure 3.6**). This prediction was based on the overlap *P*-value, which measures the significance of the overlap between dataset genes and genes regulated by the transcriptional regulator (control vs. BAC C12, P = 2.02E-12; control vs BAC C16, P = 4.37E-07). SCAP activation was predicted in both IPA comparisons based on the expression pattern of a variety of DEGs involved in sterol and lipid biosynthesis and transport (**Table 3.1**). SCAP is an escort protein required for cholesterol and lipid homeostasis. When sterol levels are low, SCAP, a sterol sensor, binds sterol regulatory element binding proteins (SREBPs) and mediates their

transport from the endoplasmic reticulum (ER) to the Golgi (Camargo, Smit, and Verheijen, 2009), where SREBPs are cleaved by proteases. Cleaved cytoplasmic portion of SREBPs subsequently translocates to the nucleus and activate genes involved in sterol and lipid biosynthesis, transport, and metabolism. SREBP1c governs the activation of genes involved in fatty acid and triacylglyceride biosynthesis, whereas SREBP2 is involved in cholesterol biosynthesis (Camargo et al., 2009).

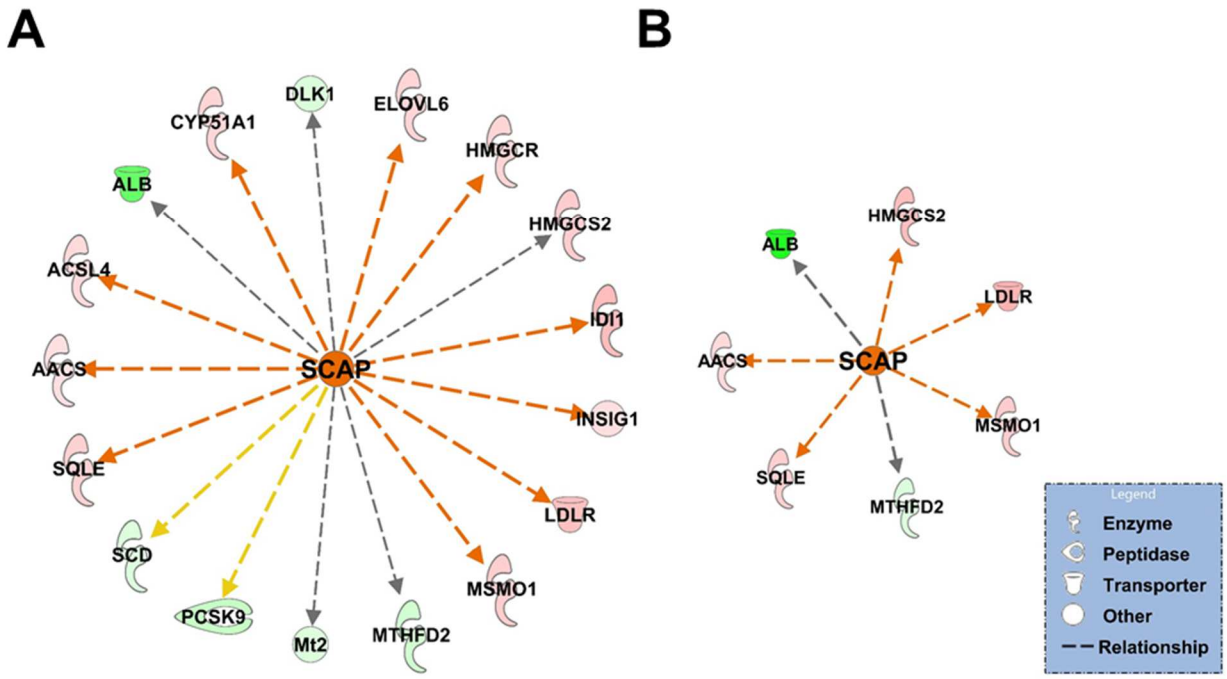

Figure 3.6. Ingenuity pathway analysis identifies the upstream regulator SCAP as significantly activated in neonatal brains exposed *in utero* to BAC C12 (A) or BAC C16 (B). Red, increased gene expression; green, decreased gene expression; orange, predicted activation; yellow, findings inconsistent with state of downstream molecule; grey, effect not predicted. n = 4 biological replicates per condition; adjusted P <0.05.

Table 3.1. Differentially expressed genes regulated by SCAP in neonatal brains exposed *in utero* to BAC C12 or BAC C16. *n*=4 biological replicates per condition; adjusted *P* <0.05.

		BAC C12		**BAC C16**	
Gene ID	**Description**	**Log2 (FC)**	**Adjusted *P* Value**	**Log2 (FC)**	**Adjusted *P* Value**
AACS	acetoacetyl-CoA synthetase	0.42	9.81E-03	0.35	3.84E-02
ACSL4	acyl-CoA synthetase long chain family member 4	0.51	4.44E-03		
ALB	albumin	-2.19	4.44E-03	-3.69	9.98E-03
CYP51	cytochrome P450, family 51	0.58	3.23E-02		
DLK1	delta like non-canonical Notch ligand 1	-0.53	2.70E-02		
ELOVL6	ELOVL family member 6, elongation of long chain fatty acids	0.58	4.44E-03		
HMGCR	3-hydroxy-3-methylglutaryl-CoenzymeA reductase	0.57	4.44E-03		
HMGCS2	3-hydroxy-3-methylglutaryl-CoenzymeA synthase 2	0.69	4.44E-03	0.61	9.98E-03
IDI1	isopentenyl-diphosphate delta isomerase	0.91	4.44E-03		
INSIG1	insulin induced gene 1	0.41	9.81E-03		
LDLR	low density lipoprotein receptor	0.87	4.44E-03	0.73	9.98E-03
MSMO1	methylsterol monoxygenase 1	0.66	4.44E-03	0.48	9.98E-03
MT2	metallothionein 2	-0.48	1.66E-02		
MTHFD2	methylenetetrahydrofolate cyclohydrolase	-0.66	4.44E-03	-0.53	9.98E-03
PCSK9	proprotein convertase subtilisin/kexin type 9	-0.81	4.44E-03		
SCD	stearoyl-Coenzyme A desaturase	-0.36	1.98E-02		
SQLE	squalene epoxidase	0.62	4.44E-03	0.45	9.98E-03

Hierarchical clustering analysis of DEGs involved in sterol and lipid metabolism

Given the identification of canonical signaling pathways, prediction of upstream regulators of sterol and lipid homeostasis, and the apparent sterol- and lipid- lowering effects of BACs on neonatal brains, expression patterns of genes involved in sterol- and lipid-homeostasis were examined in detail. DAVID functional annotation clustering analysis identified an enriched subset of genes functionally-related to sterol and lipid metabolism in both control versus BAC C12 and control versus BAC C16 comparisons (**Table S.5**). The gene cluster related to sterol and lipid homeostasis was found to be enriched in both BAC C12 (37 genes) and BAC C16 (19 genes) groups, with an enrichment score of 3.33 and 2.00, respectively (**Table S.6**). Two-way hierarchical clustering analysis revealed distinct gene expression patterns between the control and exposed samples for each comparison (**Figure 3.7**), except for 1 BAC C16- sample which clustered remotely with the controls. For the BAC C12 versus control comparison group, increased expression of genes known to play key roles in sterol biosynthesis and homeostasis was observed in the exposed group (**Figure 3.7A; Table S.5**), including *Hmgcs2*, *Idi1*, *Cyp51*, *Ldlr*, *Sqle*, *Dhcr24*, *Insig1*, *Hmgcr*, *Hsd17b7* and *Msmo1.* Increases in *Hmgcs2, Ldlr, Sqle, Dhcr24, Hsd17b7, and Msmo1* was also observed in the BAC C16 samples (Figure 3.7B; Table S.6). Both BACs also decreased the expression of genes encoding lipoproteins, including *Apoa1*, *Apoa2*, *Apoc1*, indicating decreased transport of lipids.

Targeted validation of sterol- and lipid- related genes identified by RNA sequencing

DEGs involved in sterol and lipid homeostasis were validated using RT-qPCR (**Figure 3.8**). RT-qPCR results were consistent with the RNA sequencing data, with BAC C12 showing a more significant effect than BAC C16 (**Figure 3.8A-B**). Genes involved in cholesterol biosynthesis, including *Dhcr24, Hmgcr, Hmgcs2,* and *Sqle* were significantly increased by both BACs in the RNA sequencing analyses, but significant increases were only observed with BAC

C12 exposure when validated by RT-qPCR although the trend was consistent. Changes in genes involved in the regulation of sterol and lipid biosynthesis and uptake were also assessed using RT-qPCR. *Insig1*, which was significantly altered by exposure to either BAC in the RNA sequencing analyses, also showed significant increases in expression with BAC C12 when measured by RT-qPCR. Although not significantly increased based on the RNA sequencing analysis, *Scap, Srebf1*, and *Srebf2* were also included in the RT-qPCR analysis, as *Scap* had been predicted as an activated upstream regulator in the IPA analysis. *Scap* and *Srebf2* showed a trend toward increased expression in the BAC C12 samples, but not the control or BAC C16 samples (**Figure 3.8B**).

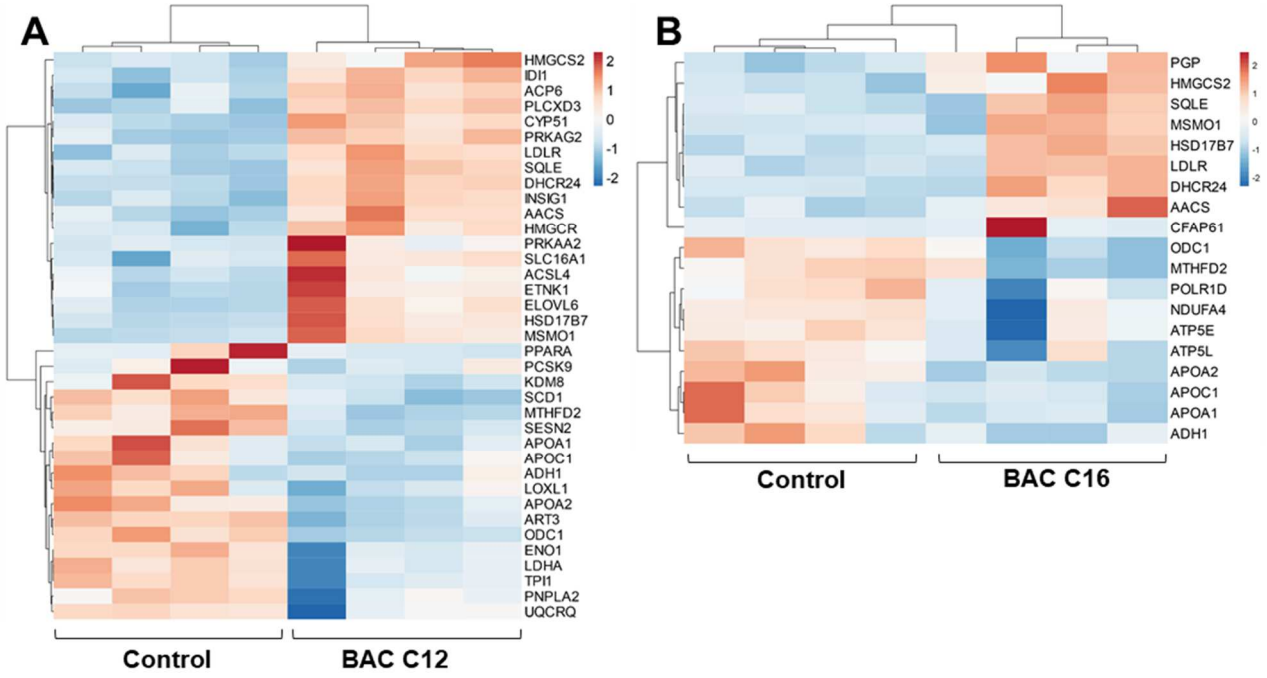

Figure 3.7. Two-way hierarchical clustering dendrograms of differentially expressed genes involved in sterol and lipid homeostasis in neonatal brains exposed *in utero* to (A) BAC C12 or (B) BAC C16; adjusted $P < 0.05$. $n = 4$ biological replicates were tested for each group (shown as columns). Each row represents a different gene. Dendrogram was generated for each comparison (A) control versus BAC C12 and (B) control versus BAC C16 using standardized means and correlation distance and average linkage was used for clustering both rows and columns. Adjusted $P < 0.05$.

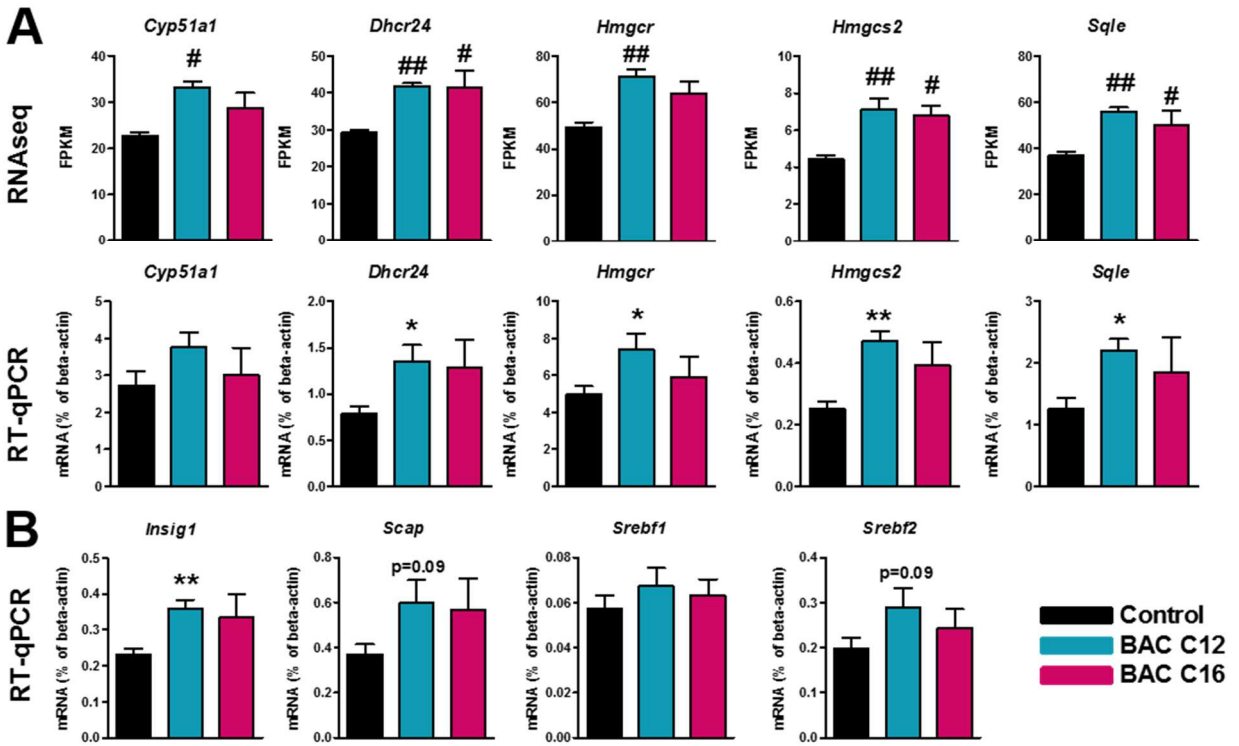

Figure 3.8. Validation of sterol- and lipid-related DEGs using RT-qPCR. (A) BAC C12 and BAC C16 exposure increased the expression of cholesterol biosynthetic genes. (B) Genes involved in regulation of sterol biosynthesis trended toward increased expression in neonatal brains exposed *in utero* to BAC C12. For RNA sequencing, differentially expressed genes met the criteria of having an adjusted *P* value < 0.05, corresponding to the allowed false discovery rate of 5; $^{\#}$ *P* <0.05, $^{\#\#}$ *P* <0.005; *n*= 4 biological replicates per condition. For RT-qPCR, all statistical analyses are relative to control using Student's *t*-test assuming unequal variances, * *P* <0.05, ** *P* <0.005; *n* = 4 biological replicates per condition.

Joint pathway analysis of genes and metabolites

MetaboAnalyst 4.0 was used to conduct joint pathway analysis which integrates significant features generated from mass spectrometry and transcriptomic analyses. In both BAC C12 and BAC C16 exposed neonatal brains, joint pathway analysis of DEGs and significantly altered sterols and lipids confirmed the importance of steroid biosynthesis. This pathway was the top-most enriched pathway identified, based on the significantly altered genes, sterols, and lipids, in BAC C12 (adjusted *P* value = 0.01, Impact = 0.76) and BAC C16 (adjusted *P* value = 0.34, Impact = 0.53) -exposed neonatal brains (**Figure 3.9**). This pathway was more significantly enriched in BAC C12 exposed brains, which corresponds with previous findings that BAC C12 is more effective at altering sterol homeostasis.

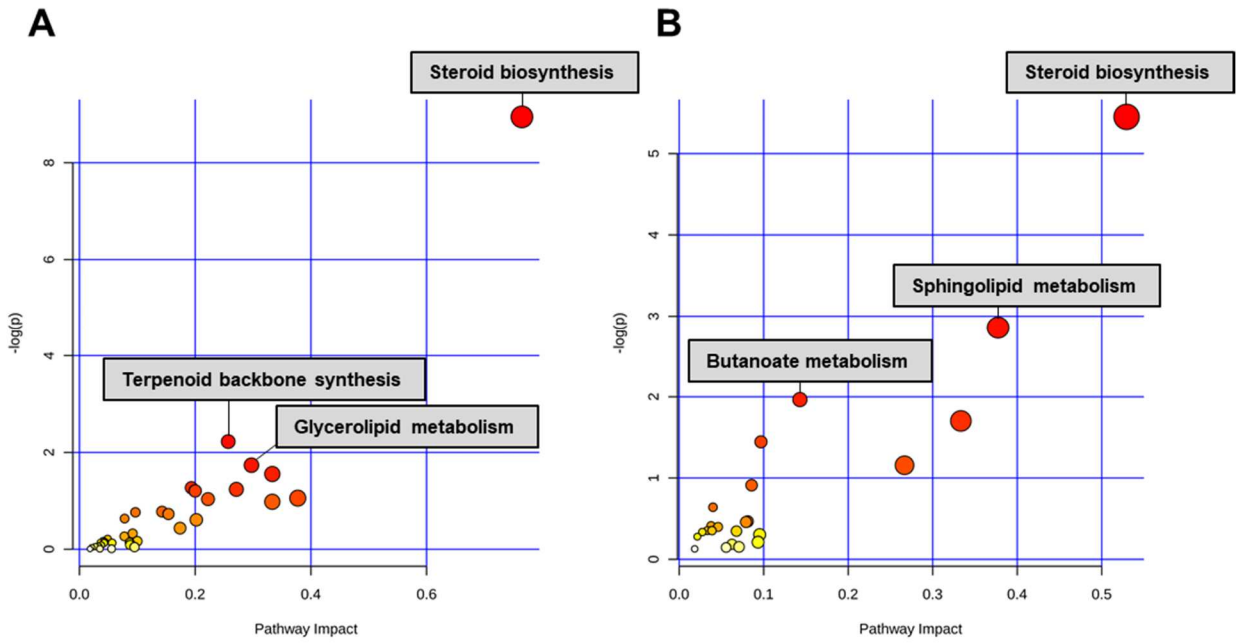

Figure 3.9. Joint pathway analysis of significantly altered genes, sterols, and lipids from (A) BAC C12- and (B) BAC C16- exposed neonatal brains. Pathway enrichment determined by hypergeometric test and reported with –log (*P* value) on y-axis and pathway impact determined by degree centrality measures and reported by pathway impact values on x-axis.

3.3. Discussion

We previously demonstrated that BAC disinfectants can alter sterol and lipid homeostasis in neuronal cells (Herron et al., 2016; Hines et al., 2017). The current study aimed at determining whether BACs could alter sterol and lipid homeostasis in a similar manner in the developing mouse brain. This study demonstrated for the first time that BACs can accumulate in the neonatal brain and alter the transcriptome, sterol profiles, and the lipidome following *in utero* exposure. Specifically, decreases in levels of sterols in the post-squalene cholesterol biosynthetic pathway and in a variety of lipid species, particularly TGs and DGs, were observed in neonatal brains exposed *in utero* to BAC C12 or BAC C16. Given the important roles of sterols and lipids during neurodevelopment, these data provide further evidence that *in utero* exposure to BACs may have significant adverse effects on neurodevelopment.

BACs directly inhibit cholesterol biosynthesis in neuronal cell lines, as evidenced by altered sterol levels and increases in the sterol and lipid biosynthetic genes *Hmgcr, Dhcr7, Ebp, Srebf2,* and *Fasn* (Herron et al., 2016). In the current study, no 7-DHC was accumulated in BAC C12-treated neonatal brains, but both BACs inhibited cholesterol biosynthesis. The decreases in the levels of lanosterol (the first sterol in the pathway) and other cholesterol precursors suggest that the inhibition of cholesterol biosynthesis by BACs occurs before the formation of lanosterol. Further transcriptomic studies revealed the "Superpathway of Cholesterol Biosynthesis" as one of the most significantly altered canonical pathways in neonatal brains exposed to either BAC compound. Consistent with our previous results in neuronal cell lines, *in utero* BAC exposure upregulated genes involved in sterol biosynthesis in the neonatal brain, including *Dhcr24, Hmgcr, Hmgcs2,* and *Sqle,* supporting direct inhibition of cholesterol biosynthesis by BACs. BACs also significantly upregulated *Insig*, with a trend toward upregulation of *Srebf2* and *Scap*, which are all involved in the regulation of sterol and

lipid biosynthesis. When sterol levels are low, SCAP binds SREBPs and mediates the translocation of the protein complex from the ER to the Golgi. Cleaved SREBPs subsequently increase the expression of sterol biosynthetic genes upon translocation to the nucleus. Decreased sterol levels observed in both BAC C12 and BAC C16-exposed neonatal brains are consistent with the finding that BACs upregulate sterol biosynthesis via SCAP signaling.

The LXR/RXR signaling pathway was predicted to be inhibited by IPA in neonatal brains exposed to either BAC. LXR is responsive to intracellular cholesterol homeostasis as the cholesterol precursor, desmosterol, and cholesterol-derived side-chain oxysterols serve as ligands for LXR signaling (Janowski et al., 1999; Yang et al., 2006). Thus, the downregulation of desmosterol (Figure 2) could contribute to the inhibition of LXR signaling.

Of interest, is the fact that liver X receptors (LXRs) have been shown to regulate both cholesterol homeostasis and neurodevelopment. LXRs form heterodimers with Retinoid X Receptors (RXRs) to bind sequence-specific elements which initiates the transcription of genes such as apolipoprotein E (*ApoE*) (Laffitte et al., 2001; Mak et al., 2002), a lipoprotein that mediates lipid transport between astrocytes and neurons, and the cholesterol efflux transporters, *Abca1* and *Abcg1* (Venkateswaran et al., 2000). Moreover, LXR regulates lipogenesis, upregulating fatty acid synthase (FAS) expression through direct interaction with the FAS promoter when the pathway is activated (Joseph et al., 2002; Schultz et al., 2000). Finally, LXR has been shown to play a role in a variety of neurodevelopmental processes, including formation of the cortical layers (Fan, Kim, Bouton, Warner, and Gustafsson, 2008), neuronal migration (Xing, Fan, and Ying, 2010), myelination (Makoukji et al., 2011; Meffre et al., 2015), and neurogenesis (Theofilopoulos et al., 2013).

When LXR signaling is inhibited, lipogenesis is expected to be downregulated, including the synthesis of TGs (Joseph et al., 2002; Schultz et al., 2000). Previously, we have shown that BACs alter the lipidome of neuronal cells, including significant changes to several lipid

classes, such as glycerides, sphingolipids, and phospholipids (Hines et al., 2017). In this study, we found that TGs and DGs are downregulated by BACs, which further supports the notion that BAC exposure leads to the inhibition of LXR/RXR signaling.

Sphingolipids, such as HexCers and Cers, were also significantly affected in neonatal brains exposed to either BAC. The exact mechanism underlying these changes is not clear, but inhibition of LXR signaling and downregulation of lipid synthesis could be contributing factors. Regardless, sphingolipids, including HexCers and Cers, play fundamental roles in a variety of cellular processes, which could be another way that BAC exposure can affect neurodevelopment (Ishibashi, Kohyama-Koganeya, and Hirabayashi, 2013).

Another novel finding of this study was the effect of BAC exposure on genes in the glutamate receptor signaling pathway, one of the top 5 significantly altered canonical pathways in BAC-exposed neonatal brains. Genes encoding various glutamate ionotropic and metabotropic receptors as well as proteins involved in glutamate signaling at the synapse were affected by both BACs (**Table S.2**). Glutamatergic signaling regulates various aspects of neurodevelopment, including neuronal migration, differentiation, neurite outgrowth, synaptogenesis and survival (Choudhury, Lahiri, and Rajamma, 2012). Glutamate also plays essential roles in motor control, synaptic plasticity, learning and memory, and cognition (Choudhury et al., 2012). Of particular relevance to the current study is the fact that lipid rafts, membrane domains enriched in cholesterol, sphingolipids, and gangliosides, are critical for various aspects of synaptic signaling, including glutamate receptor signaling (Wang, 2014; Hering, Lin, and Sheng, 2003). It has been hypothesized that changes in cholesterol biosynthesis and subsequent alterations in membrane raft events could contribute to SLOS pathophysiology (Korade and Kenworthy, 2008). Brain raft fractions prepared from AY9944-treated rats show altered gel electrophoresis profiles, suggesting that altered sterol composition perturbs raft protein content (Keller, Arnold, and Fliesler, 2004). SLOS pathology

also includes impaired neuronal response to glutamate (Wassif et al., 2001). Therefore, the altered sterol and lipid homeostasis observed in BAC-exposed neonatal brains could very well contribute to the alterations in glutamate receptor signaling pathway, which may have significant consequences in neurodevelopment.

This study is not without limitations. First, although two different BACs were evaluated for their effects on the neonatal brain, the use of a single dose prohibited the evaluation of a dose-response relationship. However, the selected dose was derived from the 2017 study by Hrubec et al., which found an increase in NTDs and late gestation fetal deaths with exposure to a mixture of BAC-containing QACs (Hrubec et al., 2017). Second, the effects of BACs at a single time-point of development was examined in this study. The mouse embryo depends on maternal cholesterol until embryonic day 11 (E11) (Herrara and Ortega-Senovilla, 2010; Tint et al., 2006). Therefore, earlier time-points, such as the transition from maternal- to embryonic-derived cholesterol, might be more susceptible to the effects of BACs.

In conclusion, we have demonstrated that BAC disinfectants cross the blood-placental barrier and embryonic blood-brain barrier and alter sterol and lipid homeostasis (**Figure 3.10**). Alterations in signaling pathways important for neurodevelopment (*i.e.* LXR/RXR and glutamatergic signaling) were also observed in this study, possibly arising from altered sterol and lipid homeostasis. Since the developmental neurotoxicants ethanol and retinoic acid are known to modulate cholesterol homeostasis, the potential for BACs to cause adverse neurodevelopmental outcomes should be seriously considered. Therefore, for future work, it is imperative to characterize the neurological phenotype resulting from *in utero* exposure to BAC disinfectants, including morphological and behavioral outcomes.

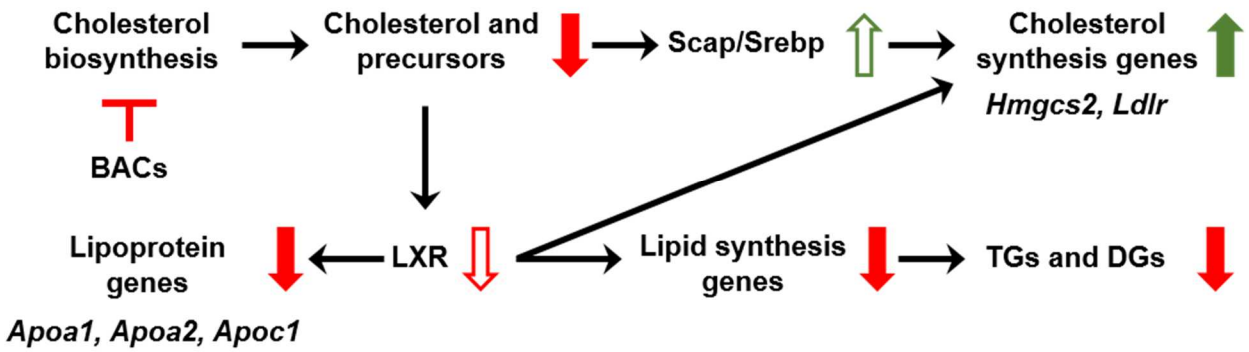

Figure 3.10. Summary of observed alterations in sterol and lipid homeostasis resulting from *in utero* exposure to BAC disinfectants. Inhibition of cholesterol biosynthesis by BACs leads to decreased levels of sterols, which results in increased SCAP-mediated signaling and expression of cholesterol synthesis genes. Downregulation of the cholesterol precursor desmosterol, which is an LXR ligand, could contribute to the predicted inhibition of LXR signaling. Inhibition of LXR signaling leads to downregulation of apolipoprotein genes and lipogenesis genes, the latter of which subsequently results in downregulation of TGs and DGs that were observed by lipidomics.

3.4. Materials and Methods

Chemicals

Optima LC/MS solvents (acetonitrile, chloroform, methanol, methylene chloride, and water), 2-methylbutane, ammonium acetate (Optima LC/MS), formic acid (Optima LC/MS), and sodium chloride were purchased from Thermo Fisher Scientific (Grand Island, NY, USA). The deuterated (d_7-) sterol standard d_7-7-dehydrocholesterol was prepared as reported previously (Xu et al., 2011a; Xu, et al., 2011b). d_7-cholesterol was purchased from Avanti Polar Lipids (Alabaster, AL, USA). $^{13}C_3$-desmosterol and $^{13}C_3$-lanosterol were purchased from Kerafast (Boston, MA, USA). d_7-BAC C12 and d_7-BAC C16 were prepared as described previously (Herron et al., 2016).

Animals

C57BL/6J mice were purchased from Jackson Laboratories (Bar Harbor, MN, USA). The University of Washington Institutional Animal Care and Use Committee approved all

animal protocols. Experiments conducted were also in accordance with the Guiding Principles in the Use of Animals in Toxicology. Adult male and female mice (4 to 6 months old) were acclimated to untreated Nutra-Gel diet (Product #F5769, Bio-Serv, Frenchtown, NJ, USA) for 1 week prior to dietary BAC exposure (**Figure 3.1A**). Our previous pilot studies have shown that exogenous BAC contamination on the mass spectrometer source led to artifact levels of BAC in control samples, preventing accurate quantitation. Therefore, to accurately quantify the ability of BACs to enter the neonatal brain, deuterated BACs were used. Thus, females were randomly assigned to exposure groups (n = 3-4 per group) as described: control Nutra-Gel diet, 120 mg/kg body weight/day d_7-BAC C12 in Nutra-Gel diet, or 120 mg/kg body weight/day d_7-BAC C16 in Nutra-Gel diet. Excess gel diet was provided fresh each day so as not to restrict food intake. No difference in food consumption was observed between exposure groups.

Following the 1-week acclimation period, females were exposed to control or BAC diet for 1 week prior to mating. Breeding pairs consisted of 1 male per 2 females (2 breeding cages per exposure group) and were housed together for 1 week. Sires were then removed from the cage and dams were fed the control or BAC diet throughout gestation until postnatal day 0 (PND0). At PND0, neonates were sacrificed, and the brain and liver were dissected, flash-frozen in 2-methylbutane on dry ice and stored at -80°C until subsequent analyses. Sex was not determined at this age. The weight of each frozen tissue was recorded. Dams were sacrificed at this time to collect blood samples for BAC measurements.

Lipid extraction

Prior to lipid extraction, isotopically labeled sterol internal standards (to be used for quantification in the sterols analysis) and unlabeled d_0-BAC C12 and d_0-BAC C16 internal standards (to be used for quantification of the fed d_7-BAC in tissues and fluids) were added to each tissue (sagittal-cut half PND0 brain, PND0 liver, or dam blood). Note that the other

half of the PND0 brain was used for RNA-sequencing analysis as described below. For sterols analysis, 5 µg of d_7-cholesterol and d_7-7-dehydrocholesterol, and 1 µg of $^{13}C_3$-lanosterol and $^{13}C_3$-desmosterol were added to each sample. For BAC analysis, 0.03 nmol of d_0-BAC C12 and d_0-BAC C16 were added to each sample. Lipid extraction was carried out as previously described in detail (Herron, Hines, and Xu, 2018). To extract the lipids, samples were homogenized in Folch solution [4 mL chloroform/methanol (2/1, v/v)], using a blade homogenizer. NaCl aqueous solution (0.9% (w/v), 1 mL) was added and the resulting mixture was briefly vortexed and then centrifuged for 5 minutes in a clinical tabletop centrifuge at 10°C. The lower (organic) phase was recovered, transferred to a separate glass tube, and the solvent was removed *in vacuo* using a SpeedVac® (Thermo Fisher Savant). Finally, the resulting dried tissue or blood extracts were re-dissolved in 0.3 mL methylene chloride prior to analysis.

UHPLC-MS/MS analysis of BAC and BAC-metabolite levels

Analysis of BAC levels was performed by ultra-high performance liquid chromatography tandem mass spectrometry (UHPLC-MS/MS) using a triple-quadrupole mass spectrometer (API 6500™; SCIEX, Vaughan, ON, CA) equipped with electrospray ionization (ESI). For analysis, 40 µL of lipid extract was transferred to an LC vial, dried under a stream of argon, and reconstituted in 40 µL water/methanol (1/1, v/v). Reverse-phase chromatography was performed with the following conditions: C18 column (Hypersil GOLD®, 100 mm x 2.1 mm, 1.9 µm particle diameter; ThermoFisher Scientific, Grand Island, NY, USA); flow rate, 0.4 mL/min; and gradient elution method with solvent A (0.1% formic acid, 2 mM ammonium formate in water) and solvent B (acetonitrile) was used: 0 min, 30% B; 9.5 min, 85% B; 10-12 min, 30% B. MS conditions: declustering potential, 50 V; entrance potential, 10 V; collision energy, 31 V; collision cell exit potential, 10 V. ESI parameters: spray voltage 3500 V; temperature, 400°C; curtain gas, 35 psi; ion source gas, 45 psi. For

MS analysis, selective reaction monitoring (SRM) was employed to monitor the mass-to-charge ratio (*m/z*) of the parent ion (Q1) for each BAC (isotopically-labelled analyte and corresponding internal standard) and the *m/z* of the characteristic fragment (Q3), formed from the loss of benzyl group (C_7H_8) (see **Table 3.2** for mass transitions). d_7-BAC concentrations were calculated based on the ratio of the analyte peak area to the internal standard peak area and internal standard concentration in each sample. The major BAC metabolites were also monitored, including the +1O- and +1O-2H- metabolites of d_7-BAC C12 and the +1O-metabolite of d_7-BAC C16 in dam blood and neonatal brain samples (see **Table 3.2** for mass transitions). Presence of a metabolite peak was confirmed by comparison to a standard sample containing BAC metabolites that had been generated in NADPH-fortified human liver microsomes (for further details on generation and characterization of BAC metabolites see Seguin et al., 2019). All data are presented as mean ± standard deviation. Statistical analyses relative to control were conducted using Student's *t*-test assuming unequal variance (*P* value < 0.05).

UHPLC-MS/MS analysis of sterol levels

Analysis of sterols was performed by UHPLC-MS/MS using a triple-quadrupole mass spectrometer (API 4000™; AB SCIEX, Vaughan, ON, CA) equipped with atmospheric pressure chemical ionization (APCI) as described previously (Herron, Hines, and Xu, 2018). For analysis, 10 µL of lipid extract was transferred to an LC vial, dried under a stream of argon, and reconstituted in 100 µL 90% MeOH with 0.1% formic acid. See previously published protocol for further details on UHPLC-MS/MS analysis, including MS conditions and quantification method (Herron, Hines, and Xu, 2018). Data are presented as mean ± standard deviation. Statistical analyses relative to control were conducted using Student's *t*-test assuming unequal variance (*P* value < 0.05).

Table 3.2. The *m/z* of the parent ion (Q1) and characteristic fragment (Q3) for each BAC analyte of interest was monitored, including the isotopically-labelled analyte, major metabolite/s, and corresponding internal standard.

Analyte	**Q1 Parent Ion (*m/z*)**	**Q3 Fragment Ion (*m/z*)**
d_7-BAC C12	311.2	212.2
d_7-BAC C12 +1O	327.2	228.2
d_7-BAC C12 +1O-2H	325.2	226.2
d_0-BAC C12	304.2	212.2
d_7-BAC C16	367.2	268.2
d_7-BAC C16 +1O	383.2	284.2
d_0-BAC C16	360.2	268.2

UHPLC-MS/MS analysis of sterol levels

Analysis of sterols was performed by UHPLC-MS/MS using a triple-quadrupole mass spectrometer (API 4000™; AB SCIEX, Vaughan, ON, CA) equipped with atmospheric pressure chemical ionization (APCI) as described previously (Herron, Hines, and Xu, 2018). For analysis, 10 µL of lipid extract was transferred to an LC vial, dried under a stream of argon, and reconstituted in 100 µL 90% MeOH with 0.1% formic acid. See previously published protocol for further details on UHPLC-MS/MS analysis, including MS conditions and quantification method (Herron, Hines, and Xu, 2018). Data are presented as mean ± standard deviation. Statistical analyses relative to control were conducted using Student's *t*-test assuming unequal variance (P value < 0.05).

Untargeted lipidomics and data analysis

Chromatographic separation was performed using a Waters Acquity FTN ultra-performance liquid chromatography (Waters Corp., Milford, MA, USA) with a hydrophilic interaction column (HILIC; Phenomenex Kinetex, 2.1 × 100 mm, 1.7 µm) maintained at 40°C. An injection volume of 5 µL was used. Ion mobility-mass spectrometry (IM-MS) analysis was performed on a Waters Synapt G2-Si HDMS (Waters Corp., Milford, MA, USA) equipped with an ESI source. Detailed chromatographic and IM-MS conditions and mass calibration parameters were as previously published (Hines, Herron, and Xu, 2017). Data alignment, peak detection, and normalization were performed in Progenesis QI (Nonlinear Dynamics). The chromatographic region from 0.4 to 8.4 min was considered for peak detection. The reference sample for alignment was automatically selected by Progenesis QI, and data were normalized to tissue weight. The resulting data set was filtered by ANOVA P value < 0.05. Principal components analysis was performed in EZInfo (Umetrics). Lipid identifications were made against the METLIN database within 20 ppm mass accuracy. Data are presented as mean ± standard deviation. Statistical analyses relative to control were conducted using Student's t-test assuming unequal variance with a Bonferroni correction for multiple comparisons (P value < 0.025).

Total RNA isolation

PND0 brain halves (sagittal-cut) from control, BAC C12, or BAC C16 exposure groups (n = 4 per exposure group) were homogenized in 1 mL of QIAzol Lysis Reagent (Qiagen) using a blade homogenizer. Total RNA was extracted from each sample using the RNeasy Lipid Tissue Mini Kit (Qiagen, Germantown, MD, USA) according to the manufacturer's protocol. RNA concentration was quantified using a microplate spectrophotometer (Bio-Tek, Winooski, VT, USA) to quantify the absorbance at 260 nm. The RNA integrity was evaluated by formaldehyde agarose gel electrophoresis to visualize the 18S and 28S rRNA bands.

Novogene (Chula Vista, CA, USA) performed the cDNA library construction and sequencing using the Illumina NovaSeq 6000 platform (150 base pairs paired-end, with sequencing depth above 20 million reads per sample). Novogene confirmed the RNA integrity and purity using the Agilent 2100 BioAnalyzer (Agilent Technologies Inc., Santa Clara, CA, USA). Samples with RNA Integrity Number (RIN) of 8.6 or above were submitted to RNA sequencing.

RNA sequencing and data analysis

Raw RNA sequencing reads in FASTQ format were mapped to the mouse genome using HISAT (https://ccb.jhu.edu/software/hisat/), and format conversions were performed using Samtools. Cufflinks (http://cole-trapnell-lab.github.io/cufflinks/) was used to estimate relative abundances of transcripts from each RNA sample. Cuffdiff, a module of Cufflinks, was then used to determine differentially expressed genes (DEGs) between comparison control versus BAC C12 or control versus BAC C16. DEGs met the following criteria: adjusted *P* value < 0.05 (corresponding to the allowed false discovery rate of 5%).

DEGs were plotted in a Venn diagram to identify the common and uniquely expressed genes for each exposure (BAC C12 or BAC C16). Canonical Pathway analysis and Upstream Regulator analysis of DEGs was performed using the Core Analysis feature of Ingenuity Pathway Analysis (IPA, Ingenuity Systems). The Database for Annotation, Visualization and Integrated Discovery (DAVID; https://david.ncifcrf.gov/summary.jsp) annotation enrichment analysis was used to identify enriched lists of DEGs related to sterol and lipid metabolism from each comparison pair (control versus BAC C12 or control versus BAC C16) (Huang, Sherman, and Lempicki, 2009). A 2-way hierarchical clustering dendrogram was conducted on the enriched lists of DEGs related to sterol and lipid metabolism for the control versus BAC C12 comparison and the control versus BAC C16 comparison using ClustVis (https://biit.cs.ut.ee/clustvis/) (Metsalu and Vilo, 2015). Correlation distance and average linkage was used for clustering of rows and columns.

Validation of genes using real-time quantitative polymerase chain reaction (RT-qPCR)

A subset of genes related to sterol and lipid metabolism were selected for validation using RT-qPCR. Total RNA isolated from the PND0 brains (n = 4 per exposure group) was reverse-transcribed into cDNA using the SuperScript IV First-Strand Synthesis System (Invitrogen, Carlsbad, CA, USA). The resulting cDNA was amplified by qPCR, using the TaqMan Gene Expression Mastermix (Thermo Fisher Scientific, Waltham, MA, USA) in a StepOnePlus Real-Time PCR System (Thermo Fisher Scientific, Waltham, MA, USA). TaqMan gene expression assays were used for all qPCR reactions, see **Table S.7** for assay ID (Thermo Fisher Scientific, Waltham, MA, USA). Data are expressed as mean percentage of the expression of the housekeeping gene β-actin ± standard error of the mean. Statistical analyses relative to control were conducted using Student's *t*-test assuming unequal variance (P value < 0.05).

Joint pathway analysis of genes and metabolites

To integrate results obtained from sterols analysis, untargeted lipidomics, and transcriptomics analyses, the joint pathway analysis module of MetaboAnalyst 4.0 (https://www.metaboanalyst.ca/MetaboAnalyst/faces/home.xhtml) was used. Joint pathway analysis exploits the KEGG (Kyoto Encyclopedia of Genes and Genomes) metabolic pathway database to discover pathways involved in underlying biological processes using gene expression and metabolite data. Lists of DEGs and significantly altered sterols and lipids from either BAC C12 or BAC C16 exposed neonatal brains were uploaded into the module. Features were then mapped to KEGG metabolic pathways for over-representation analysis and pathway topology analysis. For over-representation analysis, pathway enrichment was determined by Hypergeometric test and reported with an FDR-adjusted *P*-value. For topology analysis, degree centrality was used to assess the position of a gene or compound within a pathway.

3.5. Acknowledgements

This chapter contains the research article: Josi M. Herron, Kelly M. Hines, Hideaki Tomita, Ryan P. Seguin, Julia Yue Cui, and Libin Xu, Multi-omics Investigation Reveals Benzalkonium Chloride Disinfectants Alter Sterol and Lipid Homeostasis in the Mouse Neonatal Brain. *Toxicological Sciences* 2019, 171(1): 32-45.

The work was supported by the University of Washington Environmental Pathology/ Toxicology Training Program (NIH T32 ES007032-39), the NICHD (R01HD092659), the University of Washington Interdisciplinary Center for Exposures, Diseases, Genomics and Environment (UW EDGE) (P30ES007033), and the University of Washington's Department of Medicinal Chemistry. We also thank Drs. Theo Bammler and Lu Wang of the UW EDGE Center for assisting with the Ingenuity Pathway Analysis.

3.6. References

Bieberich, E. (2012). It"s a lipid"s world: bioactive lipid metabolism and signaling in neural stem cell differentiation. *Neurochemical Research*, *37*(6), 1208–1229. http://doi.org/10.1007/s11064-011-0698-5

Bjorkhem, I., and Meaney, S. (2004) Brain cholesterol: long secret life behind a barrier, *Arterioscler. Thromb. Vasc. Biol. 24*, 806-815.

Camargo, N., Smit, A. B., and Verheijen, M. H. G. (2009). SREBPs: SREBP function in glia-neuron interactions. *The FEBS Journal*, *276*(3), 628–636. http://doi.org/10.1111/j.1742-4658.2008.06808.x

Chen, J., Costa, L. G., and Guizzetti, M. (2011). Retinoic acid isomers up-regulate ATP binding cassette A1 and G1 and cholesterol efflux in rat astrocytes: implications for their therapeutic and teratogenic effects. *The Journal of Pharmacology and Experimental Therapeutics*, *338*(3), 870–878. http://doi.org/10.1124/jpet.111.182196

Choudhury, P. R., Lahiri, S., and Rajamma, U. (2012). Glutamate mediated signaling in the pathophysiology of autism spectrum disorders. *Pharmacology, Biochemistry, and Behavior*, *100*(4), 841–849. http://doi.org/10.1016/j.pbb.2011.06.023

Coti Bertrand, P., O'Kusky, J. R., and Innis, S. M. (2006). Maternal dietary (n-3) fatty acid deficiency alters neurogenesis in the embryonic rat brain. *The Journal of Nutrition*, *136*(6), 1570–1575.

Dietschy, J. M., and Turley, S. D. (2004). Thematic review series: brain Lipids. Cholesterol metabolism in the central nervous system during early development and in the mature animal. *The Journal of Lipid Research*, *45*(8), 1375–1397. http://doi.org/10.1194/jlr.R400004-JLR200

Edmond, J. (1992). Energy metabolism in developing brain cells. *Canadian Journal of Physiology and Pharmacology*, *70 Suppl*, S118–29.

EPA, U. S., Programs, O. O. P., AD. (2006). US EPA - Pesticides - Registration Eligibility Decision for Alkyl Dimethyl Benzyl Ammonium Chloride (ADBAC), 1–126.

Fan, X., Kim, H.-J., Bouton, D., Warner, M., and Gustafsson, J.-A. (2008). Expression of liver X receptor beta is essential for formation of superficial cortical layers and migration of later-born neurons. *Proceedings of the National Academy of Sciences of the United States of America*, *105*(36), 13445–13450. http://doi.org/10.1073/pnas.0806974105

Gilbert, P., and Moore, L. E. (2005). Cationic antiseptics: diversity of action under a common epithet. *Journal of Applied Microbiology*, *99*(4), 703–715. http://doi.org/10.1111/j.1365-2672.2005.02664.x

Hering, H., Lin, C.-C., and Sheng, M. (2003). Lipid rafts in the maintenance of synapses, dendritic spines, and surface AMPA receptor stability. *The Journal of Neuroscience : the Official Journal of the Society for Neuroscience*, *23*(8), 3262–3271.

Herron, J., Hines, K. M., and Xu, L. (2018). Assessment of Altered Cholesterol Homeostasis by Xenobiotics Using Ultra-High Performance Liquid Chromatography-Tandem Mass Spectrometry. *Current Protocols in Toxicology*, *16*(5), e65. http://doi.org/10.1002/cptx.65

Herron, J., Reese, R. C., Tallman, K. A., Narayanaswamy, R., Porter, N. A., and Xu, L. (2016). Identification of Environmental Quaternary Ammonium Compounds as Direct Inhibitors of Cholesterol Biosynthesis. *Toxicological Sciences : an Official Journal of the Society of Toxicology*, *151*(2), 261–270. http://doi.org/10.1093/toxsci/kfw041

Hines, K. M., Herron, J., and Xu, L. (2017). Assessment of altered lipid homeostasis by HILIC-ion mobility-mass spectrometry-based lipidomics. *Journal of Lipid Research*, *58*(4), 809–819. http://doi.org/10.1194/jlr.D074724

Hirata, H., Tomita, K., Bessho, Y., and Kageyama, R. (2001). Hes1 and Hes3 regulate maintenance of the isthmic organizer and development of the mid/hindbrain. *The EMBO Journal*, *20*(16), 4454–4466. http://doi.org/10.1093/emboj/20.16.4454

Holah, J. T., Taylor, J. H., Dawson, D. J., and Hall, K. E. (2002). Biocide use in the food industry and the disinfectant resistance of persistent strains of Listeria monocytogenes and Escherichia coli. *Symposium Series (Society for Applied Microbiology)*, (31), 111S–120S.

Hrubec, T. C., Melin, V. E., Shea, C. S., Ferguson, E. E., Garofola, C., Repine, C. M., et al. (2017). Ambient and dosed exposure to quaternary ammonium disinfectants causes neural tube defects in rodents. *Birth Defects Research*, *16*(Suppl A), 81–13. http://doi.org/10.1002/bdr2.1064

Huang, D. W., Sherman, B. T., and Lempicki, R. A. (2009). Systematic and integrative analysis of large gene lists using DAVID bioinformatics resources. *Nature Protocols*, *4*(1), 44–57. http://doi.org/10.1038/nprot.2008.211

Ishibashi, M., Ang, S. L., Shiota, K., Nakanishi, S., Kageyama, R., and Guillemot, F. (1995). Targeted disruption of mammalian hairy and Enhancer of split homolog-1 (HES-1) leads to up-regulation of neural helix-loop-helix factors, premature neurogenesis, and severe neural tube defects. *Genes and Development*, *9*(24), 3136–3148.

Ishibashi, Y., Kohyama-Koganeya, A., and Hirabayashi, Y. (2013). New insights on

glucosylated lipids: metabolism and functions. *Biochimica Et Biophysica Acta*, *1831*(9), 1475–1485. http://doi.org/10.1016/j.bbalip.2013.06.001

Janowski, B. A., Grogan, M. J., Jones, S. A., Wisely, G. B., Kliewer, S. A., Corey, E. J., and Mangelsdorf, D. J. (1999). Structural requirements of ligands for the oxysterol liver X receptors LXRalpha and LXRbeta. *Proceedings of the National Academy of Sciences of the United States of America*, *96*(1), 266–271.

Joseph, S. B., Laffitte, B. A., Patel, P. H., Watson, M. A., Matsukuma, K. E., Walczak, R., et al. (2002). Direct and indirect mechanisms for regulation of fatty acid synthase gene expression by liver X receptors. *Journal of Biological Chemistry*, *277*(13), 11019–11025. http://doi.org/10.1074/jbc.M111041200

Katakura, M., Hashimoto, M., Shahdat, H. M., Gamoh, S., Okui, T., Matsuzaki, K., and Shido, O. (2009). Docosahexaenoic acid promotes neuronal differentiation by regulating basic helix-loop-helix transcription factors and cell cycle in neural stem cells. *Neuroscience*, *160*(3), 651–660. http://doi.org/10.1016/j.neuroscience.2009.02.057

Keller, R. K., Arnold, T. P., and Fliesler, S. J. (2004). Formation of 7-dehydrocholesterol-containing membrane rafts in vitro and in vivo, with relevance to the Smith-Lemli-Opitz syndrome. *The Journal of Lipid Research*, *45*(2), 347–355. http://doi.org/10.1194/jlr.M300232-JLR200

Knobloch, M., Braun, S. M. G., Zurkirchen, L., Schoultz, von, C., Zamboni, N., Araúzo-Bravo, M. J., et al. (2013). Metabolic control of adult neural stem cell activity by Fasn-dependent lipogenesis. *Nature*, *493*(7431), 226–230. http://doi.org/10.1038/nature11689

Kolf-Clauw, M., Chevy, F., Wolf, C., Siliart, B., Citadelle, D., and Roux, C. (1996). Inhibition of 7-dehydrocholesterol reductase by the teratogen AY9944: a rat model for Smith-Lemli-Opitz syndrome. *Teratology*, *54*(3), 115–125. http://doi.org/10.1002/(SICI)1096-9926(199609)54:3<115::AID-TERA1>3.0.CO;2-2

Komada, M., Saitsu, H., Kinboshi, M., Miura, T., Shiota, K., and Ishibashi, M. (2008). Hedgehog signaling is involved in development of the neocortex. *Development (Cambridge, England)*, *135*(16), 2717–2727. http://doi.org/10.1242/dev.015891

Korade, Z., and Kenworthy, A. K. (2008). Lipid rafts, cholesterol, and the brain. *Neuropharmacology*, *55*(8), 1265–1273. http://doi.org/10.1016/j.neuropharm.2008.02.019

Koudinov, A. R., and Koudinova, N. V. (2001). Essential role for cholesterol in synaptic plasticity and neuronal degeneration. *FASEB Journal : Official Publication of the Federation of American Societies for Experimental Biology*, *15*(10), 1858–1860.

Laffitte, B. A., Repa, J. J., Joseph, S. B., Wilpitz, D. C., Kast, H. R., Mangelsdorf, D. J., and Tontonoz, P. (2001). LXRs control lipid-inducible expression of the apolipoprotein E gene in macrophages and adipocytes. *Proceedings of the National Academy of Sciences of the United States of America*, *98*(2), 507–512. http://doi.org/10.1073/pnas.021488798

Mak, P. A., Laffitte, B. A., Desrumaux, C., Joseph, S. B., Curtiss, L. K., Mangelsdorf, D. J., et al. (2002). Regulated expression of the apolipoprotein E/C-I/C-IV/C-II gene cluster in murine and human macrophages. A critical role for nuclear liver X receptors alpha and beta. *Journal of Biological Chemistry*, *277*(35), 31900–31908. http://doi.org/10.1074/jbc.M202993200

Makoukji, J., Shackleford, G., Meffre, D., Grenier, J., Liere, P., Lobaccaro, J.-M. A., et al. (2011). Interplay between LXR and Wnt/β-catenin signaling in the negative regulation of

peripheral myelin genes by oxysterols. *The Journal of Neuroscience : the Official Journal of the Society for Neuroscience*, *31*(26), 9620–9629. http://doi.org/10.1523/JNEUROSCI.0761-11.2011

Mauch, D. H., Nägler, K., Schumacher, S., Göritz, C., Müller, E. C., Otto, A., and Pfrieger, F. W. (2001). CNS synaptogenesis promoted by glia-derived cholesterol. *Science*, *294*(5545), 1354–1357. http://doi.org/10.1126/science.294.5545.1354

McDonnell, G., and Russell, A. D. (1999). Antiseptics and disinfectants: activity, action, and resistance. *Clinical Microbiology Reviews*, *12*(1), 147–179.

Meffre, D., Shackleford, G., Hichor, M., Gorgievski, V., Tzavara, E. T., Trousson, A., et al. (2015). Liver X receptors alpha and beta promote myelination and remyelination in the cerebellum. *Proceedings of the National Academy of Sciences of the United States of America*, *112*(24), 7587–7592. http://doi.org/10.1073/pnas.1424951112

Metsalu, T., and Vilo, J. (2015). ClustVis: a web tool for visualizing clustering of multivariate data using Principal Component Analysis and heatmap. *Nucleic Acids Research*, *43*(W1), W566–70. http://doi.org/10.1093/nar/gkv468

Porter, F. D., and Herman, G. E. (2010). Malformation syndromes caused by disorders of cholesterol synthesis. *The Journal of Lipid Research*, *52*(1), 6–34. http://doi.org/10.1194/jlr.R009548

Porter, J. A., Young, K. E., and Beachy, P. A. (1996). Cholesterol modification of hedgehog signaling proteins in animal development. *Science*, *274*(5285), 255–259.

Ratani, S. S., Siletzky, R. M., Dutta, V., Yildirim, S., Osborne, J. A., Lin, W., et al. (2012). Heavy metal and disinfectant resistance of Listeria monocytogenes from foods and food processing plants. *Applied and Environmental Microbiology*, *78*(19), 6938–6945. http://doi.org/10.1128/AEM.01553-12

Roux, C., Dupuis, R., Horvath, C., and Talbot, J. N. (1980). Teratogenic effect of an inhibitor of cholesterol synthesis (AY 9944) in rats: correlation with maternal cholesterolemia. *The Journal of Nutrition*, *110*(11), 2310–2312. http://doi.org/10.1093/jn/110.11.2310

Roux, C., Horvath, C., and Dupuis, R. (1979). Teratogenic action and embryo lethality of AY 9944R. Prevention by a hypercholesterolemia-provoking diet. *Teratology*, *19*(1), 35–38. http://doi.org/10.1002/tera.1420190106

Saher, G., Brügger, B., Lappe-Siefke, C., Möbius, W., Tozawa, R.-I., Wehr, M. C., et al. (2005). High cholesterol level is essential for myelin membrane growth. *Nature Neuroscience*, *8*(4), 468–475. http://doi.org/10.1038/nn1426

Salem, N., Litman, B., Kim, H. Y., and Gawrisch, K. (2001). Mechanisms of action of docosahexaenoic acid in the nervous system. *Lipids*, *36*(9), 945–959.

Seguin, R.P., Herron, J.M., Lopez, V., Dempsey, J.L., and Xu, L. (2019) Metabolism of benzalkonium chlorides by human hepatic cytochromes P450. To appear in *Chemical Research in Toxicology.*

Schultz, J. R., Tu, H., Luk, A., Repa, J. J., Medina, J. C., Li, L., et al. (2000). Role of LXRs in control of lipogenesis. *Genes and Development*, *14*(22), 2831–2838. http://doi.org/10.1101/gad.850400

Slimani, K., Féret, A., Pirotais, Y., Maris, P., Abjean, J.-P., and Hurtaud-Pessel, D. (2017). Liquid chromatography-tandem mass spectrometry multiresidue method for the analysis of quaternary ammonium compounds in cheese and milk products: Development and

validation using the total error approach. *Journal of Chromatography. A*, *1517*, 86–96. http://doi.org/10.1016/j.chroma.2017.08.034

Spitzer, J. J. (1973). CNS and fatty acid metabolism. *The Physiologist*, *16*(1), 55–68.

Takeoka, G. R., Dao, L. T., Wong, R. Y., and Harden, L. A. (2005). Identification of benzalkonium chloride in commercial grapefruit seed extracts. *Journal of Agricultural and Food Chemistry*, *53*(19), 7630–7636. http://doi.org/10.1021/jf0514064

Theofilopoulos, S., Wang, Y., Kitambi, S. S., Sacchetti, P., Sousa, K. M., Bodin, K., et al. (2013). Brain endogenous liver X receptor ligands selectively promote midbrain neurogenesis. *Nature Chemical Biology*, *9*(2), 126–133. http://doi.org/10.1038/nchembio.1156

Thurm, A., Tierney, E., Farmer, C., Albert, P., Joseph, L., Swedo, S., et al. (2016). Development, behavior, and biomarker characterization of Smith-Lemli-Opitz syndrome: an update. *Journal of Neurodevelopmental Disorders*, 1–10. http://doi.org/10.1186/s11689-016-9145-x

Tint, G. S. (2006). The use of the Dhcr7 knockout mouse to accurately determine the origin of fetal sterols. *The Journal of Lipid Research*, *47*(7), 1535–1541. http://doi.org/10.1194/jlr.M600141-JLR200

Tint, G. S., Irons, M., Elias, E. R., Batta, A. K., Frieden, R., Chen, T. S., and Salen, G. (1994). Defective cholesterol biosynthesis associated with the Smith-Lemli-Opitz syndrome. *The New England Journal of Medicine*, *330*(2), 107–113. http://doi.org/10.1056/NEJM199401133300205

Tint, G. S., Seller, M., Hughes-Benzie, R., Batta, A. K., Shefer, S., Genest, D., et al. (1995). Markedly increased tissue concentrations of 7-dehydrocholesterol combined with low levels of cholesterol are characteristic of the Smith-Lemli-Opitz syndrome. *The Journal of Lipid Research*, *36*(1), 89–95.

Venkateswaran, A., Laffitte, B. A., Joseph, S. B., Mak, P. A., Wilpitz, D. C., Edwards, P. A., and Tontonoz, P. (2000). Control of cellular cholesterol efflux by the nuclear oxysterol receptor LXR alpha. *Proceedings of the National Academy of Sciences of the United States of America*, *97*(22), 12097–12102. http://doi.org/10.1073/pnas.200367697

Wang, H. (2014). Lipid rafts: a signaling platform linking cholesterol metabolism to synaptic deficits in autism spectrum disorders. *Frontiers in Behavioral Neuroscience*, *8*(222), 104. http://doi.org/10.3389/fnbeh.2014.00104

Warshaw, J. B., and Terry, M. L. (1976). Cellular energy metabolism during fetal development. VI. Fatty acid oxidation by developing brain. *Developmental Biology*, *52*(1), 161–166.

Wassif, C. A., Zhu, P., Kratz, L., Krakowiak, P. A., Battaile, K. P., Weight, F. F., et al. (2001). Biochemical, phenotypic and neurophysiological characterization of a genetic mouse model of RSH/Smith--Lemli--Opitz syndrome. *Human Molecular Genetics*, *10*(6), 555–564.

Xing, Y., Fan, X., and Ying, D. (2010). Liver X receptor agonist treatment promotes the migration of granule neurons during cerebellar development. *Journal of Neurochemistry*, *115*(6), 1486–1494. http://doi.org/10.1111/j.1471-4159.2010.07053.x

Xu, L., Korade, Z., Rosado, D. A., Liu, W., Lamberson, C. R., and Porter, N. A. (2011a). An oxysterol biomarker for 7-dehydrocholesterol oxidation in cell/mouse models for Smith-

Lemli-Opitz syndrome. *The Journal of Lipid Research*, *52*(6), 1222–1233. http://doi.org/10.1194/jlr.M014498

Xu, L., Liu, W., Sheflin, L. G., Fliesler, S. J., and Porter, N. A. (2011b). Novel oxysterols observed in tissues and fluids of AY9944-treated rats: a model for Smith-Lemli-Opitz syndrome. *The Journal of Lipid Research*, *52*(10), 1810–1820. http://doi.org/10.1194/jlr.M018366

Yang, C., McDonald, J. G., Patel, A., Zhang, Y., Umetani, M., Xu, F., et al. (2006). Sterol intermediates from cholesterol biosynthetic pathway as liver X receptor ligands. *Journal of Biological Chemistry*, *281*(38), 27816–27826. http://doi.org/10.1074/jbc.M603781200

Zhong, W., Jiang, M. M., Schonemann, M. D., Meneses, J. J., Pedersen, R. A., Jan, L. Y., and Jan, Y. N. (2000). Mouse numb is an essential gene involved in cortical neurogenesis. *Proceedings of the National Academy of Sciences of the United States of America*, *97*(12), 6844–6849.

Zhou, C., Chen, J., Zhang, X., Costa, L. G., and Guizzetti, M. (2014). Prenatal Ethanol Exposure Up-Regulates the Cholesterol Transporters ATP-Binding Cassette A1 and G1 and Reduces Cholesterol Levels in the Developing Rat Brain. *Alcohol and Alcoholism (Oxford, Oxfordshire)*, *49*(6), 626–634. http://doi.org/10.1093/alcalc/agu049

Chapter 4: Benzalkonium Chloride Disinfectants Induce Apoptosis, Inhibit Proliferation, and Activate the Integrated Stress Response in a 3-D *In Vitro* Model of Neurodevelopment.

4.1. Introduction

Cholesterol is critical for neurodevelopment, serving an essential role in hedgehog signaling (Porter, Young, and Beachy, 1996), neurogenesis (Komada et al., 2008), synapse formation and function (Koudinov and Koudinova, 2001; Mauch et al., 2001), and myelination (Saher et al., 2005). The brain synthesizes its cholesterol locally and independently (Björkhem, Meaney, and Fogelman, 2004). Therefore, alterations in CNS cholesterol homeostasis are detrimental and have been shown to contribute to a variety of malformations and disorders. Effects on cholesterol homeostasis have also been shown to play a role in the developmental neurotoxicity of ethanol and retinoic acid (Chen et al., 2011a; Zhou et al., 2014). Recently, we demonstrated that a widely used class of disinfectants, benzalkonium chloride compounds (BACs), accumulate in the developing neonatal mouse brain at low nM concentrations and alter cholesterol biosynthesis (Herron et al., 2019), indicating that BACs might also impact neurodevelopment through this mechanism.

BACs are the most commonly used quaternary ammonium compound (QAC) disinfectants. They are applied in food processing lines, health care facilities, residential settings, and are common ingredients in over-the-counter cosmetics, hand sanitizers, and pharmaceutical products (Kim et al., 2018). Therefore, exposure to BACs is prevalent given the diversity of applications and may occur through dermal/eye contact, inhalation, and ingestion. Although BACs have been generally recognized as safe, the FDA recently called for additional safety data on the usage of BACs in healthcare and consumer antiseptic products (US FDA, 2015; US FDA, 2016).

An increased incidence of neural tube defects (NTDs) has been observed in both mice and rats exposed *in utero* to 120 mg/kg/day of an environmentally relevant QAC mixture that contained BACs (Hrubec et al., 2017). NTDs are closely associated with defects in neural progenitor cell (NPC) proliferation (Hirata et al., 2001; Ishibashi et al., 1995; Zhong et al., 2000). Indeed, rat NPCs exposed to high concentrations (1000 nM) of BACs *in vitro* show decreased proliferation, increased apoptosis, and oxidative stress (Ryu et al., 2018). However, the effects of BACs on neurodevelopment as a resulted of altered cholesterol biosynthesis has not yet been investigated.

Neurospheres are used as a three-dimensional (3-D) *in vitro* model for developmental neurotoxicity screening as they mimic key processes of brain development, including proliferation, apoptosis, differentiation, and migration (Fritsche et al., 2011). Neurospheres are free-floating structures consisting of NPCs. In the present study, the effects of BACs on cell proliferation and apoptosis was investigated in mouse neurospheres. We hypothesized that the inhibitory effects of BACs on cholesterol biosynthesis would translate to adverse effects on neurodevelopment *in vitro*.

4.2. Results

BACs alter cholesterol biosynthesis in neurospheres

Previously, treatment of neurospheres with AY9944, the positive control for cholesterol biosynthesis inhibition, resulted in increased levels of cholesterol precursors and decreased levels of desmosterol and cholesterol – alterations that are expected in the event of pathway inhibition (Herron et al., 2018; **Appendix A, Table A.4.**). In the current study, neurospheres were exposed to low nM concentrations of BACs from DIV 4 to DIV 7 and UHPLC-MS/MS analysis was conducted to quantify levels of sterols in the post-squalene cholesterol biosynthetic pathway (**Figure 4.1**). Decreased desmosterol levels were observed at 50 nM in BAC C12 exposed neurospheres and at 100 nM in BAC C16 exposed neurospheres. A trend

toward decreased cholesterol and lanosterol levels was also observed in BAC-exposed neurospheres, although this was not statistically significant. The cholesterol precursors, 7-dehydrocholesterol and 7-dehydrodesmosterol, were significantly increased in neurospheres exposed to BAC C12 at 50 nM. 8-Dehdyrocholesterol also showed significant accumulation in neurospheres to BAC C12 at 100 nM. Overall, the effects of BAC C12 on sterol levels in neurospheres are consistent with effects of AY9944, the positive control for cholesterol biosynthesis inhibition. BAC C16 is much less potent than BAC 12 in inhibiting cholesterol biosynthesis.

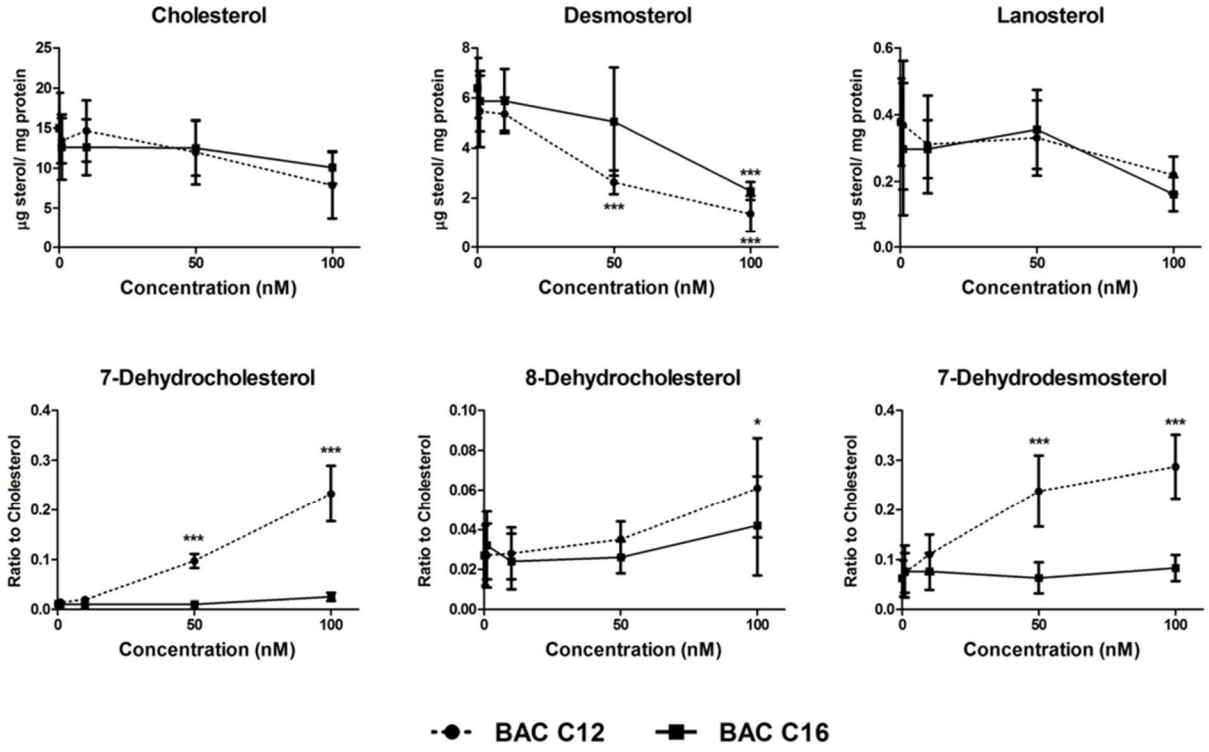

Figure 4.1. BACs alter cholesterol biosynthesis. Neurospheres exposed to vehicle control (0 nM), BAC C12 or BAC C16 at 1, 10, 50, and 100 nM from DIV 4 to DIV 7 show alterations in levels of sterols in the post-squalene cholesterol biosynthetic pathway. n=4 biological replicates per condition; adjusted *P*-value, * < 0.05; ** < 0.01; *** < 0.001.

Neurosphere growth is reduced by BACs

Alterations in neurosphere growth could indicate increased cell death and/or an impairment in the ability of NPCs to proliferate. Therefore, effects on the growth of neurospheres exposed to either BAC C12 or BAC C16 from DIV 4 to DIV 7 was investigated. Neurospheres exposed to either BAC showed a significant decrease in diameter compared to vehicle control exposed neurospheres (**Figure 4.2A-B**). The decrease in diameter was correlated with a reduction in the number of cells obtained from dissociated neurospheres (**Figure 4.2C**). These findings are not correlated with effects on cholesterol biosynthesis, as BAC C12 and BAC C16 impacted neurosphere diameter and cell count similarly while AY9944 exposure did not have significant effects on either parameter.

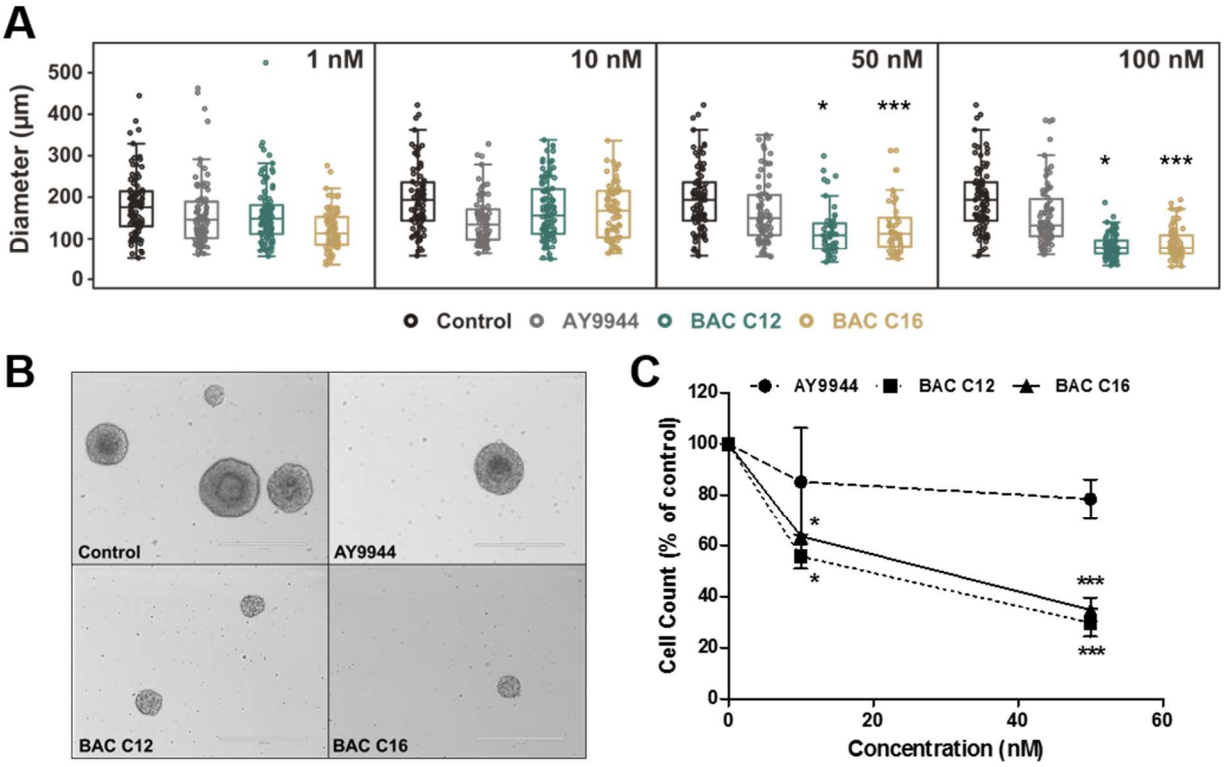

Figure 4.2. BACs reduce neurosphere growth. (A) Size distribution of neurospheres exposed to vehicle control, AY9944 (positive control), BAC C12, or BAC C16 at a concentration of 1, 10, 50, and 100 nM from DIV 4 to DIV 7. (B) Representative brightfield images of neurospheres exposed to a concentration of 50 nM from DIV 4 to DIV 7 (calibration bar: 400 µm). (C) Number of neural progenitor cells from dissociated neurospheres exposed to vehicle

control (0 nM), AY9944, BAC C12, or BAC C16 at 10 and 50 nM from DIV 4 to DIV 7. Relative to control, cell count from BAC-exposed neurospheres is decreased. n=4 biological replicates per condition; adjusted *P*-value, * < 0.05; ** < 0.01; *** < 0.001.

BACs induce apoptosis and decrease proliferation

The observed reduction in neurosphere growth could be due to decreased proliferation and/or increased apoptosis of the NPCs. To further characterize this, immunostaining for makers of these processes were employed. For apoptosis, the terminal deoxynucleotidyl transferase (TdT) dUTP nick-end labeling (TUNEL) assay was used to detect apoptotic cells. An increase in the amount of TUNEL-positive NPCs from dissociated neurospheres exposed to BACs from DIV 4 to DIV 7 was observed (**Figure 4.3A-B**). Ki67, a widely accepted cell proliferation marker, and EdU, a thymidine analog which is incorporated into DNA of proliferating cells, were used to assess the number of proliferating cells and proliferation rate (% EdU-positive cells / Ki67-positive cells). Ki67-positive cells from BAC-exposed neurospheres were decreased, although the proliferation rate was not affected (**Figure 4.3C-D**).

Additionally, cell cycle analysis using flow cytometry revealed an apparent delay of the G1/S phase transition, demonstrated by a slight, yet significant increase in G1 cells and corresponding decrease in S phase cells from BAC C12 exposed neurospheres (**Figure 4.3E**). This trend was the same for BAC C16 exposed neurospheres, although not statistically significant due to large variation between biological replicates. Therefore, these results

suggest that the reduction in neurosphere growth was due to both increased apoptosis and inhibited proliferation.

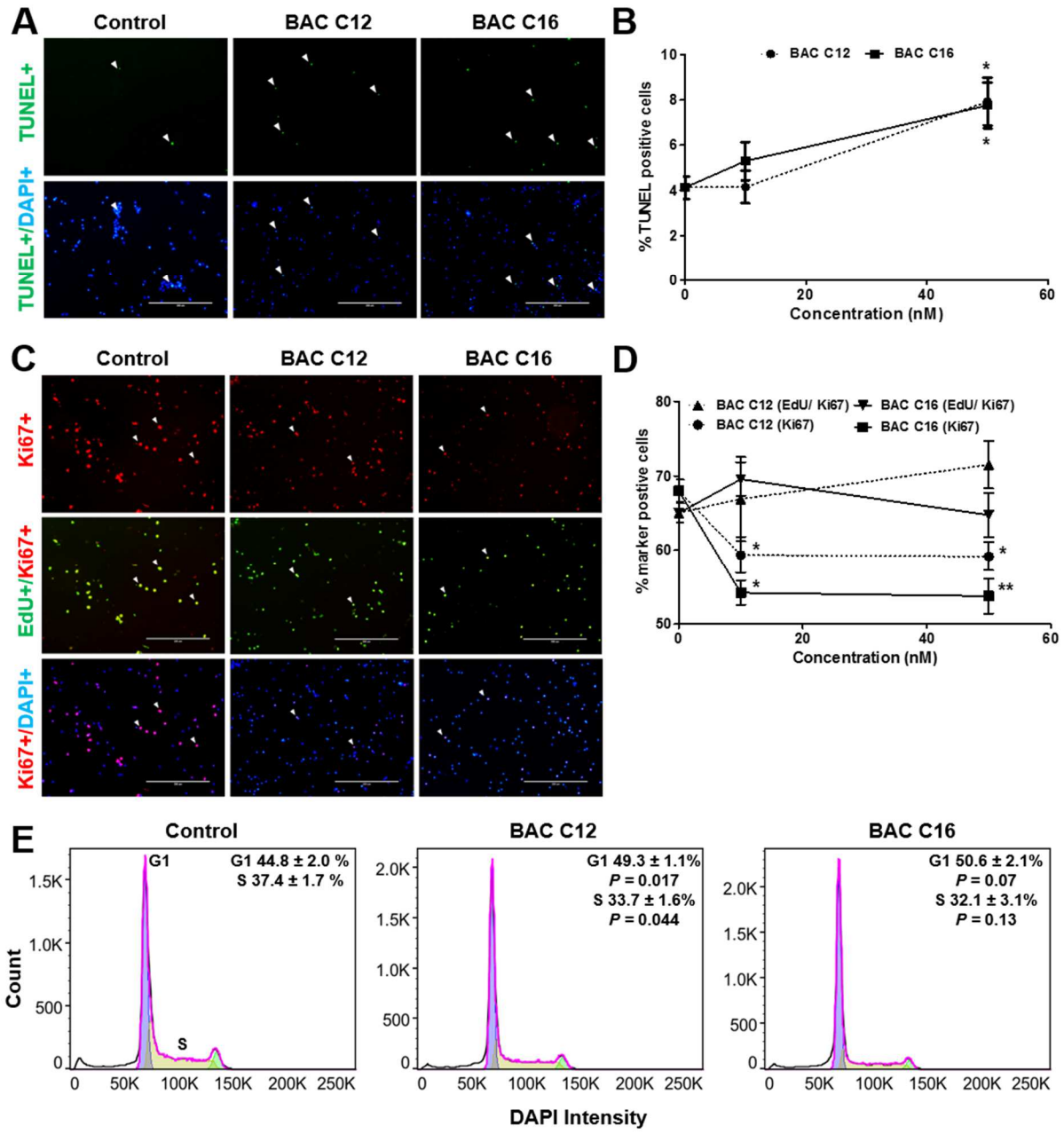

Figure 4.3. BACs induce apoptosis and decrease pool of proliferative NPCs. (A) Immunocytochemistry for TUNEL (green) counterstained with DAPI (blue) of NPCs. (B) Quantification of percentage of TUNEL-positive. (C) Immunocytochemistry for Ki67 (red) and EdU (green), counterstained with DAPI (blue) of NPCs from dissociated neurospheres exposed to vehicle control (0 nM) or 50 nM of BAC C12 or BAC C16 from DIV 4 to DIV 7. (D) Quantification of proliferation rate (Edu/Ki67) and percentage of proliferative cells (Ki67) cells.

(E) Representative histogram of cell cycle analysis for neurospheres exposed to vehicle control or 50 nM of BAC C12 or BAC C16 from DIV 4 to DIV 5. Significant differences in the percentage of G1 or S phase cells were quantified for all biological replicates, displayed as mean ± standard deviation. For all experiments, n=4 biological replicates per condition; adjusted *P*-value, * < 0.05; ** < 0.01; *** < 0.001.

Transcriptome analysis identified biological processes affected by BACs

The effects of BACs on neurosphere growth were not associated with effects on cholesterol biosynthesis. Therefore, to determine potential mechanisms underlying the effects of BAC exposure on neurosphere growth, global transcriptome analysis was conducted on mRNA isolated from neurospheres exposed to BACs from DIV 4 to DIV 5 was conducted. We identified 116 differentially expressed genes (DEGs) from BAC C12-exposed neurospheres (adjusted *P* value <0.05; **Figure 4.4A**). Only 37 DEGs were identified from BAC C16-exposed neurospheres. BAC C12 and BAC C16 co-regulated 9 genes (**Figure 4.4A**).

Functional characterization of DEGs was conducted using GO analysis of biological processes. GO analysis identified 1,143 biological processes significantly enriched by BAC C12, 445 significantly enriched by BAC C16, and 155 significantly enriched by both BACs (*P*-value < 0.05; **Figure 4.4B**). Response to stress was the top biological process enriched by both BACs, as well as cell death and the MAPK cascade (**Figure 4.4C; Table S.8**). Co-regulated genes involved in the response to stress include tribbles homolog 3 (*Trib3*)*;* fibulin 5 (*Fbln5*)*;* solute carrier family 7 member 11 (*Slc7a11*)*;* phosphoenolpyruvate carboxykinase 2, mitochondrial (*Pck2*)*;* asparagine synthetase [glutamine-hydrolyzing] (*Asns*); apolipoprotein E (*Apoe*); and calcium/calmodulin dependent protein kinase II delta (*Camk2d*) (**Figure 4.4D**). Of these, all were significantly upregulated except for *Apoe* and *Camk2d.*

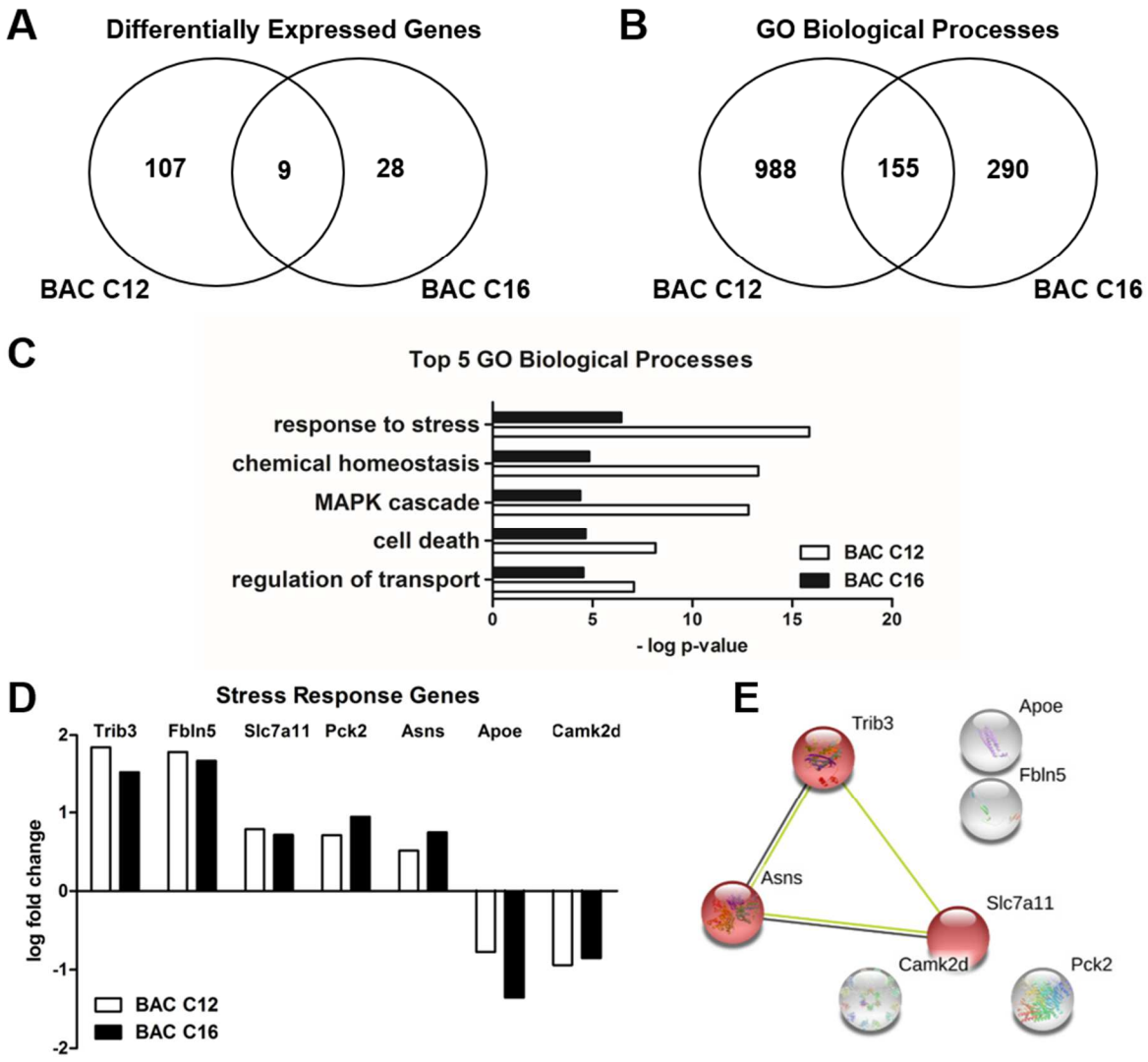

Figure 4.4. Transcriptome analysis indicates a stress response in BAC-exposed neurospheres. (A) Venn diagram of DEGs from neurospheres exposed to 50 nM BAC C12 or BAC C16 from DIV 4 to DIV 5. (B) Venn diagram of GO biological processes. (C) Top 10 significantly enriched GO biological processes. (D) Co-regulated DEGs involved in the "response to stress" biological process. (E) STRING analysis of DEGs co-regulated by both BACs. Red indicates genes involved in the integrated stress response. n=3 biological replicates per condition; adjusted *P*-value <0.05.

A cluster of co-regulated genes involved in the integrated stress response including *Trib3, Asns,* and *Slc7a11* was identified by STRING analysis (**Figure 4.4E**). The integrated stress response is an adaptive pathway activated in response to diverse stress stimuli and

can lead to cell death in cases of severe stress (Pakos-Zebrucka et al., 2016). Activating transcription factor 4 (*Atf4*), the main effector of the integrated stress response (Pakos-Zebrucka et al., 2016), was upregulated in response to BAC C12 exposure (LogFC=0.424; adjusted *P* value < 0.05), in addition to oxidative stress-related enzymes, glutathione peroxidase 3 (*Gpx3;* LogFC=0.765) and thioredoxin 1 (*Txn1;* LogFC=0.567) (**Figure 4.5**). BAC C16 affected fewer genes involved in the integrated stress response (**Figure 4.5**). However, mitochondrial electron transport (specifically cytochrome c to oxygen) was one of the top biological processes enriched in BAC C16-exposed neurospheres (**Table 4.1**) and genes encoding for subunits of mitochondrial complex IV were significantly downregulated, including cytochrome c oxidase subunit 6A1 (*Cox6a1;* LogFC= -0.547) and cytochrome c oxidase subunit 7C (*Cox7c*; LogFC=-0.569) (adjusted *P*-value < 0.05). Downregulation of genes encoding complex IV subunits may impact the formation and/or stability of complex IV which could impair mitochondrial function (Poché et al., 2016). Downregulation of genes encoding complex IV subunits may impact the formation and/or stability of complex IV which could impair mitochondrial function (Poché et al., 2016). The effect of BAC C16 on genes involved in mitochondrial electron transport is consistent with previous studies that have reported mitochondrial dysfunction in response to BAC exposure (Datta et al., 2017; Ryu et al., 2018). Altogether, these results indicate oxidative stress or mitochondrial dysfunction in BAC C12- or BAC C16-exposed neurospheres, respectively, may contribute to the activation of the integrated stress response.

Finally, and of particular relevance to neurodevelopment, was the identification of neurogenesis as one of the top biological processes enriched in BAC C12-exposed neurospheres (**Table 4.1**). Notably, the majority of DEGs involved in neurogenesis were downregulated (adjusted *P* value <0.05; **Figure 4.6**). Among these are the high mobility group family transcription factors *Sox9* (LogFC= -0.554) and *Sox10* (LogFC= -1.262), which

are required for the maintenance of the NPC pool (Kim et al., 2003; Vong et al., 2015); vascular endothelial growth factor A (*Vegf-A*; LogFC= -0.717), which has been shown to increase proliferation and/or decrease apoptosis of NPCs (Mackenzie and Ruhrberg, 2012); and noggin (*Nog*; LogFC= -1.524) which encodes a protein that has been shown to regulate neuronal differentiation (Li and LoTurco, 2000; Lim et al., 2000).

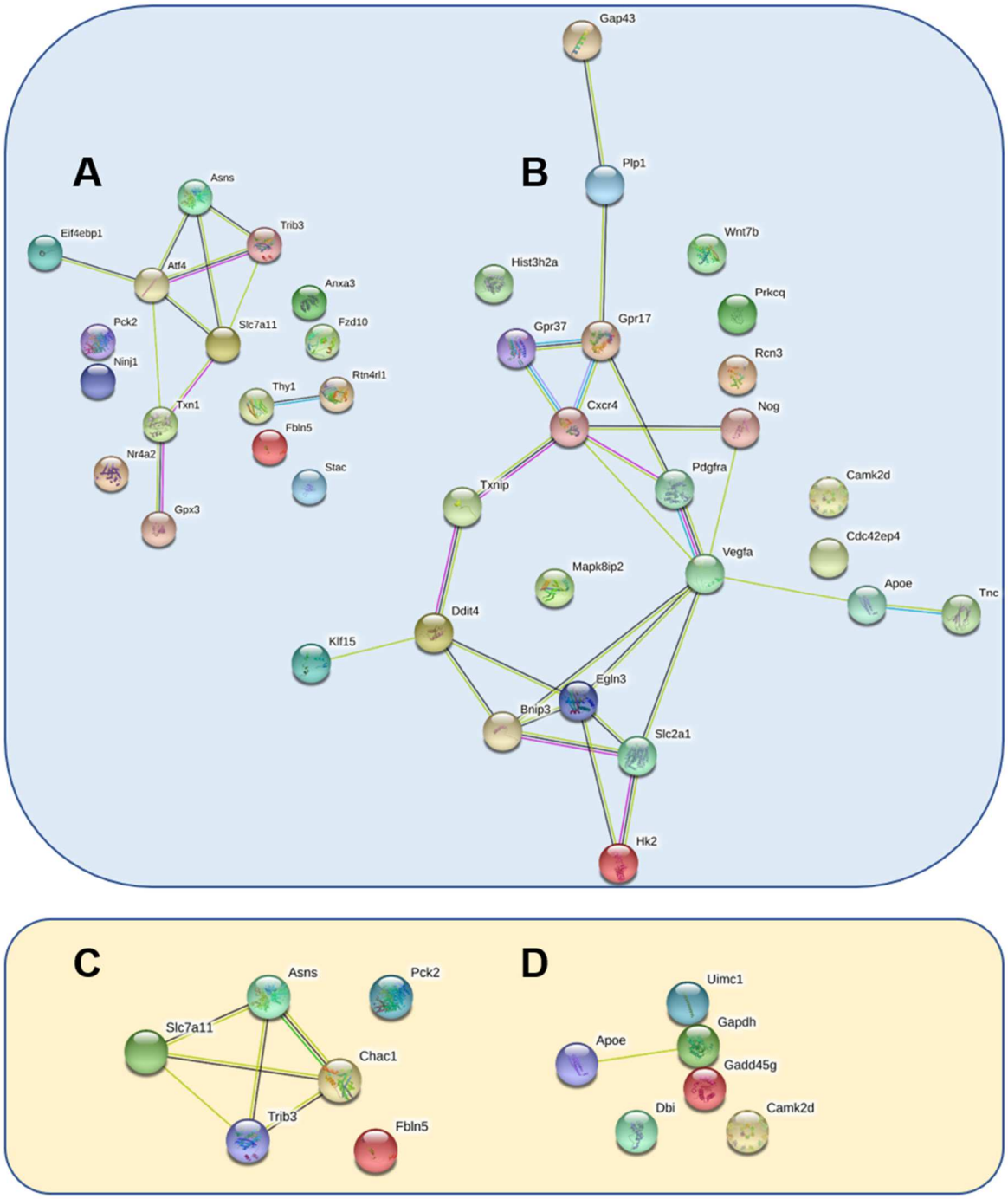

Figure 4.5. STRING networks of DEGs involved in the integrated stress response. Top: STRING networks of DEGs upregulated (A) or downregulated (B) in response to BAC C12 exposure. Bottom: STRING networks of DEGs upregulated (C) or downregulated (D) in response to BAC C16 exposure. n=3 biological replicates per condition; adjusted P-value <0.05.

Table 4.1. Top 10 biological processes altered by BAC C12 and BAC C16.

	Identifier	Name	# DEGs	# Total	-log *P*-value
BAC C12 vs. Control	GO:0061564	axon development	20	384	30.1
	GO:0007154	cell communication	63	3287	29.6
	GO:0023052	signaling	62	3249	28.7
	GO:0050896	response to stimulus	77	4701	28.0
	GO:0097485	neuron projection guidance	12	168	23.4
	GO:0022008	neurogenesis	33	1275	23.1
	GO:0040011	locomotion	31	1153	22.9
	GO: 0048869	cellular developmental process	51	2703	21.5
	GO:0048731	system development	54	2963	21.4
	GO:0009653	anatomical structure morphogenesis	39	1781	21.1
BAC C16 vs. Control	GO:0043603	cellular amide metabolic process	10	789	14.8
	GO:0043604	amide biosynthetic process	8	606	12.4
	GO:0044281	small molecule metabolic process	11	1178	12.3
	GO:0006123	mitochondrial electron transport, cytochrome c to oxygen	2	8	12.2
	GO:0097688	glutamate receptor clustering	2	9	11.9
	GO:1901617	organic hydroxy compound biosynthetic process	4	132	11.1
	GO:0045833	negative regulation of lipid metabolic process	3	55	11.1
	GO:0006641	triglyceride metabolic process	3	58	10.9
	GO:0072578	neurotransmitter-gated ion channel clustering	2	13	10.8
	GO:0019752	carboxylic acid metabolic process	7	575	10.2

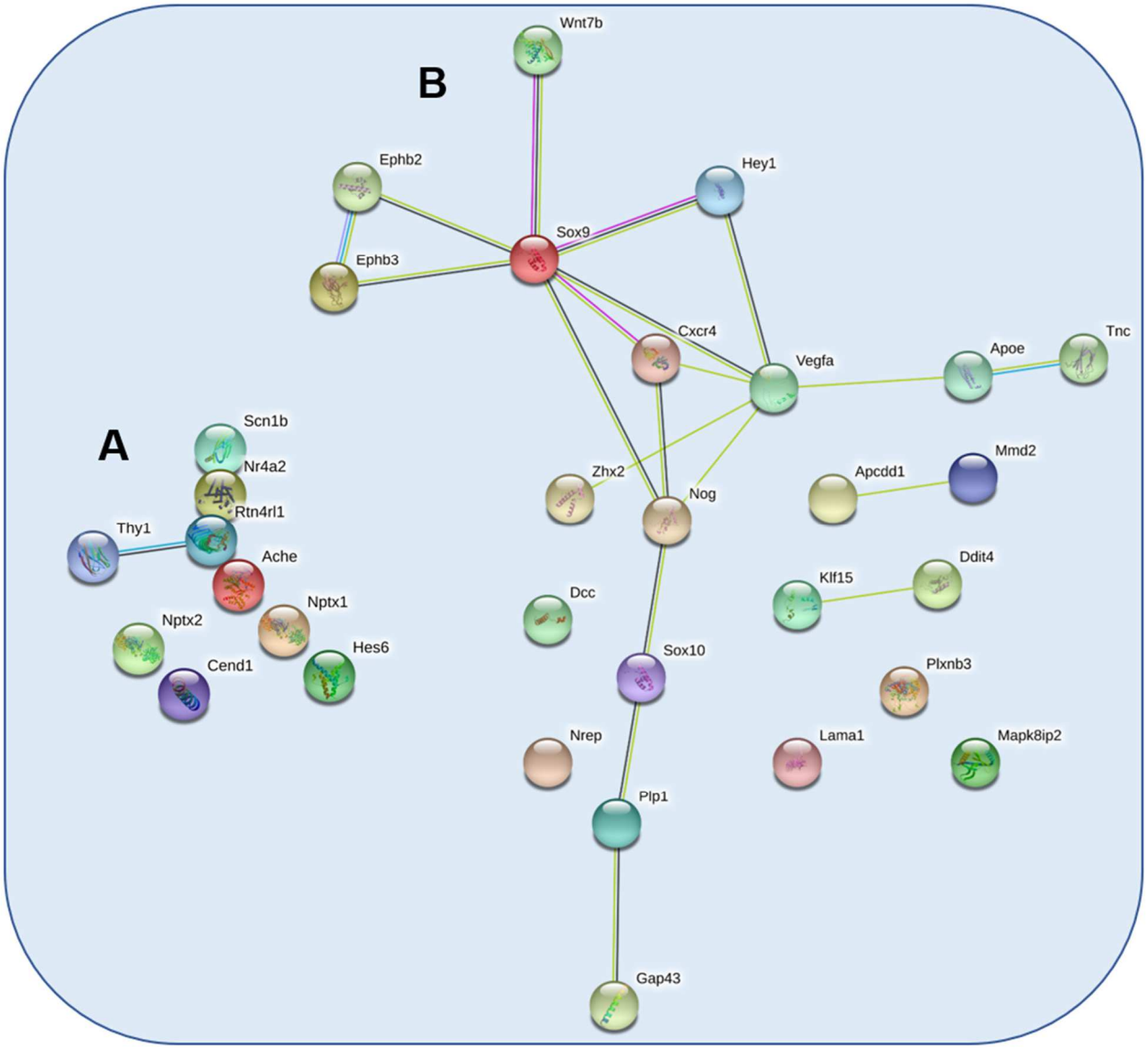

Figure 4.6. DEGs from BAC C12-exposed neurospheres involved in neurogenesis. (A) DEGs involved in the GO biological process of neurogenesis and upregulated in response to BAC C12 exposure. (B) DEGs involved in the GO biological process of neurogenesis and upregulated in response to BAC C12 exposure. n=3 biological replicates per condition; adjusted P-value <0.05.

4.3. Discussion

In the present study, we aimed to characterize the consequences of altered cholesterol biosynthesis on neurodevelopment following exposure to BACs in neurospheres – free floating clusters of NPCs used as an *in vitro* 3-D model for investigating developmental neurotoxicity. Similar to previous findings, BACs altered cholesterol biosynthesis in neurospheres (Herron et al., 2019; Herron et al., 2016) with BAC C12 being a much more potent inhibitor than BAC C16, consistent with our previous reports. However, both BACs impacted neurosphere growth by inducing apoptosis and inhibiting proliferation while AY9944 did not, which suggests that inhibition of cholesterol biosynthesis is not the underlying mechanism for the effects on neurosphere growth. To explore alternative mechanisms responsible for the observed phenotype, we carried out a comprehensive transcriptomic analysis, which revealed the integrated stress response as another potential contributing mechanism.

The integrated stress response is used by cells to adapt to a variety of stressors including endoplasmic reticulum (ER) stress, nutrient deficiency, or hypoxia (Wang et al., 2018). Oxidative stress and mitochondrial dysfunction may play a role in the activation of the integrated stress response as oxidative stress-related genes and mitochondrial complex IV genes were differentially expressed in BAC C12- and BAC C16-exposed neurospheres, respectively. *Atf4,* the main effector of the integrated stress response, transcriptionally activates *Asns, Slc7a11, and Trib3* (Evstafieva et al., 2014), which were upregulated in BAC-exposed neurospheres.

Asns converts aspartate and glutamine to asparagine and glutamate in an ATP-dependent reaction and is upregulated in response to amino acid deprivation (Balasubramanian, Butterworth, and Kilberg, 2013). Slc7a11, also known as xCT, is the light chain subunit of the cystine/glutamate antiporter system x_c^-, which transports cystine, the oxidized form of cysteine, into cells and releases glutamate into the extracellular space. This

oxidative stress-inducible system provides cysteine for the synthesis of glutathione, a major antioxidant molecule (Conrad and Sato, 2012). Therefore, upregulation of Slc7a11 in BAC-exposed neurospheres suggests an oxidative stress response. Finally, Trib3, also known as neuronal cell death inducible putative kinase (Nipk), is an important mediator of ER stress-related neuronal apoptosis (Zhang et al., 2019). Trib3 mediates apoptosis through the dephosphorylation of Akt and subsequent activation of FoxO, which leads to the increased expression of PUMA or p53 up-regulated modulator of apoptosis (Saleem and Biswas, 2017; Zou et al., 2009). Upregulation of Trib3 is consistent with the reduced growth and increased apoptosis observed in BAC-exposed neurospheres. However, these effects did not appear to be associated with altered cholesterol biosynthesis, as AY9944, the positive control for cholesterol biosynthesis inhibition, did not impact neurosphere growth (Herron et al., 2018; **Appendix A, Table A.4.**).

Recently, Ryu et al (2018) showed that BACs reduce the NPC viability through the induction of apoptotic cell death caused by overproduction of reactive oxygen species (ROS) which is associated with mitochondrial dysfunction. BACs, which are also used as eye drop preservatives, have been associated with toxic effects such as "dry eye" and trabecular meshwork degeneration (Datta et al., 2017). That study demonstrated that the underlying mechanistic basis for BACs effects on the eye were due to direct inhibition of mitochondrial function resulting in cytotoxicity of corneal epithelial cells. Therefore, it is plausible that neurospheres exposed to BACs also experience mitochondrial dysfunction, which can lead to the activation of the integrated stress response (Silva et al., 2009).

Although structure activity differences were not observed in terms of neurosphere growth reduction and apoptosis, BAC C12 altered a greater number of genes than BAC C16, many of which are involved in development. Notably, the majority of DEGs involved in neurogenesis were downregulated by BAC C12 exposure. Cholesterol metabolism is critical

for proper neurogenesis. Altered cholesterol biosynthesis has been shown to cause premature differentiation of NPCs (Driver et al., 2016; Francis et al., 2016). Additionally, Francis *et al* (2016) demonstrated that accumulation of the cholesterol precursor, 7-dehydrocholesterol, is responsible for this phenomenon. Although BAC C12 exposure lead to 7-dehydrocholesterol accumulation and downregulation of genes involved in neurogenesis, effects indicative of premature differentiation were not observed with the current experimental paradigm. Therefore, a different model may be needed to examine defects in neurogenesis related to altered cholesterol biosynthesis.

In conclusion, we have demonstrated that BACs reduce neurosphere growth through increased apoptosis and inhibited proliferation, associated with the activation of the integrated stress response. These results reinforce previous studies demonstrating that BAC exposure leads to an increased incidence of NTDs *in utero* and increased apoptosis of rat NPCs at high concentrations *in vitro.* Additionally, the fact that BAC C12 inhibits cholesterol biosynthesis and alters genes involved in neurogenesis indicates the need to more thoroughly investigate the effect of BAC C12 on neurodevelopment. The developmental neurotoxicants ethanol and retinoic acid are known to modulate cholesterol homeostasis (Chen, Costa, and Guizzetti, 2011b; Zhou et al., 2014). Therefore, future work should investigate the potential for BAC C12 to cause adverse neurodevelopmental outcomes through this and related mechanisms.

4.4. Materials and Methods

Materials

Optima LC/MS solvents (chloroform, methanol, methylene chloride, and water), formic acid (Optima LC/MS), and sodium chloride were purchased from Thermo Fisher Scientific (Grand Island, NY). Benzyldimethyldodecylammonium chloride (BAC C12) and benzyldimethylhexadecylammonium chloride (BAC C16) were purchased from Sigma Aldrich (St. Louis, MO). BAC C12 and BAC C16 were dissolved in DMSO to yield 1, 10, 50, and 100

μM stocks and stored at -80°C. The deuterated (d_7-) sterol standard d_7-7-dehydrocholesterol was prepared as reported previously (Xu et al., 2011a; Xu et al., 2011b). d_7-Cholesterol was purchased from Avanti Polar Lipids (Alabaster, AL). $^{13}C_3$-desmosterol and $^{13}C_3$-lanosterol were purchased from Kerafast (Boston, MA). The primary antibody used in immunocytochemistry was mouse anti-Ki67 at a dilution of 1:200 (BD Pharmingen™, San Jose, CA) and the secondary antibody used was Alexa Fluor-conjugated goat anti-mouse IgG at a dilution of 1:1000 (Invitrogen ™, Carlsbad, CA). 4,6-Diamidino-2-phenylindole (DAPI) was purchased from Thermo Fisher Scientific.

Cell culture

The University of Washington Institutional Animal Care and Use Committee approved all animal protocols. Male and female C57BL/6J mice (7 to 8 weeks old) were purchased from Jackson Laboratories (Bar Harbor, ME). Time-mating was conducted with breeding pairs of 2 females and each male, placed in a cage overnight and separated the following morning. On gestation day 13.5 to 14.5, the pregnant dam was euthanized, and embryos were removed from the uterus and transferred to a Petri dish in sterile 1x phosphate buffered saline (PBS). After careful removal of the meninges under a dissection microscope, cortices were dissected from each embryo, and transferred to a 60 mm culture dish containing 1 to 2 mL of neurosphere proliferation media [DMEM/F-12 medium (Gibco®, Grand Island, NY), Non-Essential Amino Acids (1x; Gibco®), GlutaMax (1x; Gibco®), Penicillin (100 IU) plus Streptomycin (100 μg/mL) Strep (Gibco®), Sodium Pyruvate (1x; Gibco®), B27 (1x; Gibco®), 20 ng/mL basic fibroblast growth factor (bFGF) and 20 ng/mL epidermal growth factor (EGF) (PeproTech®, Rocky Hill, NJ)]. Tissues in media were transferred to a 15 mL conical falcon tube and gently dissociated by trituration until clumps were no longer visible. Cells were filtered through a 40 μm sterile cell strainer and seeded in neurosphere proliferation media at either a density of 30,000 cells per well in 6-well plates for sterols analysis,

immunocytochemistry, transcriptomics, and flow cytometry experiments, or a density of 3000 cells per well in a flat-bottom, ultra-low attachment 96-well plate (Corning™, Corning, NY) for growth analysis, and cultured at 37 °C and 5% CO_2/ 95% humidified air. After 2 to 3 days, small neurospheres were formed, with peak neurosphere formation occurring at 5 to 7 days when neurospheres reached approximately 150 to 200 µm in diameter. Each preparation of neurospheres was considered one biological replicate and a minimum of 3 replicates were used for each experiment.

Drug treatment

Neurospheres were exposed to BAC C12, BAC C16, AY9944 (the positive control for cholesterol biosynthesis inhibition) or vehicle control (0.1% DMSO) from day *in vitro* 4 (DIV 4) to DIV 7for sterols analysis, growth analysis, and immunocytochemistry. For transcriptome analyses and flow cytometry, neurospheres were exposed from DIV 4 to DIV 5. Concentrations described in figures and figure legends.

Sterols analysis

On DIV 7, neurospheres exposed to BAC C12, BAC C16, or vehicle control in triplicate wells of a 6-well plate were pelleted and sonicated in ice cold 100 µL 1x PBS to lyse them. Protein mass was measured with the BioRad-DC Protein Assay Kit. Isotopically labeled sterol internal standards (to be used for quantification in the sterols analysis) were added to each neurosphere lysateas follows: 0.5 µg of d_7-cholesterol and d^7-7-dehydrocholesterol, and 0.1 µg of $^{13}C_3$-lanosterol and $^{13}C_3$-desmosterol. Lipid extraction was carried out as previously described in detail (Herron et al., 2018). To extract the lipids, Folch [4 ml chloroform/methanol (2/1, v/v)] and NaCl aqueous solutions (0.9% (w/v), 1 ml) were added to each cell lysate sample and the mixture was briefly vortexed and then centrifuged for 5 min in a clinical tabletop centrifuge at 10°C. The lower (organic) phase was recovered, transferred to a separate glass tube, and the solvent was removed *in vacuo* using a SpeedVac® (Thermo

Fisher Savant). The resulting lipid extracts were re-dissolved in 0.3 mL methylene chloride prior to analysis.

Analysis of sterols was performed by UHPLC-MS/MS using a triple-quadrupole mass spectrometer (API 4000 ™; AB SCIEX, Ontario, Canada) equipped with atmospheric pressure chemical ionization (APCI) as described previously (Herron et al., 2018). For analysis, 30 µL of lipid extract was transferred to an LC vial, dried under a stream of argon, and reconstituted in 30 µL 90% MeOH with 0.1% formic acid. Data are presented as mean ± standard deviation. Statistical analyses were conducted using ANOVA followed by Dunnet's t-test comparing multiple concentrations to a single control, with a P value < 0.05 considered statistically significant. Statistical analyses conducted using GraphPad Prism version 7.00 for Windows.

Growth analysis

Neurosphere growth was evaluated at DIV 7 after exposure to BACs, AY9944 or vehicle control in triplicate wells of a 96-well plate. Brightfield images of neurospheres were captured on an EVOS® FL Auto Imaging System (Thermo Fisher Scientific) using the 10x objective. ImageJ processing and analysis software (NIH) was used to measure the diameter of each neurosphere in each of 3 wells per condition. Only neurospheres greater than 40 µm in diameter were measured. Data are presented as box plots, with individual data-points representing each neurosphere. Statistical analyses were conducted using ANOVA followed by Dunnet's t-test comparing multiple concentrations to a single control, with a P value < 0.05 considered statistically significant. Statistical analyses conducted using GraphPad Prism version 7.00 for Windows (La Jolla, CA).

To evaluate cell count on DIV 7, neurospheres were collected from triplicate wells of a 6-well plate and mechanically dissociated into a single cell suspension for each condition. An aliquot of cell suspension was used for counting and the remaining cell suspension was used for immunocytochemistry. Data are presented as mean ± standard error of the mean.

Statistical analyses were conducted using ANOVA followed by Dunnet's t-test comparing multiple concentrations to a single control, with a *P* value < 0.05 considered statistically significant. Statistical analyses conducted using GraphPad Prism version 7.00 for Windows.

Immunocytochemistry

For determination of cell proliferation by immunocytochemistry, 5-ethynyl-2'-deoxyuridine (EdU) was added to each well at a final concentration of 10 µM for 4 hr before the end of treatment to label cells undergoing proliferation. Neurospheres exposed to BAC C12, BAC C16, or vehicle control in triplicate wells of a 6-well plate were then collected into a pellet and triturated into a single cell suspension of NPCs. NPCs were seeded in untreated neurosphere proliferation medium at a density of 100 000 cells per well in a 4-well Permanox™ plastic chamber slide (Nunc™, Thermo Fisher Scientific) freshly coated with poly-d-lysine (20 µg/mL; Sigma Aldrich) and laminin (2 µg/mL; Corning™, Corning, NY). Cells were left to adhere overnight in the incubator and then fixed with 4% paraformaldehyde (PFA) in PBS for 20 min at room temperature. PFA was aspirated and cells were washed 3 x 5 min with 1x PBS. For immunocytochemistry, the PBS was aspirated, and cells were permeabilized with 3% BSA in PBST (0.5% Triton-X 100 in PBS) for 20 min at RT.

For evaluation of proliferation, fixed cells were first exposed to 10% goat serum in PBST for 1 hr at room temperature and then exposed to Ki67 (1:200) and 5% goat serum in PBST overnight at 4°. Cells were washed with cold PBST for 5 x 5 min. Alexa 568 goat anti-mouse secondary antibody was applied for 1 hr at RT and then cells were washed with cold PBST for 5 x 10 min. After the 4th wash, cells were incubated with 1 ug/mL DAPI for 20 min and washed once again with PBST. Coverslips were applied using Aqua Poly/Mount (Polysciences, Warrington, PA). For EdU staining, the cells underwent an additional processing step prior to blocking per the manufacturer's protocol (MP 10338, Click-iT® EdU Imaging Kit, Thermo Fisher Scientific). For evaluation of apoptosis, cells on slides separate

from those used for proliferation analysis were washed in PBS for 5 min at room temperature and permeabilized in PBST for 5 min. Cells were rinsed with PBS for 2 x 5 min at room temperature. Excess liquid was removed and the TUNEL reaction was conducted per manufacturer's protocol (#TB235, DeadEnd™ Fluorometric TUNEL System, Promega). DAPI incubation was conducted as described followed by application of coverslips using Aqua Poly/Mount.

Fluorescent images of NPCs were captured on an EVOS® FL Auto Imaging System (Thermo Fisher Scientific) using the 20x objective. Images were uniformly adjusted for brightness and contrast. A cell was scored as marker-positive if the cell showed positive staining for DAPI and the marker. At least 500 DAPI-positive cells per condition per biological replicate were quantified and the experimenter was blinded to condition. Data are presented as mean ± standard error of the mean. Statistical analyses were conducted using ANOVA followed by Dunnet's t-test comparing multiple concentrations to a single control, with a *P* value < 0.05 considered statistically significant. Statistical analyses conducted using GraphPad Prism version 7.00 for Windows.

Flow cytometry analysis of cell cycle

Following exposure to vehicle control (DMSO), AY9944, BAC C12, or BAC C16 for 24 hr at 50 nM, neurospheres were pelleted and the supernatant was aspirated. The pellet was resuspended in 500 µl of 10 µg/ml DAPI and 0.1% IGEPAL CA-630 detergent (Sigma I8896) in Tris buffered saline. To lyse cells and release intact nuclei, the pellet was triturated using a 1 mL syringe with a 25-gauge needle. Isolated nuclei were filtered through a 37 µm steel mesh fitted onto a pipette tip. The nuclei suspension was analyzed using a BD™ LSR II cytometer with ultraviolet excitation and DAPI emission collected at >450 nm. Cell cycle was analyzed using the software program FlowJo™. Data are presented as mean ± standard error of the mean. Statistical analyses were conducted using paired Student's t-test with a *P* value

< 0.05 considered statistically significant. Statistical analyses conducted using Microsoft Excel spreadsheet software.

Transcriptomics analysis

Neurospheres exposed to BAC C12, BAC C16, or vehicle control from DIV 4 to DIV 5 in 4 wells of a 6-well plate were pelleted. Pellets (n = 3 biological replicates per condition) were homogenized in 1 mL of QIAzol Lysis Reagent (Qiagen, Germantown, MD). Total RNA was extracted from each sample using the RNeasy Mini Kit (Qiagen) according to the manufacturer's protocol. RNA concentration was quantified using a microplate spectrophotometer (Bio-Tek, Winooski, VT) to quantify the absorbance at 260 nm. RNA integrity was evaluated by formaldehyde agarose gel electrophoresis to visualize the 18S and 28S rRNA bands. Novogene (Chula Vista, CA) confirmed the RNA integrity and purity using an Agilent 2100 BioAnalyzer (Agilent Technologies Inc., Santa Clara, California). Samples with RNA Integrity Number (RIN) of 10.0 or above were submitted for RNA sequencing. Novogene performed the cDNA library construction and sequencing using the Illumina NovaSeq 6000 platform (150 base pairs paired-end, with sequencing depth above 20 million reads per sample).

Raw RNA sequencing reads in FASTQ format were mapped to the mouse genome using HISAT (https://ccb.jhu.edu/software/hisat/index.shtml; Last accessed 8/14/2019) and format conversions were performed using Samtools. Cufflinks (http://cufflinks.cbcb.umd.edu/; Last accessed 8/14/2019) was used to estimate relative abundances of transcripts from each RNA sample. Cuffdiff, a module of Cufflinks, was used to determine differentially expressed genes (DEGs) between comparison control versus BAC C12 and control versus BAC C16. DEGs met the criterion of an adjusted *P* value < 0.05 (corresponding to the allowed false discovery rate of 5%). DEGs were plotted in a Venn diagram to identify common and uniquely expressed genes for each condition. Analysis of

gene ontology (GO) terms for biological processes was performed using iPathwayGuide (Advaita). DEGs were also submitted for STRING (Search Tool for the Retrieval of Interacting Genes/ Proteins) analysis (https://string-db.org/; Last accessed 9/16/2019).

4.5. Acknowledgments

This chapter contains the research article: Josi M. Herron, Hideaki Tomita, Collin W. White, Terrance J. Kavanagh, and Libin Xu, Benzalkonium Chloride Disinfectants Induce Apoptosis, Inhibit Proliferation, and Activate the Integrated Stress Response in a 3-D I*n Vitro* Model of Neurodevelopment*.* Submitted for review to *Toxicology In Vitro*.

The work was supported by the University of Washington Environmental Pathology/ Toxicology Training Program (NIH T32 ES007032-39), the NICHD (R01HD092659), the University of Washington Interdisciplinary Center for Exposures, Diseases, Genomics and Environment (UW EDGE) (P30ES007033), and the University of Washington's Department of Medicinal Chemistry.

4.6. References

Balasubramanian, M. N., Butterworth, E. A., and Kilberg, M. S. (2013, April 15). Asparagine synthetase: Regulation by cell stress and involvement in tumor biology. *American Journal of Physiology - Endocrinology and Metabolism*, Vol. 304. https://doi.org/10.1152/ajpendo.00015.2013

Björkhem, I., Meaney, S., and Fogelman, A. M. (2004). Brain Cholesterol: Long Secret Life behind a Barrier. *Arteriosclerosis, Thrombosis, and Vascular Biology*, Vol. 24, pp. 806–815. https://doi.org/10.1161/01.ATV.0000120374.59826.1b

Chen, J., Costa, L. G., and Guizzetti, M. (2011a). Retinoic acid isomers up-regulate ATP binding cassette A1 and G1 and cholesterol efflux in rat astrocytes: Implications for their therapeutic and teratogenic effects. *Journal of Pharmacology and Experimental Therapeutics*, *338*(3), 870–878. https://doi.org/10.1124/jpet.111.182196

Chen, J., Costa, L. G., and Guizzetti, M. (2011b). Retinoic acid isomers up-regulate ATP binding cassette A1 and G1 and cholesterol efflux in rat astrocytes: Implications for their therapeutic and teratogenic effects. *Journal of Pharmacology and Experimental Therapeutics*, *338*(3), 870–878. https://doi.org/10.1124/jpet.111.182196

Conrad, M., and Sato, H. (2012). The oxidative stress-inducible cystine/glutamate antiporter, system x (c) (-): cystine supplier and beyond. *Amino Acids*, *42*(1), 231–246. https://doi.org/10.1007/s00726-011-0867-5

Datta, S., Baudouin, C., Brignole-Baudouin, F., Denoyer, A., and Cortopassi, G. A. (2017). The Eye Drop Preservative Benzalkonium Chloride Potently Induces Mitochondrial Dysfunction and Preferentially Affects LHON Mutant Cells. *Investigative Ophthalmology and Visual Science*, *58*(4), 2406–2412. https://doi.org/10.1167/iovs.16-20903

Driver, A. M., Kratz, L. E., Kelley, R. I., and Stottmann, R. W. (2016). Altered cholesterol biosynthesis causes precocious neurogenesis in the developing mouse forebrain. *Neurobiology of Disease*, *91*, 69–82. https://doi.org/10.1016/j.nbd.2016.02.017

Evstafieva, A. G., Garaeva, A. A., Khutornenko, A. A., Klepikova, A. V., Logacheva, M. D., Penin, A. A., … Chumakov, P. M. (2014). A sustained deficiency of mitochondrial respiratory complex III induces an apoptotic cell death through the p53-mediated inhibition of pro-survival activities of the activating transcription factor 4. *Cell Death and Disease*, *5*(11). https://doi.org/10.1038/cddis.2014.469

Francis, K. R., Ton, A. N., Xin, Y., O'Halloran, P. E., Wassif, C. A., Malik, N., … Porter, F. D. (2016). Modeling Smith-Lemli-Opitz syndrome with induced pluripotent stem cells reveals a causal role for Wnt/β-catenin defects in neuronal cholesterol synthesis phenotypes. *Nature Medicine*, *22*(4), 388–396. https://doi.org/10.1038/nm.4067

Fritsche, E., Gassmann, K., and Schreiber, T. (2011). Neurospheres as a model for developmental neurotoxicity testing. *Methods in Molecular Biology*, *758*, 99–114. https://doi.org/10.1007/978-1-61779-170-3_7

Herron, J., Hines, K. M., and Xu, L. (2018). Assessment of Altered Cholesterol Homeostasis by Xenobiotics Using Ultra-High Performance Liquid Chromatography–Tandem Mass Spectrometry. *Current Protocols in Toxicology*, *78*(1), e65. https://doi.org/10.1002/cptx.65

Herron, J. M., Hines, K. M., Tomita, H., Seguin, R. P., Cui, J. Y., and Xu, L. (2019). Multiomics Investigation Reveals Benzalkonium Chloride Disinfectants Alter Sterol and Lipid Homeostasis in the Mouse Neonatal Brain. *Toxicological Sciences*, *171*(1), 32–45. https://doi.org/10.1093/toxsci/kfz139

Herron, J., Reese, R. C., Tallman, K. A., Narayanaswamy, R., Porter, N. A., and Xu, L. (2016). Identification of environmental quaternary ammonium compounds as direct inhibitors of cholesterol biosynthesis. *Toxicological Sciences*, *151*(2), 261–270. https://doi.org/10.1093/toxsci/kfw041

Hirata, H., Tomita, K., Bessho, Y., and Kageyama, R. (2001). Hes1 and Hes3 regulate maintenance of the isthmic organizer and development of the mid/hindbrain. *EMBO Journal*, *20*(16), 4454–4466. https://doi.org/10.1093/emboj/20.16.4454

Hrubec, T. C., Melin, V. E., Shea, C. S., Ferguson, E. E., Garofola, C., Repine, C. M., … Hunt, P. A. (2017). Ambient and Dosed Exposure to Quaternary Ammonium Disinfectants Causes Neural Tube Defects in Rodents. *Birth Defects Research*, *109*(14), 1166–1178. https://doi.org/10.1002/bdr2.1064

Ishibashi, M., Ang, S. L., Shiota, K., Nakanishi, S., Kageyama, R., and Guillemot, F. (1995). Targeted disruption of mammalian hairy and Enhancer of split homolog-1 (HES-1) leads to up-regulation of neural helix-loop-helix factors, premature neurogenesis, and severe neural tube defects. *Genes and Development*, *9*(24), 3136–3148. https://doi.org/10.1101/gad.9.24.3136

Kim, J., Lo, L., Dormand, E., and Anderson, D. J. (2003). SOX10 maintains multipotency and inhibits neuronal differentiation of neural crest stem cells. *Neuron*, *38*(1), 17–31.

https://doi.org/10.1016/S0896-6273(03)00163-6

Kim, M., Weigand, M. R., Oh, S., Hatt, J. K., Krishnan, R., Tezel, U., … Konstantinidis, K. T. (2018). Widely used benzalkonium chloride disinfectants can promote antibiotic resistance. *Applied and Environmental Microbiology*, *84*(17). https://doi.org/10.1128/AEM.01201-18

Komada, M., Saitsu, H., Kinboshi, M., Miura, T., Shiota, K., and Ishibashi, M. (2008). Hedgehog signaling is involved in development of the neocortex. *Development*, *135*(16), 2717–2727. https://doi.org/10.1242/dev.015891

KOUDINOV, A. R., and KOUDINOVA, N. V. (2001). Essential role for cholesterol in synaptic plasticity and neuronal degeneration. *The FASEB Journal*, *15*(10), 1858–1860. https://doi.org/10.1096/fj.00-0815fje

Li, W., and LoTurco, J. J. (2000). Noggin is a negative regulator of neuronal differentiation in developing neocortex. *Developmental Neuroscience*, *22*(1–2), 68–73. https://doi.org/10.1159/000017428

Lim, D. A., Tramontin, A. D., Trevejo, J. M., Herrera, D. G., García-Verdugo, J. M., and Alvarez-Buylla, A. (2000). Noggin antagonizes BMP signaling to create a niche for adult neurogenesis. *Neuron*, *28*(3), 713–726. https://doi.org/10.1016/S0896-6273(00)00148-3

Mackenzie, F., and Ruhrberg, C. (2012, April 15). Diverse roles for VEGF-A in the nervous system. *Development*, Vol. 139, pp. 1371–1380. https://doi.org/10.1242/dev.072348

Mauch, D. H., Nägier, K., Schumacher, S., Göritz, C., Müller, E. C., Otto, A., and Pfrieger, F. W. (2001). CNS synaptogenesis promoted by glia-derived cholesterol. *Science*, *294*(5545), 1354–1357. https://doi.org/10.1126/science.294.5545.1354

Pakos-Zebrucka, K., Koryga, I., Mnich, K., Ljujic, M., Samali, A., and Gorman, A. M. (2016). The integrated stress response. *EMBO Reports*, *17*(10), 1374–1395. https://doi.org/10.15252/embr.201642195

Poché, R. A., Zhang, M., Rueda, E. M., Tong, X., McElwee, M. L., Wong, L., … Dickinson, M. E. (2016). RONIN Is an Essential Transcriptional Regulator of Genes Required for Mitochondrial Function in the Developing Retina. *Cell Reports*, *14*(7), 1684–1697. https://doi.org/10.1016/j.celrep.2016.01.039

Porter, J. A., Young, K. E., and Beachy, P. A. (1996). Cholesterol modification of hedgehog signaling proteins in animal development. *Science*, *274*(5285), 255–259. https://doi.org/10.1126/science.274.5285.255

Ryu, O., Park, B. K., Bang, M., Cho, K. S., Lee, S. H., Gonzales, E. L. T., … Kwon, K. J. (2018). Effects of several cosmetic preservatives on ros-dependenapoptosis of rat neural progenitor cells. *Biomolecules and Therapeutics*, *26*(6), 608–615. https://doi.org/10.4062/biomolther.2017.221

Saher, G., Brügger, B., Lappe-Siefke, C., Möbius, W., Tozawa, R. I., Wehr, M. C., … Nave, K. A. (2005). High cholesterol level is essential for myelin membrane growth. *Nature Neuroscience*, *8*(4), 468–475. https://doi.org/10.1038/nn1426

Saleem, S., and Biswas, S. C. (2017). Tribbles pseudokinase 3 induces both apoptosis and autophagy in amyloid-β-induced neuronal death. *Journal of Biological Chemistry*, *292*(7), 2571–2585. https://doi.org/10.1074/jbc.M116.744730

Silva, J. M., Wong, A., Carelli, V., and Cortopassi, G. A. (2009). Inhibition of mitochondrial

function induces an integrated stress response in oligodendroglia. *Neurobiology of Disease*, *34*(2), 357–365. https://doi.org/10.1016/j.nbd.2009.02.005

Vong, K. I., Leung, C. K. Y., Behringer, R. R., and Kwan, K. M. (2015). Sox9 is critical for suppression of neurogenesis but not initiation of gliogenesis in the cerebellum. *Molecular Brain*, *8*(1). https://doi.org/10.1186/s13041-015-0115-0

Wang, S. F., Wung, C. H., Chen, M. S., Chen, C. F., Yin, P. H., Yeh, T. S., … Lee, H. C. (2018). Activated Integrated Stress Response Induced by Salubrinal Promotes Cisplatin Resistance in Human Gastric Cancer Cells via Enhanced xCT Expression and Glutathione Biosynthesis. *International Journal of Molecular Sciences*, *19*(11). https://doi.org/10.3390/ijms19113389

Xu, L., Korade, Z., Rosado, D. A., Liu, W., Lamberson, C. R., and Porter, N. A. (2011). An oxysterol biomarker for 7-dehydrocholesterol oxidation in cell/mouse models for Smith-Lemli-Opitz syndrome. *Journal of Lipid Research*, *52*(6), 1222–1233. https://doi.org/10.1194/jlr.M014498

Xu, L., Liu, W., Shefli, L. G., Fliesler, S. J., and Porter, N. A. (2011). Novel oxysterols observed in tissues and fluids of AY9944-treated rats: A model for Smith-Lemli-Opitz syndrome. *Journal of Lipid Research*, *52*(10), 1810–1820. https://doi.org/10.1194/jlr.M018366

Zhang, J., Han, Y., Zhao, Y., Li, Q., Jin, H., and Qin, J. (2019). Inhibition of TRIB3 protects against neurotoxic injury induced by kainic acid in rats. *Frontiers in Pharmacology*, *10*(MAY). https://doi.org/10.3389/fphar.2019.00585

Zhong, W., Jiang, M. M., Schonemann, M. D., Meneses, J. J., Pedersen, R. A., Jan, L. Y., and Jan, Y. N. (2000). Mouse numb is an essential gene involved in cortical neurogenesis. *Proceedings of the National Academy of Sciences of the United States of America*, *97*(12), 6844–6849. https://doi.org/10.1073/pnas.97.12.6844

Zhou, C., Chen, J., Zhang, X., Costa, L. G., and Guizzetti, M. (2014). Prenatal ethanol exposure up-regulates the cholesterol transporters ATP-binding cassette A1 and G1 and reduces cholesterol levels in the developing rat brain. *Alcohol and Alcoholism*, *49*(6), 626–634. https://doi.org/10.1093/alcalc/agu049

Zou, C. G., Cao, X. Z., Zhao, Y. S., Gao, S. Y., Li, S. De, Liu, X. Y., … Zhang, K. Q. (2009). The molecular mechanism of endoplasmic reticulum stress-induced apoptosis in PC-12 neuronal cells: The protective effect of insulin-like growth factor I. *Endocrinology*, *150*(1), 277–285. https://doi.org/10.1210/en.2008-0794

Chapter 5: Conclusions and Future Directions

Among the more than 80,000 chemicals registered for use today, only 200 have undergone developmental neurotoxicity (DNT) testing according the established guidelines, making DNT one of the least tested health effects of chemicals (Smirnova et al., 2014). This deficit results in a shortage of information on DNT hazards posed by environmental chemicals. To more efficiently characterize DNT hazards, a shift from animal-based hazard assessment to mechanistic approaches has been proposed within the Adverse Outcome Pathway (AOP) framework (Bal-Price et al., 2017). Regulatory and research institutes, including the OECD, EPA, FDA, NIEHS, along with academia and industry, have been actively advancing the development and application of AOPs to facilitate understanding of complex systems of toxicity that result in adverse outcomes (Kleinstreuer et al., 2016). However, use of the AOP framework for neurological outcomes following developmental exposure is hampered by limited knowledge on mechanisms that trigger adverse outcomes (Bal-Price and Meek, 2017). This deficiency has consequences for the development and acceptance of more efficient toxicity testing strategies for potential developmental neurotoxicants, which ultimately impacts our ability to establish regulations that prevent exposure to chemicals that pose a DNT hazard. Addressing this gap, I worked to investigate a novel mechanism by which environmental chemicals could impact neurodevelopment – through the modulation of lipid homeostasis.

Chapter 2 describes structure activity studies in which compounds structurally similar to the known cholesterol biosynthesis inhibitor, AY9944, were investigated for their ability to inhibit cholesterol biosynthesis in mouse and human neuronal cells. Of the compounds tested, a commonly used mixture of BACs exhibited high potency in inhibiting cholesterol biosynthesis at the step of DHCR7, indicated by the accumulation of cholesterol precursors and decreased cholesterol levels as quantified by LC-MS/MS. I also showed that the potency of BACs as

DHCR7 inhibitors decreases with the length of the alkyl chain. Finally, using real-time qPCR analysis, I demonstrated that BACs upregulate genes involved in cholesterol biosynthesis and downregulate genes related to cholesterol efflux, suggesting a feedback response to the inhibition. The findings of this study established the foundation from which the hypothesis of this dissertation was developed, suggesting that exposure to BACs at critical developmental stages could contribute to adverse neurodevelopmental outcomes given their effects on cholesterol homeostasis.

Building on the results from Chapter 2, the goal of the study described in Chapter 3 was to investigate the effects of *in utero* BAC exposure on sterol and lipid homeostasis and to predict the DNT mechanism of BACs using targeted and untargeted mass spectrometry and transcriptomics. In Chapter 2, I established that BACs have differential effects on cholesterol biosynthesis based on the alkyl chain length; therefore, I chose to expose dams to two BACs of different alkyl chain lengths (BAC C12 and BAC C16) at 120 mg/kg/day via diet throughout gestation. In this study, I show for the first time that BACs can cross the placenta and enter the neonatal brain, albeit at low nM concentrations. Transcriptomic analysis of neonatal brains showed that both BACs upregulated genes involved in cholesterol biosynthesis, mediated by SREBP cleavage-activating protein (SCAP)-mediated signaling. Moreover, decreased sterol and glyceride levels were observed in BAC-exposed neonatal brains consistent with the upregulation of SCAP signaling. Consistent with Chapter 2, BAC C12 altered many more genes involved in cholesterol biosynthesis and had a stronger effect on sterol and lipid levels than BAC C16. Interestingly, pathways with critical roles in neurodevelopment were also affected by BAC exposure including LXR/RXR and glutamate receptor signaling. The LXR/RXR signaling pathway was predicted to be inhibited in BAC-exposed brains, consistent with the observed decrease of the cholesterol precursor desmosterol – a ligand for LXR signaling. LXR/RXR signaling has been shown to play a role in cortical layer formation, neuronal migration,

myelination, and neurogenesis. The dysregulation of genes involved in glutamate receptor signaling is also of interest as synaptic signaling processes occur in membrane domains enriched in cholesterol and other lipids. Alterations in sterol and lipid homeostasis in BAC-exposed brains is likely associated with dysregulation of the glutamate receptor signaling pathway, which may have significant consequences for neurodevelopment.

Finally, Chapter 4 describes the effects of BACs on neurospheres, free floating structures of NPCs, which are used as a 3-D, *in vitro* model of neurodevelopment. Consistent with the work described in Chapter 2, I observed potent inhibition of cholesterol biosynthesis at the step of DHCR7 by the short-chain BAC C12, but not by BAC C16. I also show that neurospheres exposed to either BAC decreased in size; however, this was not observed in neurospheres exposed to AY9944, a known DHCR7 inhibitor, suggesting that cholesterol biosynthesis inhibition was not responsible for the reduction in neurosphere growth. Using immunocytochemistry, I further found that both BACs decreased the number of proliferating cells and increased the number of apoptotic cells. To explore mechanisms underlying the similar biological actions of both BACs, I carried out RNA sequencing on neurospheres exposed to each BAC, which revealed activation of the integrated stress response by both BACs. Atf4, the main effector of the integrated stress response, transcriptionally activates Trib3 (a mediator of ER stress-related neuronal apoptosis), Asns (asparagine synthetase), and Slc7a11 (a transporter that mediates the intracellular level of cysteine), all of which were upregulated in BAC-exposed neurospheres. Additionally, BAC C12 downregulated many genes involved in neurogenesis which is most likely associated with the effects of BAC C12 on cholesterol biosynthesis as cholesterol is critical for proper neurogenesis. However, structure activity differences were not observed in this study and future work may be needed to examine BAC C12 exposure and defects in neurogenesis related to altered cholesterol

biosynthesis. Regardless, our findings in this 3-D, *in vitro* model of neurodevelopment suggest BACs may pose a DNT hazard.

Through the work of this dissertation, I have demonstrated that a class of commonly used disinfectants, BACs, alter cholesterol and lipid homeostasis and impact neurodevelopmental processes. These findings are exciting and support a novel mechanism (*i.e*. altered lipid homeostasis) by which environmental chemicals may target neurodevelopment. Additionally, the work presented here adds to a growing body of literature reporting the adverse effects of BACs on neurodevelopment. It is my hope that this work has laid a foundation for future studies and will prompt deeper scrutiny on the use of BAC disinfectants in such a vast array of products.

Going forward, it will be important to characterize the neurological phenotype resulting from exposure to BAC disinfectants during neurodevelopment, including effects on morphology and behavior. Future studies should investigate the effects of BACs on neurogenesis and cortical layer formation as alterations in these processes have been observed in mouse and cellular models with mutations in the post-squalene cholesterol biosynthetic pathway (Driver et al., 2016; Francis et al., 2016). Characterizing effects on learning and behavior will also be of interest, as the cholesterol biosynthesis disorder SLOS has been associated with Autism Spectrum Disorder and other behavioral characteristics (Tierney et al., 2001). My dissertation work identified several, underlying mechanisms of action of BACs associated with alterations in lipid homeostasis, including effects on glutamate receptor signaling and LXR/RXR signaling pathways. Therefore, future studies could elucidate the effects of BACs on these pathways. Finally, it is known that many more males than females are diagnosed with neurodevelopmental disorders (May et al., 2019). Therefore, delineating sex differences in the susceptibility of BAC exposure should be incorporated into the aforementioned studies.

5.1. References

Bal-Price, A., Lein, P. J., Keil, K. P., Sethi, S., Shafer, T., Barenys, M., … Meek, M. E. B. (2017). Developing and applying the adverse outcome pathway concept for understanding and predicting neurotoxicity. *Neurotoxicology*, *59*, 240–255. https://doi.org/10.1016/j.neuro.2016.05.010

Bal-Price, A., and Meek, M. E. B. (2017). Adverse outcome pathways: Application to enhance mechanistic understanding of neurotoxicity. *Pharmacology and Therapeutics*, *179*, 84–95. https://doi.org/10.1016/j.pharmthera.2017.05.006

Driver, A. M., Kratz, L. E., Kelley, R. I., and Stottmann, R. W. (2016). Altered cholesterol biosynthesis causes precocious neurogenesis in the developing mouse forebrain. *Neurobiology of Disease*, *91*, 69–82. https://doi.org/10.1016/j.nbd.2016.02.017

Francis, K. R., Ton, A. N., Xin, Y., O'Halloran, P. E., Wassif, C. A., Malik, N., … Porter, F. D. (2016). Modeling Smith-Lemli-Opitz syndrome with induced pluripotent stem cells reveals a causal role for Wnt/β-catenin defects in neuronal cholesterol synthesis phenotypes. *Nature Medicine*, *22*(4), 388–396. https://doi.org/10.1038/nm.4067

Kleinstreuer, N. C., Sullivan, K., Allen, D., Edwards, S., Mendrick, D. L., Embry, M., … Casey, W. (2016). Adverse outcome pathways: From research to regulation scientific workshop report. *Regulatory Toxicology and Pharmacology : RTP*, *76*, 39–50. https://doi.org/10.1016/j.yrtph.2016.01.007

May, T., Adesina, I., McGillivray, J., and Rinehart, N. J. (2019). Sex differences in neurodevelopmental disorders. *Current Opinion in Neurology*, *32*(4), 622–626. https://doi.org/10.1097/WCO.0000000000000714

Smirnova, L., Hogberg, H. T., Leist, M., and Hartung, T. (2014). Developmental neurotoxicity - challenges in the 21st century and in vitro opportunities. *ALTEX*, *31*(2), 129–156. https://doi.org/10.14573/altex.1403271

Tierney, E., Nwokoro, N. A., Porter, F. D., Freund, L. S., Ghuman, J. K., and Kelley, R. I. (2001). Behavior phenotype in the RSH/Smith-Lemli-Opitz syndrome. *American Journal of Medical Genetics*, *98*(2), 191–200. https://doi.org/10.1002/1096-8628(20010115)98:2<191::aid-ajmg1030>3.0.co;2-m

Appendix A: Assessment of Altered Cholesterol Homeostasis by Xenobiotics Using Ultra-high Performance Liquid Chromatography-tandem Mass Spectrometry

A.1. Introduction

Cholesterol biosynthesis is a complex process involving many intermediates but can be broadly divided into two segments: pre-squalene and post-squalene syntheses. In pre-squalene synthesis, isoprenoids formed from the mevalonate pathway undergo a series of condensation reactions that lead first to squalene and then to squalene epoxide upon epoxidation. The 3-hydroxy-3-methyl-glutaryl-CoA reductase in the mevalonate pathway is the rate-determining step of the entire cholesterol synthesis pathway. In post-squalene synthesis, cyclization of squalene epoxide leads to the first sterol in the pathway, lanosterol, which is diverted into one of two pathways that both progress through a series of dehydrogenations reducations, and demethylations (see Chapter 1, **Figure 1.1**; Kelley and Herman, 2001). Once formed, cholesterol is further metabolized through both enzymatic (Pikuleva, 2006) and free radical (Yin, Xu, and Porter, 2011) processes to produce a variety of oxysterols (**Figure A.1**; Mutemberezi, Guillemot-Legris, and Muccioli, 2016).

As noted in previous chapters, cholesterol plays important roles in embryonic development, synapse formation and function, and myelination. Alterations in cholesterol homeostasis, especially deficiency of cholesterol and accumulation of its precursors, contribute to a variety of malformation disorders (Porter and Herman, 2010). The most common cholesterol biosynthesis disorder, Smith-Lemli-Opitz syndrome (SLOS), is characterized by multiple congenital malformations, developmental delay, cognitive impairment, and behavior problems. Cholesterol-derived oxysterols also have vast cellular

roles as lipid mediators, targeting nuclear receptors, regulatory proteins, and cell membrane receptors (Mutemberezi et al., 2016).

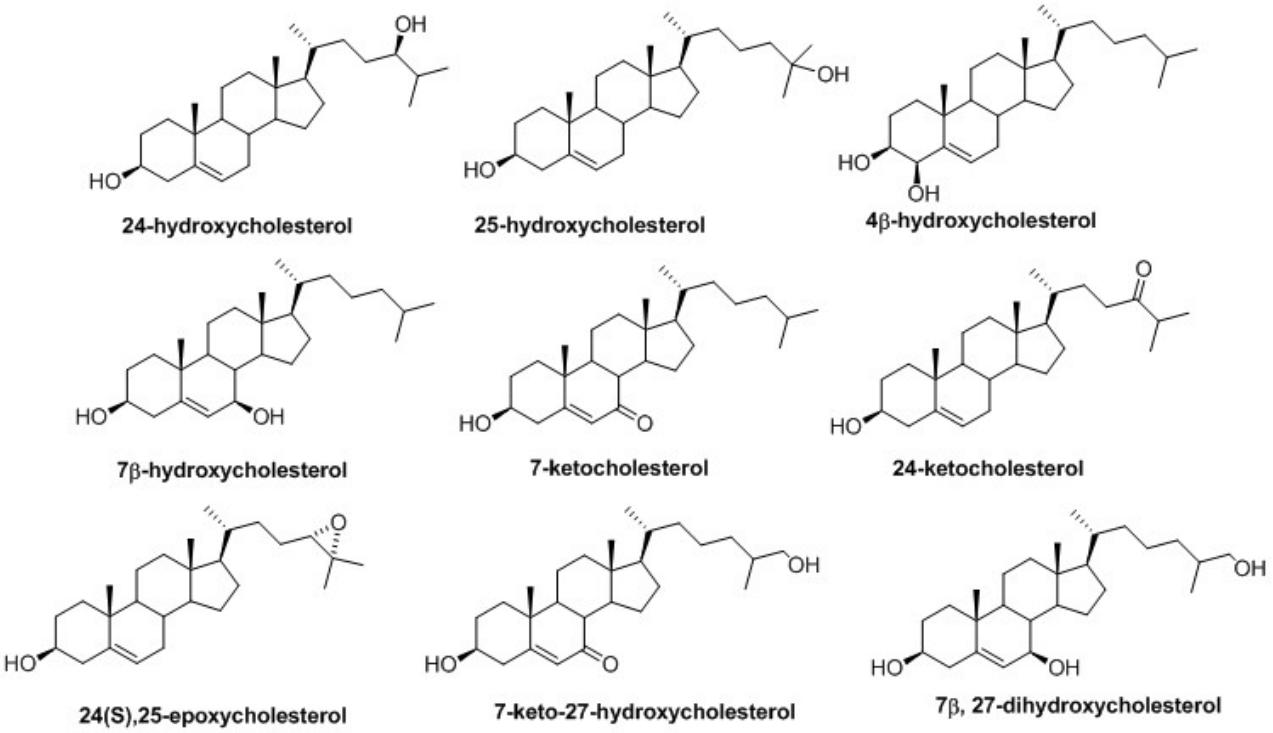

Figure A.1. Structures of the main cholesterol-derived oxysterols.

Given the biological importance of the cholesterol biosynthetic pathway, the effect of xenobiotics on cholesterol homeostasis has become increasingly of interest. Alterations in cholesterol homeostasis have been shown to play a role in the developmental toxicity of ethanol and retinoic acid (Guizzetti, Chen, and Costa, 2011). Several pharmacological agents have been found to be inhibitors of various steps of cholesterol biosynthesis (Canfran-Duque et al., 2013; de Medina et al., 2010; Hall et al., 2013; Kim et al., 2016; Korade et al., 2016). First-trimester exposure to pharmacological modulators ofDHCR7, the enzyme that converts 7-dehydrocholesterol (7-DHC) to cholesterol, is associated with adverse fetal outcomes (Boland and Tatonetti, 2016). Recently, we demonstrated that a

commonly used class of disinfectants, quaternary ammonium compounds, inhibit DHCR7 and alter cholesterol homeostasis in neuronal cells (Herron et al., 2016).

This protocol describes methods for the quantitative assessment of altered post-squalene cholesterol homeostasis and subsequent oxysterol formation in various sample types using ultra-high performance liquid chromatography-tandem mass spectrometry (UHPLC-MS/MS) and isotopically labeled internal standards.

A.2. Basic Protocol 1: Lipid Extraction

To assess changes in cholesterol homeostasis, lipids must be isolated prior to analysis. The Folch extraction method is commonly used to extract both simple and complex lipids from virtually any type of biological sample (Folch, Lees, and Sloane Stanley, 1957). With this method, a chloroform-methanol extracting solvent is used in the presence of isotopically labeled sterol and oxysterol internal standards to disrupt lipoproteins and cell membranes and to solubilize lipids from either cells grown in culture or harvested tissues. The presence of internal standards accounts for any loss of endogenous sterols or oxysterols during the extraction process and enables quantitation following UHPLC- MS/MS analysis. Finally, the addition of an aqueous sodium chloride solution yields a layered mixture with a lower organic layer containing the lipids. This lower organic layer is collected, dried, reconstituted in methylene chloride, and stored at -80°C until UHPLC-MS/MS analysis.

Materials

Cultured cells rinsed with 1 x PBS and centrifuged into a pellet or any harvested biological tissue stored at -80°C

1x phosphate buffered saline (PBS; see recipe) chilled

DC™ Protein Assay Kit II (Bio-Rad, 5000112)

Sterol internal standard (see recipe), 500/100 µg/ml and 50/10 µg/ml

Oxysterol internal standard (see recipe), 100 µg/ml and 10 µg/ml

Folch solution [chloroform:methanol = 2:1, with 1 mM butylated hydroxytoluene (BHf) and 1 mM triphenylphospine (PPh3)], chilled (see recipe)

Methylene chloride (LC-MS grade)

0.9% (w/v) sodium chloride, aqueous (see recipe)

10-ml polystyrene, disposable serological pipets (Fisherbrand, 13-678-11E) S1 pipet filler (Thermo Scientific)

10-ml disposable conical-bottom, Pyrex glass centrifuge tubes (Coming, 99502-10) Sorvall™ Legend™ Xl centrifuge, chilled to 4°C (Thermo Scientific)

Ultrasonic bath (Fisher Scientific)

Flat-bottom, clear 96-well plate for protein assay (Fisherbrand, 12-565-501) 8-channel pipettor, 10 to 100 µland 30 to 300 µl (Transferpette® S-8) Absorbance microplate reader for protein assay

Mechanical pipet pump (Bel-Art Products)

Disposable 9-in. glass Pasteur pipets (Fisherbrand, 13-678-20D) Savant™ SpeedVac™ High Capacity Concentrator (Thermo Scientific)

Savant™ Refrigerated Vapor Trap (Thermo Scientific), chilled prior to extraction Deep Vacuum Oil Pump for SpeedVac™ Concentrator (Thermo Scientific) Screw caps for 10-ml disposable glass tubes (Fisherbrand, 14-959-36A)

Glass screw-thread vials (Thermo Scientific, C40001W) Caps for screw-thread vials (Thermo Scientific, C500053B) Polytron™ PT 1200 tissue homogenizer (Kinematica)

Extraction of lipids from cultured cells

1a. For adherent cells cultured in 100-mm dishes:

i. Remove culture dishes from incubator, place on ice, and allow to chill for 5 min before proceeding.

ii. Aspirate medium from cells using a pipette filler fitted with 10-ml serological pipette.

iii. Add 5 ml chilled 1 x PBS, gently swirl dish without disrupting cells, and aspirate

iv. lx PBS.

v. Add another 5 ml chilled 1 x PBS.

vi. Using cell scraper, lift adherent cells from dish by scraping back and forth across the dish.

vii. Using a pipette filler fitted with a 10-ml serological pipette, aspirate cells suspended in 5 ml of 1 x PBS and transfer to 10-ml disposable glass centrifuge tube.

viii. Centrifuge cells into pellet for 5 min at 1693 x g, 4°C.

ix. Aspirate the supernatant and either proceed to step 2 or store pellets at - 80°C.

1b. For floating cells cultured in 150-mm dishes:

i. Collect cell suspension with a pipette filler fitted with a 10-ml serologicalpipette and transfer to 10 ml disposable glass centrifuge tube.

ii. Centrifuge cells into pellet for 5 min at 1693 x g, 4°C.

iii. Aspirate the supernatant.

iv. Add 5 ml chilled 1x PBS and pipette up and down five times to dissociate.

v. Centrifuge again for 5 min at 1693 x g, 4°C.

vi. Aspirate the supernatantand either proceed to step 2 or store pellets at - 80°C.

2. Place freshly pelleted cells or cell pellets that have been stored at - 80°C on ice.

If pellet is not already in a 10-ml glass tube, it needs to be transferred to one at this point ; otherwise proceed to step3. To t ransfer pellet, add 150 µl of 1 x *PBS to the original tube, pipette up and down to dissociate, and transfer cell suspension to a 10-ml glass tube. Add another 150 µl to the original tube, pipette up and down, and transfer to the 10-ml glass tube, ensuring that all cells have been collected. Proceed to step 3.*

3. Add 300 µl chilled 1 x PBS to each sample and pipette up and down approximately five times to dissociate cell pellet.

4. Sonicate cell suspension for 30 min to lyse cells, ensuring water in sonication bath remains ice-cold.

The lysate may be stored at -80°C until extraction; otherwise, continue with the extrac- tion and keep samples on ice.

Sonication is the preferred method of lysing cells when lipid extracts will be used for additional analyses, such as untargeted lipidomics, which is often performed in our lab. Lysis buffers can introduce unwanted background signal in such assays; therefore, sonication is used to circumvent this issue.

5. Conduct protein assay to determine the amount of protein in each cell lysate. A microplate reader is used at this step to measure absorbance and determine protein concentration.

Further details can be found in the DC Protein Assay Instruction Manual provided by Bio-Rad (LIT448).

a. Prepare the working reagent by adding 20 µl of Reagent S per each milliliter of reagent A that will be needed for the run.
b. From the 20 mg/ml BSA standard stock provided with the kit, prepare a BSA standard dilution series in 8 tubes labeled #1-8.
    i. To tube #8, add 50 µl BSA stock to 150 µl distilled H2O and mix well to yield a 5 mg/ml solution
    ii. Transfer 100 µl from tube #8 to 100 µl of distilled H2O in tube #7 and mix well to yield a 2.5 mg/ml solution.
    iii. Transfer 100 µl from tube #7 to 100 µl of distilled H2O in tube #6 and mix well to yield a 1.25 mg/ml solution.
    iv. Transfer 100 µl from tube #6 to 100 µl of distilled H2O in tube #5 and mix well to yield a 0.625 mg/ml solution.
    v. Transfer 100 µl from tube #5 to 100 µl of distilled H2O in tube #4 and mix well to yield a 0.313 mg/ml solution.
    vi. Transfer 100 µl from tube #4 to 100 µl of distilled H2O in tube #3 and mix well to yield a 0.155 mg/ml solution.

vii. Transfer 100 µl from tube #3 to 100 µl of distilled H2O in tube #2 and mix well to yield a 0.075 mg/ml solution.

viii. Add only 100 µl of distilled H2O to tube #1 to yield a 0.0 mg/ml solution.

c. Pipette 5 µl of each BSA standard into triplicate wells of a flat bottom, clear 96-well plate.

d. Pipette 5 µl of each cell lysate into duplicate wells of the flat-bottom, clear 96-well plate.

e. Add 25 µl per well of the working reagent using an 8-channel 10 to 100 µl pipettor.

f. Add 200 µl per well of Reagent B, provided in the assay kit, using an 8- channel 30 to 300 µl pipettor, in the same order in which the working reagent was added.

g. Place plate into microplate reader and mix for 5 sec if the microplate reader has a mixing function; otherwise, gently agitate the plate by hand to mix the reagents.

h. After 15 min, read absorbances using the plate reader at 750 nm.

Absorbances are stable for 1 hr.

i. To calculate protein concentration, subtract the average optical density (OD of the 0.0 mg/ml standard) from the average OD of each BSA standard.

j. Plot these data and determine the slope and y-intercept of the line.

k. Subtract the average OD of the 0.0 mg/ml standard from the average OD of each sample to obtain a corrected OD value.

l. Calculate the concentration of protein in each sample by subtracting the y-intercept from each corrected OD value and then dividing by the slope.

m. Multiply by the total volume of lysate (300 µl) to obtain the absolute amount of protein in micrograms for each sample. This value will be used as a normalization factor in step 26 in Basic Protocol 2.

6. Add 50/10 µg/ml sterol and 10 µg/ml oxysterol internal standard solutions to each sample and the extraction blank.

Note that throughout the text, sterol internal standards are annotated 50/10 or 500/100. 50 or 500 refers to the amount of d_7-cholesterol and d_7-7-DHC and 10 or 100 refers to the amount of $^{13}C_3$-lanosterol and $^{13}C_3$-desmosterol.

a. For sterols, add 0.5 µg d7-cholesterol and rd 7-DHC and 0.1 µg $^{13}C_3$-lanosterol and $^{13}C_3$-desmosterol per 100 µg protein.
b. For oxysterols, add 0.1 µg oxysterol internal standard per 100 µg protein.

7. Add 1 ml of aqueous sodium chloride solution to each sample.
8. Vortex each sample for 30 sec.
9. Add 4 ml of chilled Folch solution to each sample.
10. Vortex each sample for 30 sec.
11. Centrifuge samples for 5 min at 1693 x g, 4°C.

*Following centrifugation, the samples should separate into two layers, a lower organic phase consisting primarily of chloroform and lipids, and an upper aqueous phase consisting of methanol, water, and non-lipid contaminants. Note that a layer of protein may be visible between these layers, depending on the amount of starting material (**Figure A.2**).*

Figure A.2. Representative image of aqueous (top), protein (thin, middle layer) and lipid (bottom) layers from a cell sample.

12. Recover the lower phase using a pipet pump fitted with a 9-in. glass Pasteur pipet and transfer to a glass centrifuge tube.

    Collect a small amount of air into the pipet. Lower the glass pipet into the lower phase by gently pushing aside the protein layer. Discharge the air in the pipet to gently disperse any liquid that may have entered the pipet tip as it passed through the aqueous phase. Collect the organic phase with the pipet and discharge into a glass centrifuge tube. This may require two full pipet volumes. Leave a small amount of organic phase at the bottom of the tube to avoid collecting the protein pellet. 1f part of the protein pellet or upper phase is collected, re-disperse the sample back into the tube and repeat steps 10 to 12.

    Use of a mechanical pipet pump versus a pipet bulb is recommended here for better control when removing liquid near the aqueous-pellet-organic interface.

13. To dry samples in the SpeedVac, turn on the Savant™ Refrigerated Vapor Trap and allow to cool for 1 hr until the ready indicator light turns green.

    It is recommended that the Refrigerated Vapor Trap be chilled prior to initiating the extraction.

14. Uncap samples and place in the Savant™ SpeedVac™ High Capacity Concentrator, ensuring that the samples in the centrifuge are balanced.
15. Next, turn on the Deep Vacuum Oil Pump and adjust gas ballast control knob to position "I."

    Adjustment of the gas ballast allows any volatile organic solvent that has not be collected in the cold trap to escape the vacuum pump. This will prolong the life of the oil in the vacuum pump.

16. Finally, close the lid on the Savant™ SpeedVac1M High Capacity Concentrator, tum the Concentrator switch to "On," and set the Drying Rate switch to "Low."
17. Drying should take approximately 2 hr.
18. Once dry, reconstitute extracts by adding 300 µl methylene chloride, capping samples, and vortexing for 3 sec.

    Given the small volume of the reconstituted extract, it may be beneficial to microcentrifuge the samples briefly to collect any liquid that is on the wall of the tube.

19. Transfer reconstituted extracts to a labeled screw top vial, cap, and store at - 80°C until UHPLC-MS/MS analysis.

Extraction of lipids from biological tissues

20. Remove tissues from - 80°C and place on ice.

    If tissues are not already in a 10-ml glass tube, it needs to be transferred to one at this point. Otherwise proceed to step 21.

21. Record the weight of each tissue.

Ideally, 10 to 100 mg of tissue yield is sufficient for assessing changes in sterol homeostasis. Analysis of tissues larger than 100 mg may require additional dilution of the lipid extract prior to UHPLC-MS/MS analysis. Analysis of tissues less than 10 mg may result in low peak areas for less abundant analytes.

22. Add 500/100 µg/ml sterol and 100 µg/ml oxysterol internal standard solution separately to each sample.
    a. For sterols, add 5 µg d7-cholesterol and d7-7-dehydrocholesterol and 1 µg $^{13}C_3$- lanosterol and $^{13}C_3$-desmosterol per 100 mg tissue.
    b. For oxysterols, add 1 µg oxysterol internal standard per 100 mg tissue.
23. Add 4 ml of chilled Folch solution to each sample.
24. Vortex each sample for 30 sec.
25. Rinse the probe of the tissue homogenizer in a separate fresh, chilled Folch solution.
26. Homogenize each tissue sample thoroughly.

    Continue to rinse the blade with fresh, chilled Folch solution in between samples to prevent cross contamination.

27. Add 1 ml of aqueous 0.9% sodium chloride solution to each sample.
28. Follow steps 8 to 17, above, except for step 14. Tissue samples below 100 mg should be reconstituted in 300 µl methylene chloride and samples at or above 100 mg should be reconstituted in 1 ml methylene chloride.
29. Transfer reconstituted extracts to a labeled screw top vial, cap, and store at - 80°C until UHPLC-MS/MS analysis.

A.3. Basic Protocol 2: UHPLC-MS/MS Analysis of Cholesterol Homeostasis

This section describes the analysis of sterols or cholesterol-derived oxysterols in the lipid extracts using UHPLC-MS/MS. It should be noted that the concentration of endogenous oxysterols in biological samples is typically much lower (1/100 or less) than that of sterols. Thus, separate sample preparation and UHPLC-MS/MS analyses are conducted for sterols and oxysterols. In this protocol, lipid extracts, prepared in Basic Protocol 1, are dried and reconstituted in mobile phase, and then a 10-µl aliquot is injected into the UHPLC-MS/MS system. Reversed-phase chromatography is used to elute the sample through a C18 column with an isocratic 90% methanol mobile phase, separating the oxysterols and sterols. Selective reaction monitoring is then employed to monitor the dehydration process of the ion [M+H]+ or [M+ H-H2O] + (Finno et al., 2016; Fliesler et al., 2018). The total time for analysis is 15 min per run for sterols and oxysterols, with oxysterols eluting between 0.5 and 6.0 min and sterols eluting between 6 and 12.5 min. Subsequent quantitation is based on relative response factors (RRFs) obtained from the standard sample, which is prepared with a mix of standard sterols, oxysterols, and corresponding isotopically labeled internal standards. Using the RRF for each sterol or oxysterol analyte allows the calculation of each endogenous sterol and oxysterol con- centration based on the peak area ratio and internal standard concentration in the sample. Finally, statistical analyses are used to determine significant changes in sterol and/or cholesterol-derived oxysterol levels, which indicate changes in cholesterol homeostasis.

Materials

50/10 µg/ml sterol internal standard (see recipe) 10 µg/ml sterol standard (see recipe)

Argon source

Reconstituted extract (from Basic Protocol 1, step 12)

Mobile phase: 90% methanol with 0.1% formic acid (see recipe) 10 µg/ml oxysterol internal standard (see recipe)

10 µg/ml oxysterol standard (see recipe) Methanol (LC-MS grade)

Autosampler vials: glass crimp/snap top vials (11 mm) with fused 500-µl insert (Thermo Scientific, C40001-LV1)

Reacti-Vap™ Evaporator (Thermo Scientific) with argon gas supply

Pre-slit snap caps with PTFE lining for 11-mm glass vials (Thermo Scientific, C4011-55)

C18 column (Kinetex®, 100 mm x 2.1 mm, 1.7 µm particle diameter; Phenomenex)

Triple-quadrupole mass spectrometer equipped with an atmospheric-pressure chemical ionization source (Sciex QTRAP® 6500™ system)

ACQUITY UPLC® liquid chromatography system with binary solvent, sample, and column manager (Waters®)

Computer interface for mass spectrometer with Windows operating system Analyst® 5.1 instrument control and data processing software (2013 SCIEX

Analyst® 5.1, version 1.6.2)

Waters® ACQUITY Console instrument component software (2013 Waters®, version 1.60)

Microsoft® Excel® (Microsoft Corp.)

Sample preparation for sterols

1. On day of analysis, prepare standard sample by adding 2 µleach of the 50/10 µg/ml sterol internal standard and 10 µg/ml sterol standard to an autosampler vial.

2. Wash needles of Reacti-Vap™ Evaporator with methanol, let air-dry for 1 min.

3. Dry standard sample undera gentle flow of argon using the Reacti-Vap™ Evaporator and reconstitute in 100 µl mobile phase.

This yields a standard sample containing 1 µg/ml of d_7-7-DHC and d_7-cholesterol, 0.2 µg/ml each of $^{13}C_3$-desmosterol and $^{13}C_3$-lanosterol, and 0.2 µg/ ml all sterol standards. These amounts are similar to the amount of internal standard used in the samples. This is important as quantitation relies on single point calibration.

4. Cap with pre-slit snap cap and vortex 3 sec.

5. For each sample, prepare a 10 x dilution of reconstituted extract (from Basic Protocol 1, step 18 or 28) by transferring 10 µl to a glass autosampler vial, drying under argon, and reconstituting in 100 µl mobile phase.

   Further dilution or concentration of samples may be needed based on instrument sensitivity and nature of the sample.

6. Cap with pre-slit snap cap and vortex each sample 3 sec.

Sample preparation for oxysterols

7. On day of analysis, prepare standard sample by adding 2 µl each of the 10 µg/ml oxysterol internal standard and 10 µg/ml oxysterol standard to an autosampler vial.

8. Wash needles of Reacti-Vap™ Evaporator with methanol, and let air-dry.

9. Dry under argon using the Reacti-Vap™ Evaporator and reconstitute in 100 µl mobile phase.

   This yields a standard sample containing 0.2 µglml of oxysterol standards and internal standard, which is similar to the amount of internal standard used in the samples. This is important as quantitation relies on single point calibration.

10. Cap with pre-slit snap cap and vortex 3 sec.

11. Prepare a 1:1 dilution of the reconstituted extract from Basic Protocol 1, step 18 or 28, by transferring 40 µl to a glass autosampler vial, drying under argon using a Reacti-Vap™ Evaporator (washing needles with methanol and allowing to air-dry prior to use), and reconstituting in 40 µl mobile phase.

    Further dilution or concentration of samples may be needed based on instrument sensitivity and nature of the sample.

    A minimum volume of 40 µl is needed in the autosampler vial to provide adequate depth for the inject ion needle to draw sample.

12. Cap with pre-slit snap cap and vortex each sample 3 sec.

Analysis of sterols and oxysterols using UHPLC-MS/MS

This protocol is designed for the following instrumentation: Sciex QTRAP® 6500™ system with an atmospheric-pressure chemical ionization source and the ACQUITY UPLC® liquid chromatography system, which consists of a binary solvent manager, sample manager, and column manager. The instrumentation is controlled by the Analyst® software and the ACQUITY UPLC® Console instrument component software.

13. Build an acquisition method in the instrumentation software following the parameters outlined in **Table A.1**, including the mass transitions outlined for sterols, oxysterols, and corresponding internal standards in Tables **A.2 and A.3.**

    As noted previously, one acquisition method may be used for both sterols and oxysterols, but often the amount of oxysterols is much lower than sterols in biological samples. Therefore, two separate acquisition methods are recommended, as the samples will need to be prepared at much higher concentrations for oxysterols than for sterols. Steps 14 to 19, below, describe a general protocol for either type of analysis.

14. Equilibrate column and mass spectrometer to the parameters outlined in **Table A.1.**

Table A.1. UHPLC-MS/MS parameters.

UHPLC Conditions	
Column	Kinetex® C18, 100 mm x 2.1 mm, 1.7µm particle diameter
Injection volume	10 µL
Flow rate	0.4 mL/min
Mobile phase	90% methanol with 0.1% formic acid
MS/MS Conditions	
Declustering potential	80 V
Entrance potential	10 V
Collision energy	25 V
Collision cell exit potential	20 V
APCI Conditions	
Nebulizer current	3 mA
Temperature	300°C
Curtain gas	20 psi
Ion source gas	55 psi

Table A.2. Sterols and internal standards transitions and retention times.

Analyte Name	**Quadrupole 1 (m/z)**	**Quadrupole 3 (m/z)**	**Retention Time (min)**	**Peak ID**
7-Dehydrodesmosterol	365.3	365.3	5.88	A
Zymosterol	367.3	367.3	6.84	B
Desmosterol	367.3	367.3	7.32	C
$^{13}C_3$-Desmosterol	370.3	370.3	7.30	D
8-Dehydrocholesterol	367.3	367.3	7.81	E
d_7-7-Dehydrocholesterol	374.3	374.3	7.93	F
7-Dehydrocholesterol	367.3	367.3	8.02	G
Lathosterol	369.3	369.3	9.57	H

Analyte Name	Quadrupole 1 (m/z)	Quadrupole 3 (m/z)	Retention Time (min)	Peak ID
d_7-Cholesterol	376.3	376.3	9.96	I
Cholesterol	369.3	369.3	10.09	J
$^{13}C_3$-Lanosterol	412.3	412.3	11.53	K
Lanosterol	409.3	409.3	11.54	L

Table A.3. Oxysterols and internal standards transitions and retention times.

Analyte Name	Quadrupole 1 (m/z)	Quadrupole 3 (m/z)	Retention Time (min)	Peak ID
7β,27-dihydroxycholesterol	401.3	383.3	0.93	M
7-keto-27-hydroxycholesterol	417.3	399.3	0.97	N
24-hydroxycholesterol*	385.3	367.3	1.69	O
25-hydroxycholesterol*	385.3	367.3	1.69	O
24-ketocholesterol	383.3	365.3	1.84	P
24(S),25-epoxycholesterol	383.3	365.3	1.97	Q
7β-hydroxycholesterol	385.3	367.3	2.85	R
d_7-7-ketocholesterol	408.3	390.3	3.12	S
7-ketocholesterol	401.3	383.3	3.17	T
4β-hydroxycholesterol	385.3	367.3	5.60	U

15. Once equilibrated, inject a blank sample to verify the column is in good condition and the instrument is running properly.

16. Inject the extraction blank, which contains internal standard, and evaluate for unwanted analyte that may have been introduced in the extraction process or from the internal standard.

    In the case that analyte has been introduced into the extraction blank, see step 24, below.

17. Inject 10 µl of the standard sample and check that the chromatograms appear similar to those shown in **Figures A.3 and A.4.**

    See Troubleshooting for guidance if unexpected changes in peak intensity or retention time occur.

18. Build the sample batch so that biological samples are randomized and there is an injection of the standard sample at the beginning, middle, and end of the run.

19. Submit the sample batch to the run queue.

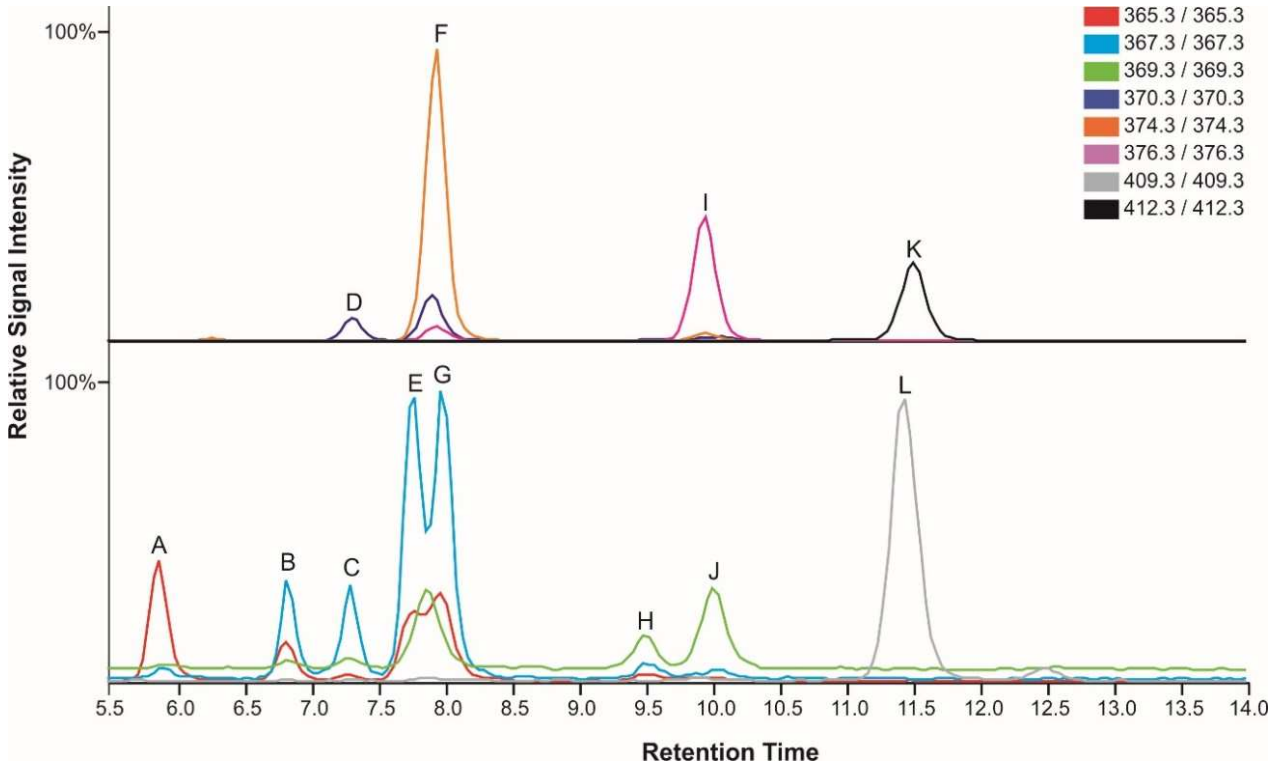

Figure A.3. LC-MS chromatogram of the sterol standard sample, including the internal standards $^{13}C_3$-desmosterol, d_7-7-DHC, d_7-cholesterol, and $^{13}C_3$-lanosterol (top panel) and all sterol standards (bottom panel). Mass transitions are denoted in color legend.

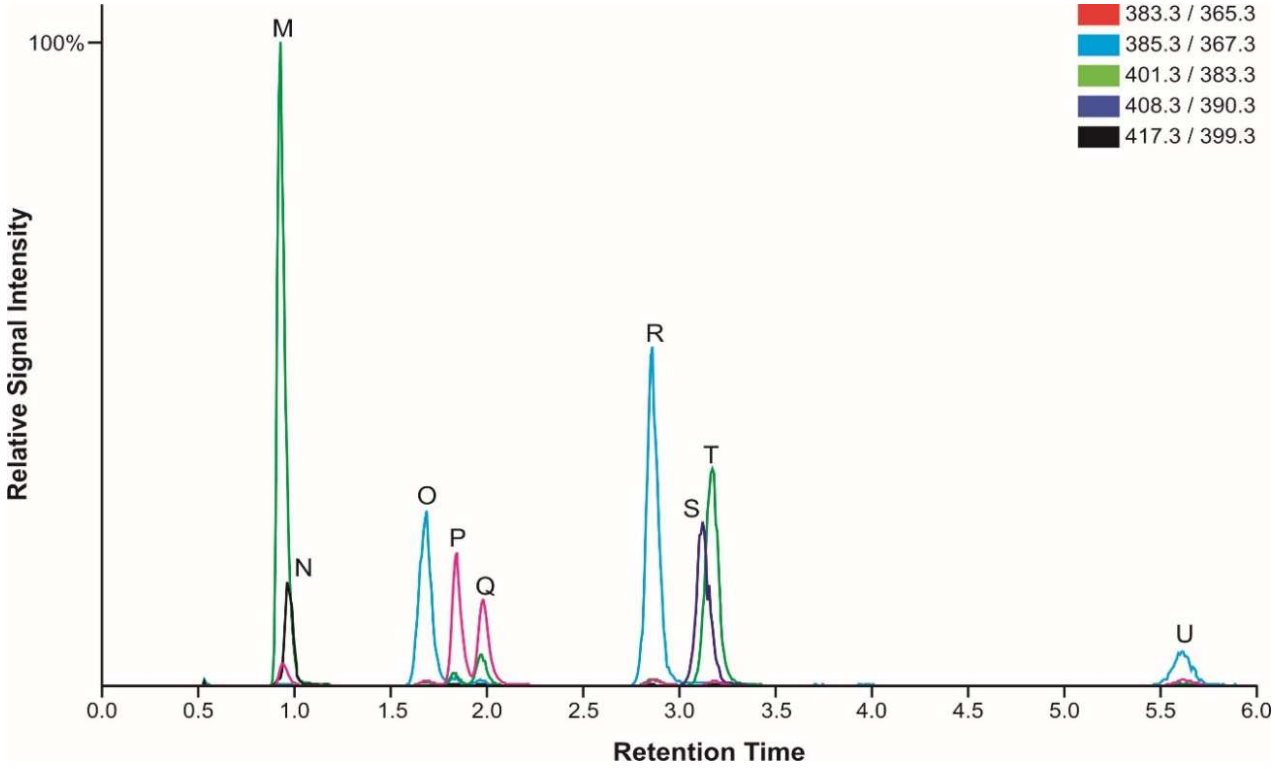

Figure A.4. LC-MS chromatogram of the oxysterol standard sample, including the internal standard d_7-7-ketocholesterol (peak S) and all oxysterol standards. Mass transitions are denoted in color legend.

Quantitation of sterols and oxysterols

20. Within the Analyst® software, set up the quantitation method to allow for automated peak integration.
    a. In quantitation mode, select a standard sample as the representative sample to use.
    b. In the internal standards table, enter each internal standard along with its mass transition.
    c. For each analyte listed in the table, select the internal standard that will be used to calculate the area ratio for that specific analyte.
    d. Select the integration tab and ensure that the correct peak is selected for

each analyte and internal standard. Adjust the retention time if needed.

21. Using the quantitation method, conduct automated peak integration.
    a. Integrate the peaks of each analyte and internal standard for all extraction blanks, samples, and standard samples injected.
    b. Review individual peaks for proper integration and consistency of peak shape, retention time, and area.
    c. Calculate the peak area ratio of the analyte to internal standard.

       Note that isotopically labeled internal standards are not available for all analytes. To overcome this problem, an alternative with similar chemical composition to that of the analyte can be substituted. For calculating the peak area ratio of zymosterol, 7-DHC, and 8-DHC, use d_7-DHC; for 7-dehydrodesmosterol (7-DHD) and desmosterol, use $^{13}C_3$ -desmosterol; for cholesterol, use d_7-cholesterol; and for lanosterol and lathosterol, use $^{13}C_3$-lanosterol. Use d_7-ketocholesterol for all cholesterol-derived oxysterols. However, users can add additional internal standards if they are available, such as d_6-24(S),25-epoxycholesterol, d_7-24-hydroxycholesterol, and d_7-4β-hydroxycholesterol.

22. Using an Excel® spreadsheet, generate the relative response factor (RRF) of each analyte from each injection of the standard sample.
    a. Calculate the response factor (RF) for each sterol and oxysterol by dividing the standard analyte peak area by its concentration in the standard sample.
    b. Calculate the RF of each internal standard in the standard sample by dividing the internal standard peak area by its concentration in the standard sample.
    c. Calculate the RRFby dividing the RFof the analyte by the RF of its corresponding internal standard.

As noted previously, this quantitation method relies on single-point calibration. For best results, the standard and internal standard concentrations should be in the range of the estimated concentration in the sample. This may require additional fine tuning to get the correct levels.

23. Average the RRFs calculated from each injection of the standard sample and use this number to account for any instrumental drift.
24. Calculate the concentration of each endogenous sterol and oxysterol in the sample, as well as the extraction blank, by multiplying the peak area ratio by the internal standard concentration in the sample and then dividing by the average RRF.

    If quantifiable levels of any analyte were introduced in the extraction blank, subtract that amount from each sample, to correct for analyte that did not originate from the cell or tissue.

25. The absolute amount of each endogenous sterol and oxysterol can by calculated by multiplying the concentration by the dilution factor and volume of mobile phase used to reconstitute extract.
26. The absolute amount of sterol or oxysterol should then be normalized to the amount of protein or tissue used in the extraction, as differences in protein content or tissue weight could yield different sterol or oxysterol levels. Alternatively, normalization of sterol precursors and/or oxysterols to cholesterol content can also be used to assess relative changes in cholesterol synthesis and/or metabolism.

Statistical analyses

These data are amenable to a variety of statistical analyses to determine significant differences in sterol and oxysterol levels between treatment groups. Student's t-test to compare two means, or analysis of variance (ANOVA) for more than two means, are two

commonly used analyses to determine if xenobiotic treatment alters sterol or oxysterol levels. Regression analyses could also be useful for determining a dose-response relationship between doses of xenobiotic and resulting sterol or oxysterol levels.

A.4. Reagents and Solutions

Folch solution (chloroform:methanol = 2:1, with 1 mM BHT and 1 mM PPh3)

Weigh out 0.131 g of PPh3 (triphenylphosphine, Sigma-Aldrich, 93092) and 0.11 g of BHT (2,6-di-tert-butyl-4-methyl-phenol, Sigma-Aldrich, B1378). Measure 167 ml methanol (LC-MS grade) in a graduated cylinder and add to 500-ml volumetric flask. Transfer PPh3 and BHT to the volumetric flask containing methanol. Fill the volumetric flask to 500 ml with chlorofom1 (LC-MS grade). Transfer solution to glass storage bottle. Make fresh and chill prior to extraction.

This recipe makes enough for approximately 125 samples.

Mobile phase: 90% methanol with 0.1% formic acid

Measure out 100 ml of water (LC-MS grade) using a graduated cylinder and add to I-liter volumetric flask. Fill the volumetric flask half-way with methanol. Add 1 ml formic acid (LC-MS grade) to volumetric flask with 1000-µl pipet. Adjust volume to 1 liter with methanol. Prepare the mobile phase fresh prior to each analysis.

Oxysterol internal standard, 10 µg/ml

Prepare a 10x dilution of the 100 µg/ml oxysterol internal standard (see recipe) in a new screw-cap vial. Store at - 80°C up to 6 months.

Oxysterol internal standard, 100 µg/ml

Prepare 100 µg/ml dr 7-ketocholesterol (Avanti Polar Lipids, Inc., 700046P) in benzene (LC-MS grade). Prepare a stock solution by dissolving 1 mg d_7-7- ketocholesterol in 1

ml benzene in a screw-cap vial. Transfer 100 µl of the 1 mg/ml mixture to a new screw-cap vial and dry under argon using the Reacti-Vap™ Evap- orator. Reconstitute in 1 ml benzene. Store at - 80°C up to 6 months.

Oxysterol standard, 10 µg/ml

Dissolve 1 mg of each oxysterol (listed below) in 1 ml of benzene (LC-MS grade). Prepare a 10x dilution of each oxysterol standard to yield a 100 µg/ml stock solution of each in benzene. Add 100 µl of each oxysterol standard from 100 µg/ml stock to the same screw-cap vial. Add 200 µl of benzene to yield a 10 µg/ml oxysterol standard solution. Cap and store at -80°C up to 6 months.

- 7 ,27-dihydroxycholesterol(Avanti Polar Lipids, Inc., 700025P)
- 7-keto-27-hydroxycholesterol (Avanti Polar Lipids, Inc., 700033P)
- 24-hydroxycholesterol (Avanti Polar Lipids, Inc., 700061P)
- 25-hydroxycholesterol (Avanti Polar Lipids, Inc., 700019P)
- 24-ketocholesterol (Steraloids, Inc., C7030-000)
- 24(S),25-epoxycholesterol (Avanti Polar Lipids, Inc., 700039P)
- 4 -hydroxycholesterol (Avanti Polar Lipids, Inc., 700036P)
- 7 -hydroxycholesterol (Avanti Polar Lipids, Inc., 700035P)
- 7-ketocholesterol (Avanti Polar Lipids, Inc., 700015P)

Phosphate-buffered saline (PBS), lx

Measure out 100 ml of 10x PBS buffer, pH 7.4 (ThermoFisher Scientific, AM9625) using a graduated cylinder and add to a I-liter glass storage bottle. Measure out 900 ml of deionized water and add to the 100 ml of 10x PBS in the glass storage bottle. Chill prior to use.

Sterol internal standard, 50/10 µg/ml

Prepare a 10x dilution of the 500/100 µg/ml sterol internal standard (see recipe) in a new screw-cap vial. Store at - 80°C up to 6 months.

Sterol internal standard, 500/100 µg/ml

Prepare a solution containing 500 µg/ml drcholesterol (Avanti Polar Lipids, Inc., 700041) and d_7-7-DHC (Avanti Polar Lipids, Inc., 700116P) and 100 µg/ml $^{13}C_3$-lanosterol (Kerafast®, EVU135) and $^{13}C_3$-desmosterol (Kerafast®, EVU127). Pre- pare a stock solution of each internal standard by dissolving solids in benzene. Aliquot an amount of each internal standard into the same screw-cap vial, depending on starting stock concentration, to achieve the desired final concentration. Dry this mixture under argon using the Reacti-Vap™ Evaporator and reconstitute in benzene (LC-MS grade) to achieve the desired final concentration of each sterol internal standard. Store at -80°C up to 6 months.

Sterol standard, 10 µglml

Dissolve 1 mg of each sterol (listed below) in 1 ml of benzene (LC-MS grade). Prepare a 10x dilution of each sterol standard to yield a 100 µg/ml stock solution in benzene. Add 100 µl of each sterol standard to the same screw-cap vial. Add 200 µl of benzene to yield a 10 µg/ml sterol standard solution. Cap and store at - 80°C up to 6 months.

- 7-dehydrodesmosterol (Avanti Polar Lipids, Inc., 700138P)
- Zymosterol (Avanti Polar Lipids, Inc., 700068P)
- Desmosterol (Avanti Polar Lipids, Inc., 700060P)
- 8-dehyrocholesterol (Avanti Polar Lipids, Inc., 700075P)
- 7-dehydrocholesterol (Avanti Polar Lipids, Inc., 700066P)
- Lathosterol (Avanti Polar Lipids, Inc., 700069P)

- Cholesterol (Sigma-Aldrich®, C8667)
- Lanosterol (Avanti Polar Lipids, Inc., 700063P)

Sodium chloride, aqueous solution (0.9% w/v)

Weigh out 0.900 g of sodium chloride (certified ACS crystalline) and transfer to a 100-ml volumetric flask. Adjust volume to 100 ml with water (LC-MS grade). Transfer to glass storage bottle. Store at room temperature up to 1 month.

A.5. Commentary

Background information

Mass spectrometry is the modern technol- ogy for sterol and oxysterol analysis, including both gas chromatography-mass spectrometry (GC-MS) and LC-MS, as well as matrix- assisted laser desorption/ionization (MALDI)- MS for imaging studies (Griffiths et al., 2017). Conventionally, sterols are analyzed by GC or GC-MS after derivatization, which is still often used, but LC-MS has become the technique of choice over the past decade (Gerst, Ruan, Pang, Wilson, and Schroepfer, 1997). In LC-MS analysis, sterols and oxys- terols can be analyzed either underivatized or with derivatization to facilitate ionization (Griffiths and Wang, 2009; Honda et al., 2008; McDonald, Thompson, McCrum, and Russell, 2007).

In the current procedure, UHPLC-MS/MS withAPCI is used to quantify the major sterols in the cholesterol biosynthetic pathway as well as the cholesterol-derived oxysterols without chemical derivatization (Finno et al., 2016; Fliesler etal., 2018; Herron etal., 2016). APCI is advantageous over GC-MS and LC-MS paired with electrospray ionization (LC- ESI-MS/MS), as sterols and oxysterols are nonvolatile and poorly ionizable. The use of APCI circumvents the need to derivatize sam- ples while still affording sufficient sensitivity. The elimination of derivatization procedures can reduce undesired ex vivo autoxidation of cholesterol and its precursors, which could interfere with the analysis of endogenous oxysterols (Lamberson et

al., 2017; Xu and Porter, 2015; Yin et al., 2011). Additionally, the UHPLC-MS/MS method in the current method has a run time of 15 min for each sample, which is quite efficient compared to previously published methods (McDonald et al., 2007).

A.6. Critical Parameters and Troubleshooting

Autoxidation of cholesterol and its precursors

Cholesterol and cholesterol precursors are highly vulnerable to autoxidation, where oxysterols can be formed from sterols in air (Lamberson et al., 2017) (Xu and Porter, 2015; Yin et al., 2011). Artifactual formation of cholesterol-derived oxysterols during freezing and thawing of samples or during extraction could hamper accurate measurements. It is im-portant to use only freshly collected or flash- frozen samples to prevent oxidation prior to homogenization in the Folch solution. In addition, antioxidants, such as BHT and PPh3, are added to the Folch solution to prevent undesired autoxidation.

UHPLC maintenance and troubleshooting

The UHPLC system, including tubing, column, injection port, and needle, can become clogged by dirty samples, precipitated salts, solvents, and even autosampler caps. There-fore, it is important to use only high-quality, HPLC-grade solvents and pre-slit autosampler caps, and to filter samples using a syringe filter prior to UHPLC-MS/MS analysis if extracts look cloudy or contain particulates. System pressure can also be an indicator of alterations in the column, mobile phase, flow rate, and temperature. It is important to record system pressure to establish a pressure reference point. If changes in pressure occur, longer column equilibration might help in stabilizing the pressure to the reference point. The mobile phase composition may change over time, so one should make it fresh prior to sample anal- ysis. If pressure problem persists, consider replacing the column, as it has a finite lifetime. Additionally, altered retention times most often indicate poor equilibration of the system and

mobile phase, as well as column contamination and flow rate. Overloading the sample or improper column equilibration might also yield distorted peak shapes that could result in inaccurate quantitation. Finally, random baseline noise spikes and disrupted flow rates might indicate gas bubbles in the UHPLC pumps, which would require mobile phase degassing or replacement of pump seals. Further information on these issues and how to avoid them can be found in the manufacturer's user guide.

Mass spectrometer maintenance

The mass spectrometer should be properly and routinely maintained for optimal performance. Loss of sensitivity, increased background noise, and additional peaks not part of the sample could be observed in the absence of proper and timely instrument maintenance, indicative of system contamination. To avoid these issues as well as damage to the mass spectrometer, follow the manufacturer's guidance on maintenance tasks and schedule.

A.7. Anticipated Results

A chromatogram for each sterol and oxysterol standard sample, each containing a mixture of sterols and oxysterols and corresponding internal standards, is shown in **Figures A.3 and A.4.** With this method, oxysterols are eluted through the column between 1 and 5 min and sterols are eluted through the column between 5 and 14 min.

The utility of this protocol is demonstrated in **Table A.4**. In this case, we investigated the effect of a known cholesterol biosynthesis inhibitor, AY9944, on cholesterol homeostasis in neurospheres, which are a three-dimensional in vitro model used for developmental neurotoxicity testing. We hypothesized that AY9944, which inhibits cholesterol biosynthesis at the step of DHCR7, would lead to an accumulation of sterol precursors and a decrease in cholesterol and cholesterol-derived oxysterols in treated neurospheres. Following a 72-hr treatment with AY9944 or vehicle control, neurospheres were collected into a cell pellet and

a protein mass assay was used to determine sample protein content. Lipid extraction and UHPLC-MS/MS analysis for sterols and oxysterols was conducted. The endogenous sterol and oxysterol content was then normalized to the protein content for each sample. The Student's t-test assuming unequal variance was used to determine statistically significant differences in sterol and oxysterol levels, using the significance value of $p<0.05$. The results of this experiment show that AY9944 is a potent inhibitor of cholesterol biosynthesis in neurospheres. This is indicated by the significant accumulation of the cholesterol precursors 7-DHC and 7-DHD, which rely on DHCR7 to be converted to cholesterol and desmosterol, respectively. Further alteration of cholesterol homeostasis was observed in the almost 5-fold decrease in 24(S), 25-epoxycholesterol and 7-fold decrease in 24/25-hyclroxycholesterol, two of the main cholesterol-derived oxysterols. Significant decreases in these cholesterol-derived oxysterols provide further evidence that cholesterol biosynthesis is downregulated in the AY9944 treated samples.

Table A.4. Treatment of neurospheres with AY9944 induced significant changes in levels of sterols and cholesterol-derived oxysterols.

Sterols	**Control**	**AY9944**	**Units**
Cholesterol	15.01 ± 4.39	2.82 ± 1.3 *	µg/mg
7-DHC	0.14 ± 0.05	11 ± 3.02 *	ng/mg
Desmosterol	6.4 ± 1.2	0.19 ± 0.15 **	µg/mg
7-DHD	0.81 ± 0.39	10.52 ± 2.57 **	ng/mg
Lanosterol	0.38 ± 0.13	0.25 ± 0.05	µg/mg
8-DHC	0.36 ± 0.02	2.52 ± 0.19	ng/mg
Zymosterol	1.01 ± 0.39	1.23 ± 0.41	ng/mg
Lathosterol	0.65 ± 0.60	0.43 ± 0.48	µg/mg
Cholesterol-derived Oxysterols			
24(S),25-epoxycholesterol	352.04 ± 176.27	76.03 ± 54.61 *	ng/mg
24-ketocholesterol	22.3 ± 7.68	38.31 ± 2.7 *	ng/mg

7-hydroxycholesterol	2.17 ± 0.52	5.55 ± 1.41 *	ng/mg
24/25-hydroxycholesterol	9.25 ± 2.45	1.32 ± 1.75 **	ng/mg
7-ketocholesterol	13.67 ± 8.32	10.81 ± 5.27	ng/mg

** denotes p≤0.05; ** denotes p≤0.005; t-test assuming unequal variances was used.*

A.8. Time Considerations

For approximately 20 cell samples, the protein assay takes 2 hr to complete. The lipid extraction for 20 cell samples takes approximately 5 hr, including drying in the Speed- Vac, reconstituting in methylene chloride, and transferring to a screw-top storage vial. For sterols and oxysterols separately, UHPLC- MS/MS analysis takes approximately 16 min per sample for a total run time of approximately 6 hr for injections of 20 cell samples, 3 standard samples (at minimum), and 1 ex- traction blank. For the same number of tissue samples, the lipid extraction and UHPLC- MS/MS analyses take approximately same amount of time.

A.9. Acknowledgments

This chapter contains the research article: Josi Herron, Kelly M. Hines, and Libin Xu, Assessment of Altered Cholesterol Homeostasis by Xenobiotics Using Ultra-High Performance Liquid Chromatography-Tandem Mass Spectrometry. *Current Protocols in Toxicology* 2018, 78, e65.

This work was supported by grants from the National Institutes of Health (R00HD073270 and R01HD092659). J.H. was also supported by a National Institute of Environmental Health Sciences training grant (T32ES007032).

A.10. References

Boland, M. R., and Tatonetti, N. P. (2016). Investigation of 7-dehydrocholesterol reductase pathway to elucidate off-target prenatal effects of pharmaceuticals: a systematic review. *The pharmacogenomics journal*, *16*(5), 411–429. Nature Publishing Group.

Canfrán-Duque, A., Casado, M. E., Pastor, O., Sánchez-Wandelmer, J., la Peña, de, G., Lerma, M., Mariscal, P., et al. (2013). Atypical antipsychotics alter cholesterol and fatty acid metabolism in vitro. *Journal of Lipid Research*, *54*(2), 310–324.

de Medina, P., Paillasse, M. R., Segala, G., Poirot, M., Silvente-Poirot, S., and Mangelsdorf, D. J. (2010). Identification and pharmacological characterization of cholesterol-5,6-epoxide hydrolase as a target for tamoxifen and AEBS ligands. *Proceedings of the National Academy of Sciences of the United States of America*, *107*(30), 13520–13525. National Academy of Sciences.

Finno, C. J., Bordbari, M. H., Valberg, S. J., Lee, D., Herron, J., Hines, K., Monsour, T., et al. (2016). Transcriptome profiling of equine vitamin E deficient neuroaxonal dystrophy identifies upregulation of liver X receptor target genes. *Free Radical Biology and Medicine*, *101*, 261–271.

Fliesler, S. J., Peachey, N. S., Herron, J., Hines, K. M., Weinstock, N. I., Ramachandra Rao, S., and Xu, L. (2018). Prevention of Retinal Degeneration in a Rat Model of Smith-Lemli-Opitz Syndrome. *Scientific reports*, *8*(1), 1286. Nature Publishing Group.

Folch, J., Lees, M., and Sloane Stanley, G. H. (1957). A simple method for the isolation and purification of total lipides from animal tissues. *Journal of Biological Chemistry*, *226*(1), 497–509.

Gerst, N., Ruan, B., Pang, J., Wilson, W. K., and Schroepfer, G. J. (1997). An updated look at the analysis of unsaturated C27 sterols by gas chromatography and mass spectrometry. *The Journal of Lipid Research*, *38*(8), 1685–1701.

Griffiths, W. J., and Wang, Y. (2009). Analysis of neurosterols by GC-MS and LC-MS/MS. *Journal of chromatography. B, Analytical technologies in the biomedical and life sciences*, *877*(26), 2778–2805.

Griffiths, W. J., Abdel-Khalik, J., Yutuc, E., Morgan, A. H., Gilmore, I., Hearn, T., and Wang, Y. (2017). Cholesterolomics: An update. *Analytical biochemistry*, *524*, 56–67.

Guizzetti, M., Chen, J., and Costa, L.G. (2011) Chapter 65: Disruption of cholesterol homeostasis in developmental neurotoxicity. In R.C. Gupta (Ed.), *Reproductive and Developmental Toxicology* (pp. 855-862). Academic Press.

Hall, P., Michels, V., Gavrilov, D., Matern, D., Oglesbee, D., Raymond, K., Rinaldo, P., et al. (2013). Aripiprazole and trazodone cause elevations of 7-dehydrocholesterol in the absence of Smith-Lemli-Opitz Syndrome. *Molecular genetics and metabolism*, *110*(1-2), 176–178.

Herron, J., Reese, R. C., Tallman, K. A., Narayanaswamy, R., Porter, N. A., and Xu, L. (2016). Identification of Environmental Quaternary Ammonium Compounds as Direct Inhibitors of Cholesterol Biosynthesis. *Toxicological Sciences : an official journal of the Society of Toxicology*, *151*(2), 261–270.

Honda, A., Yamashita, K., Miyazaki, H., Shirai, M., Ikegami, T., Xu, G., Numazawa, M., et al. (2008). Highly sensitive analysis of sterol profiles in human serum by LC-ESI-MS/MS. *The Journal of Lipid Research*, *49*(9), 2063–2073.

Kelley, R. I., and Herman, G. E. (2001). Inborn errors of sterol biosynthesis. *Annual review of genomics and human genetics*, *2*(1), 299–341.

Kim, H.-Y. H., Korade, Z., Tallman, K. A., Liu, W., Weaver, C. D., Mirnics, K., and Porter, N. A. (2016). Inhibitors of 7-Dehydrocholesterol Reductase: Screening of a Collection of Pharmacologically Active Compounds in Neuro2a Cells. *Chemical research in toxicology*, *29*(5), 892–900.

Korade, Z., Kim, H.-Y. H., Tallman, K. A., Liu, W., Koczok, K., Balogh, I., Xu, L., et al.

(2016). The Effect of Small Molecules on Sterol Homeostasis: Measuring 7-Dehydrocholesterol in Dhcr7-Deficient Neuro2a Cells and Human Fibroblasts. *Journal of medicinal chemistry*, *59*(3), 1102–1115.

Lamberson, C. R., Muchalski, H., McDuffee, K. B., Tallman, K. A., Xu, L., and Porter, N. A. (2017). Propagation rate constants for the peroxidation of sterols on the biosynthetic pathway to cholesterol. *Chemistry and physics of lipids*, *207*(Pt B), 51–58.

McDonald, J. G., Thompson, B. M., McCrum, E. C., and Russell, D. W. (2007). Extraction and analysis of sterols in biological matrices by high performance liquid chromatography electrospray ionization mass spectrometry. *Methods in enzymology*, *432*, 145–170. Elsevier.

Mutemberezi, V., Guillemot-Legris, O., and Muccioli, G. G. (2016). Oxysterols: From cholesterol metabolites to key mediators. *Progress in lipid research*, *64*, 152–169.

Pikuleva, I. A. (2006). Cholesterol-metabolizing cytochromes P450. *Drug metabolism and disposition: the biological fate of chemicals*, *34*(4), 513–520. American Society for Pharmacology and Experimental Therapeutics.

Porter, F. D., and Herman, G. E. (2010). Malformation syndromes caused by disorders of cholesterol synthesis. *The Journal of Lipid Research*, *52*(1), 6–34.

Xu, L., and Porter, N. A. (2015). Free radical oxidation of cholesterol and its precursors: Implications in cholesterol biosynthesis disorders. *Free radical research*, *49*(7), 835–849.

Yin, H., Xu, L., and Porter, N. A. (2011). Free radical lipid peroxidation: mechanisms and analysis. *Chemical reviews*, *111*(10), 5944–5972.

Appendix B: Curriculum Vitae

Josi M. Herron

Department of Environmental and Occupational Health Sciences
1959 NE Pacific Street, Box 357234
Seattle, WA 98105
jh0618@uw.edu

Education

Ph.D. in Environmental Toxicology – Environmental Health
Emphasis: Human Health Risk Assessment
09/2014 – 12/2019
University of Washington, Seattle, WA
Advisor: Dr. Libin Xu

Dissertation: The Effects of Benzalkonium Chloride Disinfectants on Lipid Homeostasis and Neurodevelopment

Bachelor of Arts in Biology
Summa Cum Laude
8/2009 – 5/2013
University of Great Falls, Great Falls, MT

Research Experience

Graduate Research Assistant

- Elucidated the neurotoxic effects of benzalkonium chloride disinfectants in a 3-D *in vitro* model of neurodevelopment.
- Evaluated the effect of *in utero* exposure to benzalkonium chloride disinfectants on sterol and lipid homeostasis in neonate brains using targeted and untargeted mass spectrometry, RNA-sequencing, and bioinformatics.
- Developed and implemented a method for the quantitative assessment of altered cholesterol homeostasis by xenobiotics utilizing ultra-high performance liquid chromatography-tandem mass spectrometry.
- Characterized the lipidome of neuronal cells treated with benzalkonium chloride disinfectants.
- Investigated the structure activity and toxicity of quaternary ammonium compound disinfectants in neuronal cell lines.

Honors, Awards, and Fellowships

- 10/2018 – **Awarded Best Graduate Platform Presentation** at the Pacific Northwest Association of Toxicologists Annual Meeting.
- 09/2017 – **Awarded Best Graduate Poster Presentation** at the Pacific Northwest Association of Toxicologists Annual Meeting.
- 07/2017 – **Selected for Predoctoral Trainee Oral Presentation** at the Environmental Pathology/ Toxicology Training Grant Annual Retreat.
- 01/2017 – **Awarded the Environmental Pathology/Toxicology Training Grant** (NIH T32 ES007032-39) which provides stipend and tuition to trainees actively involved in research on cellular and molecular mechanisms of toxicity.
- 12/2016 – **Awarded Poster of Exceptional Merit** at the University of Washington Biological Basis of Autism Research Symposium.

Publications

9. **Herron, J.M,** Tomita, H., White, C.W., Kavanagh, T.J, and Xu, L. (2019) Benzalkonium chloride disinfectants inhibit proliferation and induce cell death in an in vitro model of neurodevelopment. Submitted for review to *Toxicology In Vitro.*

8. Seguin, R.P., **Herron, J.M.,** Lopez, V., Dempsey, J.L., and Xu, L. (2019) Metabolism of benzalkonium chlorides by human hepatic cytochromes P450. *Chem. Res. Toxicol.* 2019, XXXX, XXX, XXX-XXX.

7. **Herron, J. M.,** Hines, K. M., Tomita, H., Seguin, R. P., Cui, J. Y., and Xu, L. (2019). Multiomics investigation reveals benzalkonium chloride disinfectants alter sterol and lipid homeostasis in the mouse neonatal brain. *Toxicol. Sci.*, *171*(1), 32–45.

   Article featured as a Tox Spotlight article in the September 2019 issue, a recognition from the editor to highlight papers of interest.

6. Weber, E.J., Lidberg, K.A., Wang, L., Bammler, T.K., MacDonald, J.W., Li, M.J., Redhair, M., Atkins, W.M., Tran, C., Hines, K.M., **Herron, J.**, Xu, L., et al. (2018) Human kidney on a chip assessment of polymyxin antibiotic nephrotoxicity. *JCI Insight 3*(24), e123673.

5. **Herron, J.**, Hines, K.M., Xu, L. (2018) Assessment of altered cholesterol homeostasis by xenobiotics using ultra-high performance liquid chromatography-tandem mass spectrometry. *Curr Protoc Toxicol*, 78(1): e65.

4. Fliesler, S.J., Peachey, N.S., **Herron, J.**, Hines, K.M., Weinstock, N.I., Rao, S.R., Xu, L. (2018). Prevention of retinal degeneration in a rat model of Smith-Lemli-Opitz syndrome. *Sci Rep.* 8(1):1286.

3. Hines, K. M., **Herron, J**., Xu, L. (2017). Assessment of altered lipid homeostasis by HILIC-ion mobility-mass spectrometry-based lipidomics*. Journal of Lipid Research*, 58(4), 809–819.

2. **Herron, J**., Reese, R.C., Tallman, K.A., Narayanaswamy, R., Porter, N.A., Xu, L. (2016) Identification of environmental quaternary ammonium compounds as direct inhibitors of cholesterol biosynthesis. *Toxicol. Sci. 151*(2):261-270.

1. Finno, C. J., Bordbari, M. H., Valberg, S. J., Lee, D., **Herron, J.,** Hines, K., et al. (2016). Transcriptome profiling of equine vitamin E deficient neuroaxonal dystrophy

identifies upregulation of liver X receptor target genes. Free Radical Biology and Medicine, 101, 261–271.

Oral Presentations

American Society for Mass Spectrometry Annual Conference
Atlanta, GA, 06/2019
Title: Multiomics investigation reveals benzalkonium chloride disinfectants alter sterol and lipid homeostasis in the mouse neonatal brain.

Pacific Northwest Association of Toxicologists Annual Meeting
Seattle Genetics, Bothell, WA, 10/2018
Title: *In utero* exposure to the disinfectant benzalkonium chloride alters sterol and lipid homeostasis in the neonate mouse brain.
Awarded Best Graduate Platform Presentation

Environmental Pathology/ Toxicology Training Grant Annual Retreat
University of Washington, Seattle, WA, 07/2017
Title: The effect of quaternary ammonium compounds on lipid homeostasis and neurogenesis.

Environmental and Molecular Toxicology Research Day
Oregon State University, Corvallis, OR 01/2016
Title: Investigating a mechanism of developmental neurotoxicity: Quaternary ammonium compounds and their effect on cholesterol biosynthesis.

Poster Presentations

Society of Toxicology 58th Annual Meeting
Baltimore, MD, 03/2019
Title: Altered sterol homeostasis during neurodevelopment, *in vivo* and *in vitro*, is a common target for benzalkonium chloride disinfectants

Society of Toxicology 57th Annual Meeting
San Antonio, TX, 03/2018
Title: The impact of benzalkonium chloride on lipid homeostasis and neurodevelopment.

Pacific Northwest Association of Toxicologists Annual Meeting
Seattle Genetics, Bothell, WA, 10/2018
Title: Investigating a novel mechanism of developmental neurotoxicity: The impact of quaternary ammonium compounds on neurodevelopment through modulation of lipid homeostasis.
Awarded Best Graduate Poster Presentation

Tenth World Congress: Alternatives and Animal Use in the Life Sciences
Seattle, WA, 08/2017
Title: Investigating a novel mechanism of developmental neurotoxicity: The impact of quaternary ammonium compounds on neurodevelopment through modulation of lipid homeostasis.

CHDD Biological Basis of Autism Research Symposium
University of Washington, Seattle, WA, 12/2016
Title: Disruption of lipid homeostasis by environmental chemicals: Implication for

neurodevelopmental disorders
Awarded Presentation of Exceptional Merit

Pacific Northwest Association of Toxicologists Annual Meeting
Oregon State University, Corvallis, OR, 09/2016
Title: Investigating a mechanism of developmental neurotoxicity: Quaternary ammonium compounds and their effect on cholesterol biosynthesis.
Poster selected for flash talk presentation.

Society of Toxicology 55th Annual Meeting
New Orleans, LA, 03/2016
Title: Investigating a mechanism of developmental neurotoxicity: Quaternary ammonium compounds and their effect on cholesterol biosynthesis.
Poster selected for flash talk presentation.

Professional Experience

Toxicologist (Intern)
06/2019-09/2019
The Boeing Company, Renton, WA

Supervisor: Katherine Skordal

- Supported health hazard assessments.
- Provided employee safety recommendations related to materials used in company operations.
- Ensured US EPA Toxic Substances Control Act (TSCA) regulatory compliance.

Laboratory Technician
09/2013-06/2014
Malteurop North America, Great Falls, MT

Supervisor: Andrea Stern

- Implemented laboratory research and tasks in a team driven setting to support quality assurance objectives.
- Produced and maintained records of observations, measurements, and results.
- Complied with pre-established guidelines to perform functions of the job.
- Assessed result validity prior to reporting to manufacturing or customers.
- Provided technical support to the sales function of the company by preparing special samples and analytical information.

Teaching Experience

Graduate Mentor
06/2015-12/2019
University of Washington, Seattle, WA

- Trained 6 students (graduate and undergraduate): Brianna Morgan, Amy Li, Cecilia Tran, Tania Velasco, Vanessa Lopez, Quynh Do
- Instructed students in cell culture, molecular assays, mouse colony management, tissue dissection, lipid extraction from biological samples, ultra-high performance liquid

chromatography-tandem mass spectrometry operation, RNA isolation and sequencing, data analysis and bioinformatics

Organic Chemistry Teaching Assistant
08/2012-05/2013
University of Great Falls, Great Falls, MT

- Supervised laboratory activities for undergraduates
- Complied with chemical hygiene and safety regulations
- Provide guidance to students on experimental procedures and calculations
- Facilitated recitation sessions, reviewing problem sets and providing additional review of lecture topics

Professional Memberships

- 2019 – Present, American Society for Mass Spectrometry
- 2018 – Present, Society of Toxicology Women in Toxicology Special Interest Group
- 2017 – Present, Society of Toxicology Neurotoxicology Specialty Section
- 2016 – Present, Pacific Northwest Association of Toxicologists
- 2015 – Present, Society of Toxicology

Professional Service

- 2017 – 2019, **Communications Subcommittee Member**, Society of Toxicology Graduate Student Leadership Committee
- 2017 – 2019, **Graduate Student Representative**, Pacific Northwest Association of Toxicologists

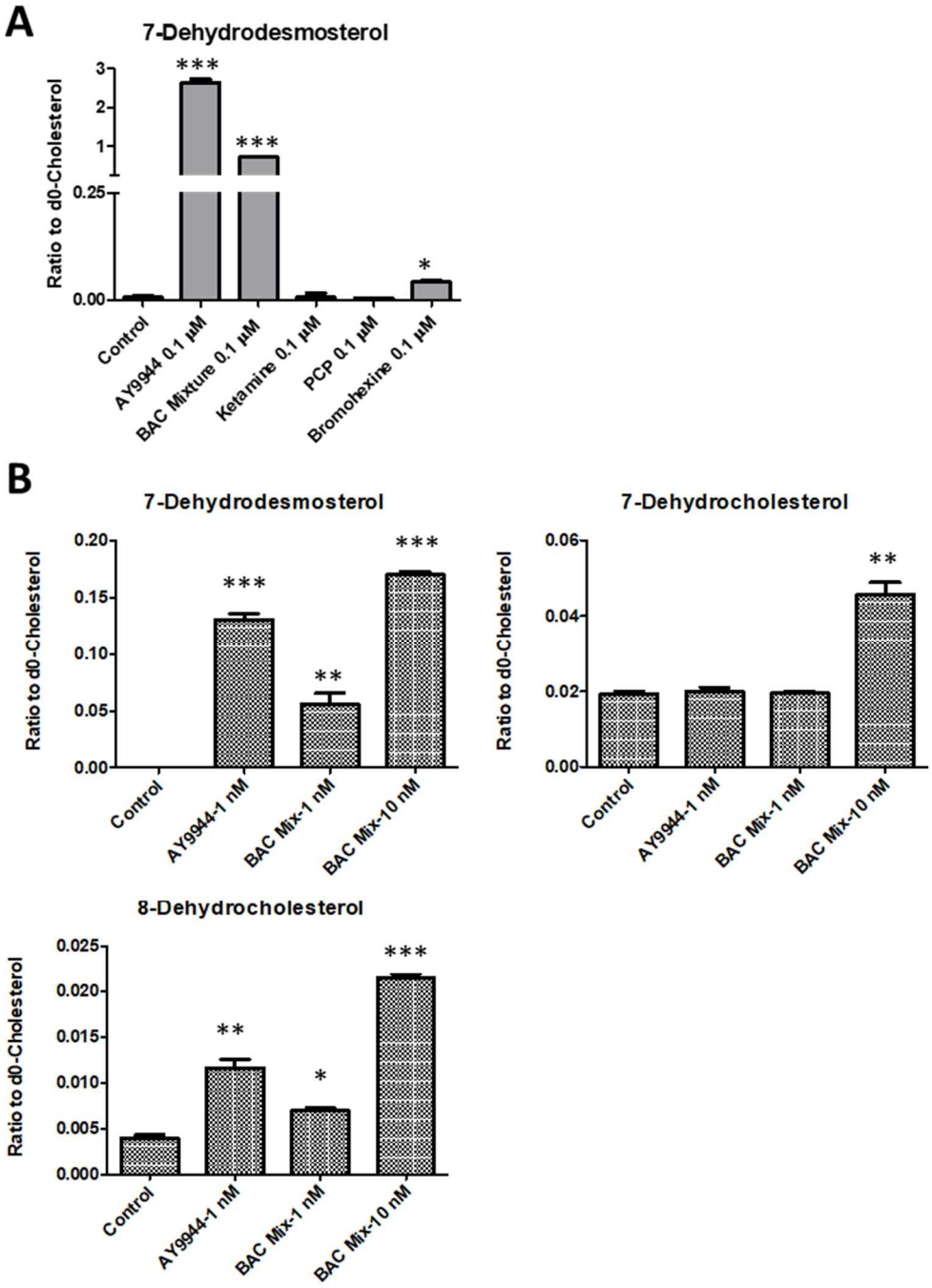

Figure S.1. (A) Effect of different compounds similar to AY9944 on cholesterol biosynthesis in Neuro2a cells on the levels of 7-dehydrodesmosterol (7-DHD) after 48 hrs of treatment. (B) Effect of different concentrations of BACs on 7-DHC, 7-DHD and 8-DHC in Neuro2a cells after 48 hrs of treatment.

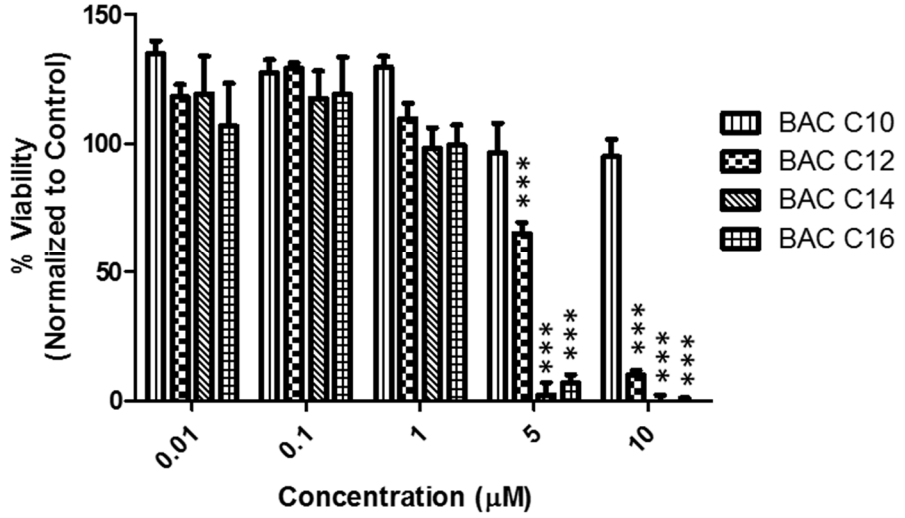

Figure S.2. Cytotoxicity of individual BACs on Neuro2a cells after 24 hrs of treatment.

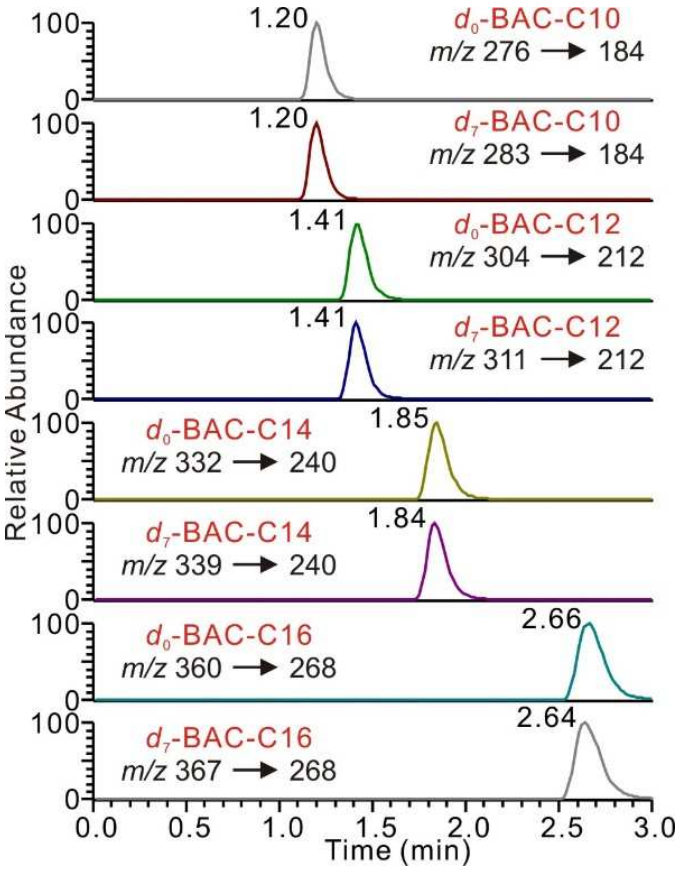

Figure S.3. Reverse phase UPLC-MS/MS analysis of BACs using d_7-BACs as internal standards.

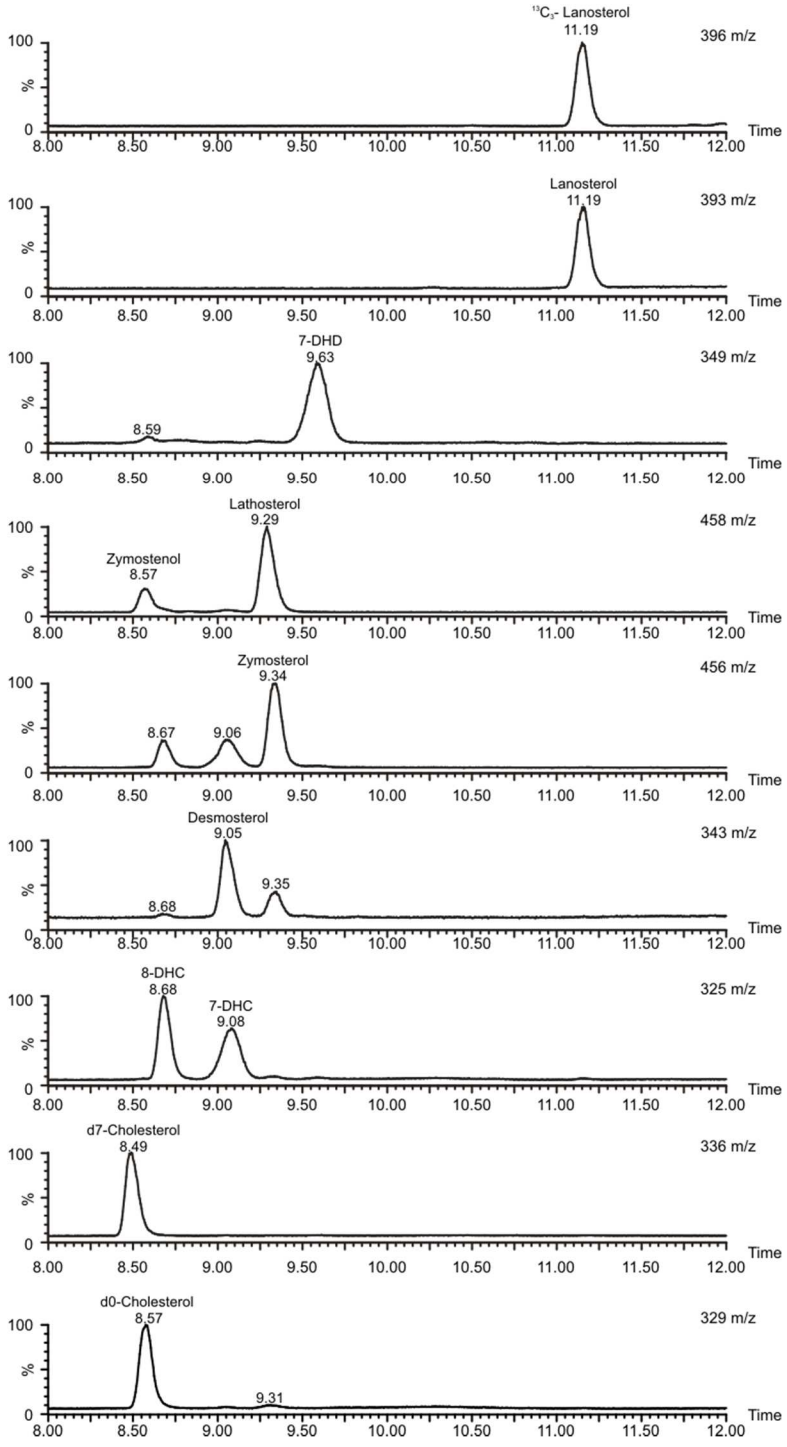

Figure S.4. Representative chromatogram of analysis of standards of cholesterol and its precursors using GC-MS.

Supporting Information for Chapter 3

Table S.1. Altered lipids in neonatal brains exposed *in utero* to BAC C12 or BAC C16.

	m/z	Retention Time (min)	Mass Accuracy (ppm)	Abundance in Control	Fold Change[a,b]	
					BAC C12	BAC C16
DG 34:6 Na	639.498	0.5	11.0	453 ± 59	0.8 *	0.9
DG 36:6	595.473	0.4	0.7	481 ± 33	0.8	0.9
DG 36:2	659.501	0.4	8.0	882 ± 73	0.8	0.9
DG 32:1	549.488	0.4	3.2	1741 ± 343	0.6 **	0.8
DG 34:2	575.504	0.4	6.0	1928 ± 204	0.7 **	0.8
DG 36:1	605.551	0.4	10.7	2268 ± 197	0.7 *	0.8
DG 34:1	577.520	0.5	2.5	7228 ± 1083	0.6 ***	0.8
TG 50:5	842.723	0.5	18.3	354 ± 29	0.9	0.8
TG 48:2	820.739	0.5	6.8	737 ± 105	0.5 *	0.5
TG 54:2	904.833	0.5	11.5	1094 ± 149	0.5 *	0.6
TG 48:1	822.755	0.5	6.1	2301 ± 305	0.4 *	0.4
TG 50:2	848.770	0.5	4.4	2846 ± 497	0.5 *	0.6
TG 50:1	850.786	0.5	5.8	4284 ± 600	0.4 **	0.5
TG 52:2	876.802	0.5	5.0	6303 ± 893	0.5 *	0.6
Cer (d18:1/26:1)	658.650	0.5	10.1	174 ± 27	1.2	0.8
Cer (d18:1/20:0)	558.562	0.5	11.9	295 ± 35	1.0	0.8 *
Cer (d18:0/24:0)	634.650	0.5	19.1	501 ± 84	1.0	0.7 *
Cer (d18:1/16:1)	536.504	0.5	1.2	3880 ± 301	0.9	0.8 **
Cer (d18:1/18:0)	566.551	0.5	0.5	4272 ± 507	1.0	0.8 *
Cer (d18:1/16:0)	502.499	0.5	3.7	4487 ± 779	1.1	0.8
Cer (d18:1/22:0)	604.603	0.5	3.3	5649 ± 907	1.1	0.7 *
Cer (d18:0/16:0)	520.510	0.5	2.9	53136 ± 7419	1.0	0.8 *
Cer (d18:0/18:0)	548.541	0.5	5.1	113197 ± 14647	1.0	0.8 *
HexCer (d18:0/22:0)	750.662	0.7	15.9	222 ± 28	0.9	0.8 **
HexCer (d18:1/20:1)	770.614	0.7	6.4	312 ± 35	0.8	0.7 **
HexCer (d18:1/22:0)	766.656	0.7	16.5	313 ± 66	0.9	0.6 *
HexCer (d18:1/20:0)	738.625	0.7	13.6	400 ± 60	0.8	0.6 **
HexCer (d18:1/16:0)	700.572	0.7	13.8	1024 ± 122	0.9	0.7 *
HexCer (d18:1/20:0)	756.635	0.7	17.0	1165 ± 131	0.9	0.8 **
HexCer (d18:1/18:0)	728.604	0.7	9.5	1537 ± 231	0.9	0.7 *
HexCer (d18:1/16:0)	682.562	0.7	2.9	3639 ± 578	0.9	0.6 **
HexCer (d18:1/18:0)	750.585	0.7	4.5	5534 ± 863	0.9	0.7 **

HexCer (d18:1/18:0)	710.594	0.7	2.6	8699 ± 1622	0.9	0.6 *
PI O-40:2	927.630	3.6	17.6	84 ± 16	0.7 *	0.9
PI 40:9	887.507	3.9	17.6	217 ± 44	0.7	0.6 **
PE p34:2	722.510	5.1	7.6	3560 ± 360	0.8	0.9
SM(d18:1/18:1)	729.591	7.1	6.9	1216 ± 234	0.8	1.2

[a]Fold-change relative to control.

[b]Student's *t*-test against control with Bonferroni correction for multiple comparisons; * P <0.025, ** P <0.0025, ** P <0.00025.

Table S.2. Top 5 significantly altered canonical pathways of DEGs in BAC C12 and BAC C16 exposed neonatal brains.

Comparison Groups	IPA Canonical Pathway	- log (P-value)	Molecules
BAC C12 vs Control	Superpathway of Cholesterol Biosynthesis	7.03	HMGCS2, SQLE, DHCR24, IDI1, HMGCR, HSD17B7, CYP51A1, MSMO1
	LXR/RXR Activation	6.49	GC, ITIH4, MMP9, HMGCR, LDLR, NGFR, SCD, APOA2, SERPINA1, APOA1, CYP51A1, HPX, TTR, ALB
	TR/RXR Activation	5.10	FGFR1, LDLR, HP, COL6A3, CAMK4, TRH, SLC2A1, ENO1, NCOA2, SLC16A3, KLF9
	Glutamate Receptor Signaling	4.60	HOMER1, GNB3, GRIA2, CAMK4,SLC1A2, GRIN2C, GRIN2B, GRM3
	Acute Phase Response Signaling	3.95	ITIH4, JAK2, SERPINA3, FN1, HP, NGFR, APOA2, SERPINA1, APOA1, HPX, RBP3, TTR, ALB
BAC C16 vs Control	EIF2 Signaling	9.37	RPL21, RPS24, RPL37A, RPL26, RPS13, RPL9, ATF4, EIF3E, RPL22L1, RPS27A, RPL36A, RPS21, RPL10
	Superpathway of Cholesterol Biosynthesis	6.37	HMGCS2, SQLE, DHCR24, HSD17B7, MSMO1
	LXR/RXR Activation	5.30	LDLR, MMP9, APOA2, APOA1, AHSG, TTR, ALB
	Glutamate Receptor Signaling	3.55	SLC17A7, GRIA2, GRIN2B, GRM3
	Acute Phase Response Signaling	3.35	APOA2, APOA1, SERPINA3, AHSG, TTR, ALB

Table S.3. Transcriptional regulators and endogenous factors predicted as upstream regulators with the Ingenuity Pathway Analysis in BAC C12 exposed neonatal brains.

Upstream Regulator	Molecule Type	Predicted Activation State	Activation z-score	p-value of overlap
ATP7B	transporter	Activated	2.50	1.10E-12
SCAP	other	Activated	2.86	2.02E-12
HTT	transcription regulator	Inhibited	-2.16	1.67E-09
beta-estradiol	endogenous chemical	Inhibited	-2.30	3.17E-09
TGFB1	growth factor	Inhibited	-2.57	5.52E-08
SREBF2	transcription regulator		1.66	6.80E-08
SREBF1	transcription regulator		1.05	1.91E-07
T3-TR-RXR	complex		-1.19	2.02E-07
FGF2	growth factor	Inhibited	-2.22	2.29E-07
SP1	transcription regulator		-1.69	3.00E-07
EGF	growth factor	Inhibited	-2.50	3.55E-07
INSIG1	other	Inhibited	-2.29	3.60E-07
D-glucose	endogenous chemical		-0.86	8.55E-07
MED13	transcription regulator		-0.45	1.37E-06
HIF1A	transcription regulator		-1.97	1.45E-06
BDNF	growth factor		1.42	1.88E-06
ERBB2	kinase		0.01	4.62E-06
PPARG	ligand-dependent nuclear receptor		1.84	6.30E-06
APP	other		-0.78	6.38E-06
oleic acid	endogenous chemical		-0.61	7.76E-06
Vegf	group		-0.20	8.19E-06

Table S.4. Transcriptional regulators and endogenous factors predicted as upstream regulators with the Ingenuity Pathway Analysis in BAC C16 exposed neonatal brains.

Upstream Regulator	Molecule Type	Predicted Activation State	Activation z-score	*P*-value of overlap
RICTOR	other	Activated	3.61	3.94E-09
L-triiodothyronine	endogenous chemical		-0.62	2.19E-07
SCAP	other	Activated	2.23	4.37E-07
dihydrotestosterone	endogenous chemical		0.97	5.81E-07
MYCN	transcription regulator	Inhibited	-2.35	6.55E-07
ATP7B	transporter	Activated	2.24	2.72E-06
SREBF1	transcription regulator		1.21	1.44E-05
IGF1R	transmembrane receptor		-1.39	2.27E-05
beta-estradiol	endogenous chemical		-1.01	2.56E-05
INSIG1	other		-1.67	2.60E-05
SREBF2	transcription regulator		1.29	6.50E-05
FOS	transcription regulator		-0.13	6.69E-05
SOX4	Transcription regulator		-1.20	9.62E-05
ABCA1	transporter		-0.64	1.36E-04
ERBB4	kinase		1.46	1.41E-04
FGF2	growth factor		-1.45	2.84E-04
fatty acid	endogenous chemical		-0.56	3.85E-04
BDNF	growth factor		1.25	4.43E-04
estrogen receptor	group		1.22	4.45E-04
GH1	growth factor		1.22	5.14E-04
Vegf	group		0.42	6.54E-04

Table S.5. Differentially expressed genes involved in sterol and lipid homeostasis in neonatal brains exposed *in utero* to BAC C12; adjusted *P* <0.05. Genes identified as related to sterol and lipid metabolism using DAVID functional annotation clustering.

Gene ID	Description	Log2 (FC)	Adjusted *P* value
AACS	acetoacetyl-CoA synthetase	0.42	9.81E-03
ACP6	acid phosphatase 6, lysophosphatidic	0.81	1.81E-02
ACSL4	acyl-CoA synthetase long-chain family member 4	0.51	4.44E-03
ADH1	alcohol dehydrogenase 1 (class I)	-1.31	2.97E-02
APOA1	apolipoprotein A-I	-1.89	4.44E-03
APOA2	apolipoprotein A-II	-2.14	4.44E-03
APOC1	apolipoprotein C-I	-1.74	1.81E-02
ART3	ADP-ribosyltransferase 3	-1.53	4.44E-03
CYP51	cytochrome P450, family 51	0.58	3.23E-02
DHCR24	24-dehydrocholesterol reductase	0.54	4.44E-03
ELOVL6	ELOVL family member 6, elongation of long chain fatty acids (yeast)	0.58	4.44E-03
ENO1	enolase 1, alpha non-neuron	-0.36	1.81E-02
ETNK1	ethanolamine kinase 1	0.31	4.11E-02
HMGCR	3-hydroxy-3-methylglutaryl-Coenzyme A reductase	0.57	4.44E-03
HMGCS2	3-hydroxy-3-methylglutaryl-Coenzyme A synthase 2	0.69	4.44E-03
HSD17B7	hydroxysteroid (17-beta) dehydrogenase 7	1.07	4.44E-03
IDI1	isopentenyl-diphosphate delta isomerase	0.91	4.44E-03
INSIG1	insulin induced gene 1	0.41	9.81E-03
KDM8	lysine (K)-specific demethylase 8	-0.77	4.44E-03
LDHA	lactate dehydrogenase A	-0.40	4.44E-03
LDLR	low density lipoprotein receptor	0.87	4.44E-03
LOXL1	lysyl oxidase-like 1	-0.43	4.53E-02
MSMO1	methylsterol monooxygenase 1	0.66	4.44E-03
MTHFD2	methylenetetrahydrofolate dehydrogenase (NAD+ dependent), methenyltetrahydrofolate cyclohydrolase	-0.66	4.44E-03
ODC1	ornithine decarboxylase, structural 1	-0.81	4.44E-03
PCSK9	proprotein convertase subtilisin/kexin type 9	-0.81	4.44E-03
PLCXD3	phosphatidylinositol-specific phospholipase C, X domain containing 3	0.55	4.44E-03
PNPLA2	patatin-like phospholipase domain containing 2	-0.52	2.56E-02
PPARA	peroxisome proliferator activated receptor alpha	-1.46	4.33E-02
PRKAA2	protein kinase, AMP-activated, alpha 2 catalytic subunit	0.40	7.33E-03
PRKAG2	protein kinase, AMP-activated, gamma 2 non-catalytic subunit	0.47	2.36E-02
SCD1	stearoyl-Coenzyme A desaturase 1	-0.36	1.98E-02
SESN2	sestrin 2	-0.61	4.44E-03
SLC16A1	solute carrier family 16 (monocarboxylic acid transporters), member 1	0.48	4.44E-03
SQLE	squalene epoxidase	0.62	4.44E-03
TPI1	triosephosphate isomerase 1	-0.45	4.44E-03
UQCRQ	ubiquinol-cytochrome c reductase, complex III subunit VII	-0.53	4.86E-02

Table S.6. Differentially expressed genes involved in sterol and lipid homeostasis in neonate brains exposed *in utero* to BAC C16; adjusted *P* <0.05. Genes identified as related to sterol and lipid metabolism using DAVID functional annotation clustering.

Gene ID	Description	Log2 (FC)	Adjusted *P* value
AACS	acetoacetyl-CoA synthetase	0.35	3.84E-02
ADH1	alcohol dehydrogenase 1 (class I)	-1.40	2.92E-02
APOA1	apolipoprotein A-I	-2.10	9.98E-03
APOA2	apolipoprotein A-II	-2.75	9.98E-03
APOC1	apolipoprotein C-I	-1.54	3.35E-02
ATP5E	ATP synthase, H+ transporting, mitochondrial F1 complex, epsilon subunit	-0.35	2.38E-02
ATP5L	ATP synthase, H+ transporting, mitochondrial F0 complex, subunit G	-0.40	9.98E-03
CFAP61	cilia and flagella associated protein 61	1.95	2.38E-02
DHCR24	24-dehydrocholesterol reductase	0.49	9.98E-03
HMGCS2	3-hydroxy-3-methylglutaryl-Coenzyme A synthase 2	0.61	9.98E-03
HSD17B7	hydroxysteroid (17-beta) dehydrogenase 7	0.71	9.98E-03
LDLR	low density lipoprotein receptor	0.73	9.98E-03
MSMO1	methylsterol monoxygenase 1	0.48	9.98E-03
MTHFD2	methylenetetrahydrofolate dehydrogenase (NAD+ dependent), methenyltetrahydrofolate cyclohydrolase	-0.53	9.98E-03
NDUFA4	NADH dehydrogenase (ubiquinone) 1 alpha subcomplex, 4	-0.32	2.92E-02
ODC1	ornithine decarboxylase, structural 1	-0.69	9.98E-03
PGP	phosphoglycolate phosphatase	0.42	2.38E-02
POLR1D	polymerase (RNA) I polypeptide D	-0.40	9.98E-03
SQLE	squalene epoxidase	0.45	9.98E-03

Table S.7. Genes selected for qPCR validation and purchased from ThermoFisher Scientific.

Gene	TaqMan™ Assay ID
ACTB	Mm00607939_s1
CYP51	Mm00490968_m1
DHCR24	Mm00519071_m1
HMGCR	Mm01282499_m1
HMGCS2	Mm00550050_m1
INSIG1	Mm00463389_m1
SCAP	Mm01250176_m1
SQLE	Mm00436772_m1
SREBF1	Mm00550338_m1
SREBF2	Mm01306292_m1

Table S.8. Top 10 biological processes altered by BACs.

GO Biological Process	BAC C12 vs. Control			BAC C16 vs. Control		
	# DEGs	# Total	-log *P*-value	# DEGs	# Total	-log *P*-value
response to stress	41	2214	15.84	12	2205	6.44
phosphate-containing compound metabolic process	18	674	13.29	5	665	4.84
Phosphorylation	15	508	13.29	4	499	4.38
cell death	26	1523	8.29	8	1508	4.34
programmed cell death	25	1453	8.16	8	1446	4.65
apoptotic process	21	1216	7.06	7	1201	4.54
regulation of transport	31	2084	6.67	10	2066	4.39
small molecule metabolic process	22	1337	6.55	8	1331	5.28
chemical homeostasis	21	1308	5.94	8	1301	5.46
MAPK cascade	19	1193	5.37	11	1178	12.29